Study on diffusion behavior of radionuclides in compacted bentonite(Dissertation_全文)

AUTHOR(S):

Ishidera, Takamitsu

Study on diffusion behavior of radionuclides in compacted bentonite

2008

Takamitsu Ishidera

Contents

Chapter 1
Introduction

1.1 Introduction

In Japan, spent nuclear fuel from nuclear power plant is reprocessed in order to extract uranium and plutonium. In the reprocessing process, high-level radioactive waste (HLW) containing fission products and actinides is generated as a residue of reprocessing. HLW is, therefore, planned to be disposed in deep geological environment[1)]. In addition to HLW, radioactive waste containing transuranic nuclides (TRU waste) is generated from the reprocessing of spent nuclear fuel and from the mixed oxide (MOX) fuel processing plant. Such TRU waste contains relatively large concentrations of both alpha-emitting radionuclides and other long-lived isotopes. Therefore, TRU waste is also planned for geological disposal[2)].

Long-term safety of geological disposal is ensured by a multi-barrier system. The multi-barrier system of HLW disposal consists of an engineered barrier system (EBS) that includes a vitrified waste, an overpack and a buffer material, and host rock as natural barrier as shown in Fig.1-1. In geological disposal of TRU waste, the engineered barrier system consists of waste package, backfill and buffer material.

The geological disposal of HLW and TRU waste possibly affects the human environment by migration of radionuclides to the biosphere via groundwater. After the disposal repository is closed, compacted bentonite used as the buffer material is saturated with groundwater. In geological disposal of HLW, groundwater corrodes the overpack, and then the overpack has a mechanical failure due to the corrosion. When groundwater comes into contact with the vitrified waste due to the failure of overpack, radionuclides contained in the waste will dissolve into the groundwater. In geological disposal of TRU waste, radionuclides contained in waste package will dissolve into groundwater immediately after the groundwater come into contact with the waste package through compacted bentonite. The radionuclides diffuse through the compacted bentonite, and then migrate in host rock to the biosphere. In safety assessment of geological disposal, radiation dose in human environment is estimated based on this groundwater scenario.

Because of low permeability of compacted bentonite, radionuclides are transported by diffusion from a high concentration region to a low concentration region. The diffusion through compacted bentonite is one of important processes of radionuclides migration. In

safety assessment of geological disposal, the diffusion coefficients of radionuclides are determined based on the experimental studies for diffusion behavior in compacted bentonite. However, the studies for phenomena affecting the diffusion behavior of radionuclides in compacted bentonite are not sufficient to predict the effects of these phenomena on the diffusion coefficients. The items listed below are the phenomena which have a possibility to increase diffusion coefficients of radionuclides.

(a) Temperature dependence of diffusion coefficients

Most of diffusion experiments in compacted bentonites have been carried out at room temperature. The diffusion coefficients obtained at room temperature should be corrected to those at 60^{o}C, which is assumed to be the repository temperature[1)], for the safety assessment. However, there are no available data on the temperature dependence of effective diffusion coefficients, although the temperature dependence of apparent diffusion coefficient has been reported[3-5)]. The temperature correction is based on the activation energy for diffusion. The effective diffusion coefficient, which can be obtained from steady-state diffusion experiments such as the through-diffusion method, does not include retardation by sorption, while the apparent diffusion coefficient, which can be obtained from transient diffusion experiment such as the in-diffusion method, includes retardation. As the temperature dependence of apparent diffusion coefficient contains the activation energy of sorption, the activation energy of effective diffusion coefficient can not be calculated from that of apparent diffusion coefficient. For the activation energy of effective diffusion coefficient, it is proposed to use that in free water[1)]. However, the electrostatic interaction between diffusive chemical species and bentonite surface is considered to affect the activation energy. Thus, the activation energy of effective diffusion coefficients in compacted bentonite should be determined based on experimental data.

(b) Effect of salinity on diffusion of anions

Anions are considered to be excluded from negatively charged smectite surfaces by electric repulsion in compacted bentonite. As this anion exclusion decreases with increasing salinity of porewater, the effective diffusion coefficient of anions has been reported to increase with increasing salinity[6-8)]. However, only a few reports are available for the salinity dependence of effective diffusion coefficient of anions in compacted bentonite. Also, there is little available

information on the effects of sodium nitrate, which is contained in TRU waste abundantly, on the diffusion of anions. Therefore, the salinity dependence of effective diffusion coefficient should be studied considering sodium nitrate.

(c) Effect of iron corrosion products

In geological disposal of HLW, groundwater corrodes an overpack, and subsequently the corrosion products of carbon steel, which is a candidate material for the overpack, migrates into compacted bentonite. After the overpack has a mechanical failure due to the corrosion, radionuclides contained in vitrified waste dissolve into the groundwater and diffuse through the compacted bentonite. Therefore, diffusion behavior of radionuclides could possibly be affected by the corrosion of carbon steel. Corrosion of iron have been reported to affect the diffusion behavior of radionuclides in compacted bentonite[9-17]. However, in order to estimate the effect of carbon steel corrosion, the corrosion process and the form of corrosion products present in compacted bentonite should be clarified. In addition, the corrosion products may cause the alteration of smectite in compacted bentonite. The possibility of alteration of Na^+-adsorbed smectite (Na-smectite) to Fe^{2+}-adsorbed smectite (Fe-smectite) has been reported by experimental studies[18-20]. The presence of iron has been reported to cause the alteration of smectite to other minerals[21-24]. These alterations of smectite possibly increase the diffusion coefficient of radionuclides in compacted bentonite. Unfortunately, most of the alteration experiments have been, however, performed by batch experiments. There is a little available information for alteration of smectite in compacted bentonite due to corrosion products.

On the backgrounds mentioned above, the experimental studies are carried out to clarify the effects, which have a possibility to increase the diffusion coefficient of radionuclides in compacted bentonite.

In chapter 2, through-diffusion experiments of deuterated water (HDO) are conducted at elevated temperatures. The effect of temperature on diffusivity of HDO in compacted sodium bentonite is studied in term of activation energy.

In chapter 3, effective diffusion coefficients for Cl^- and I^- in compacted bentonite are determined as a function of $NaNO_3$ concentrations. The effect of salinity on diffusion of anions in compacted bentonite is discussed.

In chapter 4, the corrosion of carbon steel and its effect on neptunium diffusion are studied by corrosion experiments of carbon steel and neptunium diffusion experiments with and without carbon steel. The form of corrosion products is discussed from the thermodynamic prediction considering the condition of pore water of compacted bentonite. The effect of corrosion products on neptunium diffusion is discussed by considering the oxidation state of neptunium.

In chapter 5, carbon steel is left in contact with compacted bentonite under reducing conditions for 3 to 4 years at room temperature. The form of corrosion products from the carbon steel into compacted bentonite is identified by selective dissolution analysis, to estimate crystallinity of Fe-bearing compounds, and by spectrophotometry to determine the valence of iron in the corrosion products. The alteration of smectite to Fe-smectite in compacted bentonite is analyzed by X-ray diffraction (XRD).

In chapter 6, carbon steel in contact with compacted bentonite for 10 years at 80^{o}C was investigated. The form of corrosion products distributed in the compacted bentonite is determined by selective dissolution analysis, by valence analysis and by XRD. The possibility of montmorillonite alteration in compacted bentonite is investigated by XRD and by the cation exchange capacity (CEC) analysis.

In Chapter 7, the conclusions of these studies are summarized.

References

1) Japan Nuclear Cycle Development Institute (JNC), *H12: Project to establish the technical basis for HLW disposal in Japan, Supporting report 3, Safety assessment of the geological system*, JNC TN1410 2000-004, (2000)
2) Japan Nuclear Cycle Development Institute and The Federation of Electric Power Companies, *Progress report on disposal concept for TRU waste in Japan*, JNC TY1400 2000-002, (2000).
3) T. Kozaki, H. Sato, A. Fujishima, S. Sato and H. Ohashi, "Activation Energy for Diffusion of Cesium in Compacted Sodium Montmorillonite," *J. Nucl. Sci. Technol*., 33, 522-524 (1996).
4) T. Kozaki, H. Sato, A. Fujishima, N. Saito, S. Sato and H. Ohashi, "Effect of Dry Density on Activation Energy for Diffusion of Strontium in Compacted Sodium Bentonite," *Mat.*

Res. Soc. Symp. Proc., 465, 893 -900 (1997).

5) H. Sato and M. Yui, "Diffusion of Ni in Compacted Sodium Bentonite," *J. Nucl. Sci. Technol*., 34, 334-336 (1997).
6) A. Muurinen, P. Penttila-Hiltunen and K. Uusheimo, "Diffusion of chloride and uranium in compacted sodium bentonite," *Mat. Res. Soc. Symp. Proc.*, 127, 743-748 (1989).
7) S. Suzuki, *Study on diffusion behavior of nuclide in buffer material*, JNC TN8400 2002-006, Japan Nuclear Cycle Development Institute (JNC), (2002), (in Japanese).
8) T. E. Eriksen and M. Jansson, *Diffusion of I, Cs^+ and Sr^{2+} in compacted bentonite – Anion exclusion and surface diffusion*, SKB Tech. rep. TR 96-16, Swedish Nuclear Fuel and Waste Management Co., (1996).
9) B. Torstenfelt, K. Andersson, H. Kipatsi, et al., "Diffusion Measurements in Compacted Bentonite," *Mat. Res. Soc. Symp. Proc.*, 11, 295-302 (1982).
10) B. Torstenfelt, H. Kipatsi, K. Andersson, et al., "Transport of Actinides through a Bentonite Backfill," *Mat. Res. Soc. Symp. Proc.*, 11, 659-668, (1982).
11) Y. Albinsson, R. Forsyth, G. Skarnemark, et al., "Leaching/Migration of UO_2-fuel in Compacted Bentonite," *Mat. Res. Soc. Symp. Proc.*, 176, 559-565 (1990).
12) Y. Albinsson, B. Christiansen-S□tmark, I. Engkvist et al., "Transport of Actinides and Tc through a Bentonite Backfill Containing Small Quantities of Iron or Copper," *Radiochim. Acta* 52/53, 283-286 (1991).
13) K. Idemitsu, Y. Tachi, H. Furuya, et al., "Diffusion of Uranium in Compacted Bentonites in the Reducing Condition with Corrosion Products of Iron," *Mat. Res. Soc. Symp. Proc.*, 412, 683-690 (1996).
14) Y. Kuroda, K. Idemitsu, H. Furuya et al., "Diffusion of Technetium in Compacted Bentonites in the Reducing Condition with Corrosion Products of Iron," *Mat. Res. Soc. Symp. Proc.*, 465, 909-916 (1997).
15) K. Idemitsu, Y. Tachi, H. Furuya et al., "Diffusion of Cs and Sr in Compacted Bentonites under Reducing Conditions and in the Presence of Corrosion Products of Iron," *Mat. Res. Soc. Symp. Proc.*, 506, 351-358 (1998).
16) H. Ramebäck, M. Skålberg, U. B. Eklund, et al., "Mobility of U, Np, Pu, Am and Cm from Spent Nuclear Fuel into Bentonite Clay," *Radiochim. Acta*, 82, 167-171 (1998).
17) K. Idemitsu, X. Xia, T. Ichishima, et al., "Diffusion of Plutonium in Compacted Bentonites in the Reducing Condition with Corrosion Products of Iron," *Mat. Res. Soc.*

Symp. Proc., 608, 261-266 (2000).

18) K. Idemitsu, S. Yano, X. Xia, et al., "Migration Behavior of Iron Ion in Compacted Bentonite under Reducing Condition by using Electromigration," *Mat. Res. Soc. Symp. Proc.*, 757, 657-664 (2003).

19) H.Sasamoto, T. Suyama and M. Shibata, *Laboratory Experiment of Iron-Bentonite Interaction*, JNC TN8400 2003-047, Japan Nuclear Cycle Development Institute (JNC), (2004), (in Japanese).

20) G. Kamei, C. Oda, S. Mitsui, et al., "Fe(II)-Na Ion Exchange at Interlayers of Smectite: Adsorption-desorption Experiments and a natural Analogue," *Eng. Geol.*, 54, 15-20, (1999).

21) Guillaume D., Neaman A., Cathelineau M., et al., "Experimental Study of the Transformation of Smectite at 80 and 300^{o}C in the Presence of Fe oxides," *Clay Minerals*, 39, 17-34 (2004).

22) S. Lantenois, B. Lanson, F. Muller, et al., "Experimental Study of Smectite Interaction with Metal Fe at Low Temperature: 1. Smectite Destabilization," *Clays Clay Miner.*, 53, 597-612 (2005).

23) J. Wilson, D. Savage, J. Cuadros, et al, "The Effect of Iron on Montmorillonite Stability (I) Background and Thermodynamic Considerations," *Geochim. Cosmochim. acta*, 70, 306-322 (2006).

24) J. Wilson, G. Cressey, B. Cressey, et al., "The Effect of Iron on Montmorillonite Stability (II) Experimental investigation," *Geochim. Cosmochim. acta*, 70, 323-336 (2006).

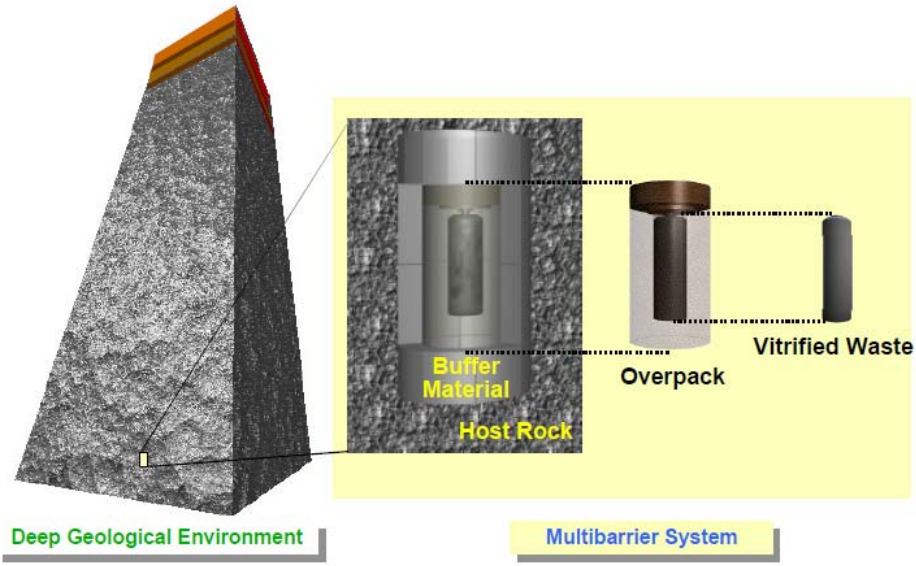

Figure 1-1 The basic concept of geological disposal in Japan[1)]

Chapter 2
Anisotropy of effective diffusion coefficient and activation energy for deuterated water in compacted sodium bentonite

2.1 Introduction

The effective diffusion coefficient, D_e, of a radionuclide in compacted bentonite used as a buffer material is an important parameter in the safety assessment of geological disposal of high-level radioactive waste. Effective diffusion coefficients of nuclides in the buffer material are affected by the conditions in the underground environment, e.g. temperature and salinity of the groundwater[1,2].

However, there have been few studies of the temperature dependence of D_e in compacted bentonite. In the H12 project report by Japan Nuclear Cycle Development (hereafter referred to as the ''H12 report'')[3], the performance of the buffer material was assessed at 333 K. As no data were available regarding D_e at 333 K, an activation energy of 15 kJ/mol for diffusion of ions in bulk water was adopted in the H12 report to calculate D_e for any nuclides in the buffer material at 333 K from D_e at 298 K using the Arrhenius equation. Kozaki et al. (1996, 1998, 2001)[2,4,5] and Nakazawa et al. (1999)[6] have determined activation energies of diffusion for Cs, HTO, Cl and Na using the apparent diffusion coefficients. Activation energies for all diffusants increased with increasing dry density from 1.0 to 1.8 Mg/m^3. Especially, the 53 kJ/mol activation energy for Cs at the dry density of 1.8 Mg/m^3 was significantly larger than the 18 kJ/mol activation energy in bulk water calculated from the results reported by Li and Gregory (1974)[4,7]. The activation energy calculated from the effective diffusion coefficient may also differ from that in bulk water, because the solute diffusivity may be affected by the properties of pore water[8] and/or the interactions between the diffusant and the mineral surface, such as sorption.

Thus, it is necessary to determine the temperature dependence of D_e in compacted bentonite directly by the through-diffusion method. Pusch et al. (1989) attempted to investigate the diffusivities of Na, Cu and U at 363 K by the through-diffusion method[9]. However, because of practical problems, they neither analyzed the effective diffusion coefficients nor measured the activation energy. To confirm the methodology, we selected deuterium-doped water (deuterated water) as an inactive diffusant and compared the values of its effective diffusion coefficient and activation energy with those of tritiated water reported previously by Sato et al.

(1992)[10] and Nakazawa et al. (1999)[6]. HTO has been used as a nonsorbing diffusant in previous studies of the effects of diffusion pathways in bentonite[11,12]. The effective diffusion coefficient of HTO was used in the safety assessment of an engineered barrier system[3]. If the diffusion behavior of HDO is comparable to that of HTO, our data can be used as an analogue of HTO diffusion.

2.2 Experimental method

2.2.1 Compacted bentonite

The bentonite material examined in this study was Kunipia F (Kunimine Industries, Japan). Kunipia F consists of Na-montmorillonite (>98 wt.%) and trace amount of quartz[13]. The chemical formula of Na-montmorillonite in Kunipia F was $(Na_{0.431},K_{0.002},Ca_{0.002})(Al_{1.560},Mg_{0.305},Fe_{0.099},Ti_{0.007})(Si_{3.949},Al_{0.051})O_{10}(OH)_2 \cdot nH_2O$ [14]. A powdered sample (mean particle size = ca. 100 μm) was compacted to obtain a dry density of 0.9 or 1.35 Mg/m^3. The dry bulk density of 0.9 Mg/m^3 was comparable to the partial dry density of the smectite component of the buffer material proposed in JNC (2000)[3], which was a mixture of silica sand and bentonite[15]. The latter dry density of 1.35 Mg/m^3 was chosen with consideration of microstructural development in compacted bentonite. According to Kozaki et al. (1998)[5], the basal spacing of montmorillonite in compacted bentonite in the saturated state changes discontinuously from 1.88 to 1.56 nm with increasing dry density. The X-ray diffraction peak related to the 1.88 nm basal spacing was only observed at dry densities lower than 1.3 Mg/m^3. The basal spacing maintained a constant distance of 1.88 nm at dry densities lower than 1.3 Mg/m^3. When the dry density was increased to 1.4 Mg/m^3, basal spacing of both 1.88 and 1.56 nm basal spacing were found in the XRD profile. Therefore, the interstitial pore space was postulated to collapse between 1.3 and 1.4 Mg/m^3 and ca. 80% of the total pore space may become the interlamellar space (1.56-1.88 nm) or the extremely narrow pores equivalent to the interlamellar space, according to calculations based on the simple microstructural model of bentonite[15].

Sato (2001) reported that bentonite particles orient perpendicularly to the direction of compaction, so the effective diffusion coefficient depends on the direction of compaction[16]. Diffusion experiments were designed to investigate the anisotropy of D_e and the activation energy. Diffusion directions are shown schematically in Fig. 2-1. Effective diffusion coefficients along the preferred orientation of the montmorillonite and normal to the

orientation are denoted by D_e^P and D_e^N, respectively.

2.2.2 Diffusion experiment

Fig. 2-2 shows the through-diffusion system and the diffusion cell used in this study. A tracer solution was circulated through a porous plastic filter on one side of the diffusion cell by a peristaltic pump (EYELA SMP-21S). A tracer-free solution was circulated through a porous plastic filter on the other side of the diffusion cell. Their flow rates were controlled by controlling the speed of the pump between 2 and 5 ml/h. The diffusion cell was kept in an incubator, while the two reservoirs containing the solutions were left outside the incubator at room temperature. The solution volume was 500 ml for the tracer solution and 100 ml for the tracer-free solution. The temperature inside the incubator was maintained within 1 K of either 298, 313, 323 or 333 K.

The size and shape of the bentonite samples used were dependent upon the diffusional direction. When the direction was parallel to the preferred orientation of the montmorillonite, the sample measured 17.5 × 17.5 × 5 mm. When the direction was normal to the orientation, samples measured 20 mm in diameter and 5 mm in thickness. A membrane filter (Millipore, pore size = 0.22 μm, ϕ = 25 mm, thickness = ca. 0.1 mm) was placed between the porous plastic filter and bentonite, to prevent leakage of montmorillonite particles after saturation. The porous plastic filter was 25 mm in diameter and 2 mm in thickness.

After assembling the diffusion cell, deionized water was circulated for 1 week on both sides of the cell to saturate the bentonite. To accelerate saturation, the diffusion cells were then left for 2 weeks under vacuum (-50 mm Hg), before placing them in the incubator. Before the solutions were circulated, the diffusion cell was equilibrated to the desired temperature.

The deuterated water tracer was prepared by adding 20-30 ml of D_2O (>99.8 wt.%; Kanto Chemical) to 500 ml of deionized water. The obtained concentration of the deuterated water was 2-3 mol/dm^3. Prior to the diffusion experiments, the solution was left at room temperature for several hours and the initial concentration of the deuterated water was measured.

To apply Eqs. (2-2) and (2-3) in the following section, the boundary conditions during the experiment were maintained as described below. A sample of 1 ml was taken from the bottle on the low-concentration side once or twice a day, and the concentration of the tracer was measured as described later. To maintain the large difference in HDO concentration between the high-concentration side (C_H) and the low-concentration side (C_L), when the concentration

C_L had risen to ca. 5% of the C_H, the whole solution in the bottle on the low-concentration side was replaced with tracer-free deionized water. As a result of this operation, the C_L changed in a sawtooth with respect to time. The cumulative quantity (or integrated flux) $Q(t)$ [mol/m^2] for HDO was, therefore, calculated as:

$$Q(t) = \frac{V}{A}\left(C_L(t) + \sum_{n=1}^{m} C_{n-1} \right); C_0 = 0 \qquad (2\text{-}1)$$

where $C_L(t)$ is the concentration of deuterated water at time t, V is the volume of solution in the low-concentration volume (100 ml), A is the cross-sectional area of the bentonite sample (3.06 cm^2 for D_e^P or 3.14 cm^2 for D_e^N) and m is the number of solution exchanges. The reservoir was exchanged at most once in this study. $C_{n\text{-}1}$ is the final concentration on the low-concentration side in the n-1th exchange of solution. The change in concentration in the tracer bottle C_H during the experiment was negligible.

The species in the deuterated water and their concentrations were investigated by Fourier transform infrared (FTIR) spectroscopy (System 2000, Perkin Elmer) with attenuated total reflectance (ATR) spectroscopy (ATR crystal: ZnSe, Spectratech). The details of the ATR/FTIR spectroscopy are described elsewhere[17]. Deionized water was used as a reference material to obtain a background spectrum. An IR absorption peak due to O-D stretching in the deuterated water was found at 2508cm^{-1}. As the peak height is essentially proportional to the concentration of deuterated water, it was used to determine the HDO concentration (Fig. 2-3). The chemical species present could be distinguished by their absorption peaks due to bond bending. The relative dose of three species, D_2O, HDO and H_2O, were determined by their respective peaks at 1216, 1453 and 1635 cm^{-1}. As the absorption peak at 1453 cm^{-1} was much larger than the peak at 1216 cm^{-1}, the most abundant chemical species in the deuterated water was HDO under the conditions used in this study.

2.2.3 Diffusion analysis

The cumulative quantity $Q(t)$ increased gradually to reach a steady state of diffusion. Consequently, $Q(t)$ reached a state whereby it increased linearly with time. D_e was determined from the diffusive flux J and the concentration gradient in the pore water in bentonite $\Delta C_p/L_b$ using the following equation[1,11]:

$$D_e = -J \frac{L_b}{\Delta C_p} \tag{2-2}$$

The diffusive flux J was obtained by linear least-squares fitting for the break-through curve at steady state, L_b is the thickness of bentonite sample, and ΔC_p is the concentration difference in pore water between each side of the bentonite sample. Assuming the concentration in the water in the surface pores on each side of the bentonite to be equal to the concentration in the corresponding solution bottles, the concentration gradient can be expressed as:

$$\frac{\Delta C_p}{L_b} = \frac{C_L - C_H}{L_b} \cong -\frac{C_H}{L_b} \tag{2-3}$$

assuming $C_H \gg C_L$.

2.3 Results and discussion

2.3.1 Anisotropy of effective diffusion coefficient and activation energy

Fig. 2-4a shows typical break-through curves of HDO for two diffusional directions and two different dry densities at 313 K. As shown in Fig. 2-4b, the flux was almost constant and fluctuated around the value determined by least-square fitting of the break-through curve (dashed lines). Thus, the steady state of diffusion was confirmed. Effective diffusion coefficients D_e for all conditions are listed in Table 1. The magnitude of D_e decreased in the order of D_e^P (ρ_{dry} = 0.9 Mg/m^3) > D_e^P(1.35) > D_e^N(0.9) > D_e^N(1.35) at the same temperature.

The rock capacity factor for HDO equals porosity of medium (0.70 for 0.9 Mg/m^3 or 0.56 for 1.35 Mg/m^3), as HDO is nonsorbing diffusant. The capacity factor can be also calculated from the time-lag method[18,19]. The time-lags determined in this study involve large errors, for example, 0.66 ± 2.05 h (D_e^P at 0.9 Mg/m^3) and 4.7 ± 3.8 h (D_e^P at 1.35 Mg/m^3) at 298 K. Because the capacity factor is proportional to the time-lag, the capacity factors cannot be available to discuss porosity related to the diffusion pathways. The very small time-intercepts and small errors in the diffusive flux result in huge errors in the capacity factor[19].

As the D_e for HDO diffusivity in Kunipia F bentonite has not been reported previously, the D_e for HDO at 298 K is compared with that for tritiated water (HTO) on an Archie's law plot

of D_e vs. porosity (ε) (Fig. 2-5) [19]. Sato (2001)[16] has already reported anisotropic diffusion of HTO in Kunipia F. D_e^P and D_e^N in the present study correspond to D_e axial and D_e perpendicular in the previous report by Sato (2001) [16], respectively. As data concerning D_e for HTO are not available, we calculate D_e from the apparent diffusion coefficient obtained by the in-diffusion method by Sato et al. (1992)[10] and Nakazawa et al. (1999)[6], assuming that the following equation holds:

$$D_e = \varepsilon D_a \tag{2-4}$$

where ε is the porosity of bentonite. In these experiments, the diffusional direction is the same as the direction of the compaction, which is normal to the preferred orientation of montmorillonite, and hence is denoted as D_e^N. Our diffusion coefficients for the two different directions are in agreement with those for HTO. Thus, effective diffusion coefficients for HDO are essentially the same as those for HTO.

The dependence of D_e for HTO and HDO on porosity is described by the modified Archie's law as:

$$\frac{D_e}{D_{water}} = \beta \varepsilon^m \tag{2-5}$$

where D_e is the D_e^P or D_e^N , D_{water} is the diffusivity of HDO in the bulk water (2.3×10^{-9} m^2/s at 298 K)[20] and ε is the porosity. β and m are the parameters for the least-square fitting. When β is equal to 1.0, Eq. (2-5) is the same as the original Archie's law. The porosity is calculated by

$$\varepsilon = 1 - \frac{\rho_{dry}}{\rho_{clay}} \tag{2-6}$$

where ρ_{clay} is the mineral density of montmorillonite (2.88 g/cm^3). The parameters β and m are determined to be $\beta = 0.29 \pm 0.03$, $m = 2.1 \pm 0.2$ for D_e^P and $\beta = 0.47 \pm 0.07$, $m = 4.3 \pm 0.3$ for D_e^N, respectively (errors were $\pm1\sigma$). Generally, the β parameter should be 1.0, assuming that the diffusivity in the pore water is the same as that in the bulk water. A value of β less

than 1.0 suggests that the diffusivity in the pore water in bentonite is less than in the bulk water. The diffusivity of water in pore water may decrease as a result of interaction of water with negatively charged montmorillonite surface, which is known as the viscoelectric effect[21]. Assuming the above considerations, the decrease in the HDO diffusivity in the pore water is calculated to be 30-50% of that in the bulk water in the present study.

To confirm Archie's law at porosity higher than 0.7, the diffusivity of water in Na-montmorillonite gel determined by pulsed-field gradient spin-echo nuclear magnetic resonance (PGSE-NMR) is plotted in Fig. 2-5[22]. The montmorillonite from the Tsukinuno mine in Japan used in the previous study corresponds to Kunipia F used in the present study. As the data reported by Nakashima (2001)[22] have been obtained at higher temperatures than 303.4 K, the diffusivity at 298 K is calculated from the activation energies also obtained in the previous study using the Arrhenius equation, while the porosity is calculated from the water contents using Eq. (10) presented in Nakashima (2003) (ε=1-ϕ_{clay})[23]. The reported diffusivity is isotropic, and is therefore denoted as D^{iso} in Fig. 2-5. The D^{iso} increases gradually until the porosity of 0.93 and then increases sharply. The D^{iso}/D_{water} value is extrapolated to 1.0 at ε = 1.0. Thus, the D^{iso} is in agreement with the original Archie's law when β = 1.0 at porosity of more than 0.93. When the porosity is less than 0.93, β will be extrapolated to about 0.3 at ε = 1.0, as with the results of D_e^P or D_e^N . Thus, the original Archie's law (β = 1.0) could not be applied to bentonite samples whose porosity is less than 0.93. The exponent m will be discussed later.

Arrhenius plots for all the D_e values are shown in Fig. 2-6. Activation energies E_{act} of D_e for each direction and for each dry density are obtained from the following relationship:

$$D_e = D_e^0 \exp\left(-\frac{E_{act}}{RT}\right) \tag{2-7}$$

where D_e^0 is the pre-exponential term [m^2/s], R [J/mol K] is the gas constant, and T [K] is absolute temperature. The data are summarized in Table 1. The magnitude of E_{act} is similar for the different diffusional directions. Thus, the activation energy may be considered to be isotropic. The activation energy at ρ_{dry} = 1.35 Mg/m^3 is slightly higher than that at 0.9 Mg/m^3. Nakazawa et al. (1999)[6] reported E_{act} for HTO as being in the range of 16-20 kJ/mol at dry densities ranging from 1.0 to 2.0 Mg/m^3. Our value of E_{act} (19-25 kJ/mol) is comparable to

those reported by Nakazawa et al. (1999)[6], taking into account the uncertainties (4-7 kJ/mol).

2.3.2 Effects of pore structure on the diffusion mechanism of HDO in bentonite

Anisotropy of the effective diffusion coefficient is due to the preferred orientation of the montmorillonite particles, and is a consequence of the pore structure in the compacted bentonite[16]. The tortuosity of the diffusion pathways is larger when the direction is normal rather than parallel to the preferred orientation (Fig. 2-7a)[24]. This has been demonstrated previously by theoretical diffusion analysis[15]. The exponent *m* obtained by Eq. (2-5) is also related to the pathways in bentonite. The exponent *m* is 1.5-2.5 for the sandstone consisting of spherical particles[19,25], but larger for the samples containing platy materials, because the plates effectively disturb the diffusion (e.g. m = 10)[25]. The degree of disturbance by the montmorillonite may be greater when HDO diffuses normal to the preferred orientation. The exponent *m* is larger for D_e^N (m = 4.3) than for D_e^P (m = 2.1), and therefore, this result is in qualitative agreement with those reported by Sen et al. (1981)[25]. However, the observation that the value of *m* for D^{iso} by NMR changed at a porosity of ca. 0.95 cannot be explained by this consideration. If there is no preferred orientation in the montmorillonite gel, the exponent *m* should be the same over the entire range of the measurement.

On the other hand, the activation energy shows isotropic behavior and its magnitude is slightly larger at the higher dry density. This will be discussed here in regards to the diffusion pathways and pore size in compacted bentonite. First, consider pore size and the diffusion pathway as a function of the dry density of bentonite. Pusch et al. (1990) reported that there are two different pore spaces in compacted bentonite: i.e. interlamellar (or interlayer) and interstitial spaces[26]. The interlamellar pores exist between layers and have a width of ca. 0.9 nm ($d_{(001)}$ = 1.88 nm; three-water layer) as demonstrated by the X-ray diffractometry[5,15]. The width of the interlamellar pore space depends on the submicrometer grain size of the montmorillonite. On the other hand, the interstitial pore space does not necessarily have a regular shape or size. Suzuki et al. (2001) has theoretically expressed the interstitial pore size *L* as a function of the dry density, assuming that the interstitial pores are planar and uniform in size in the medium as follows[15]:

$$L = n\delta\left(\frac{1}{(1+\lambda)^2}\frac{\rho_{clay}}{\rho_{dry}} - 1\right) - \left(d_{(001)} - \delta\right)(n-1) \qquad (2\text{-}8)$$

where n is the number of clay sheets in a stack, λ is the structural parameter, δ is the thickness of a montmorillonite sheet (1 nm), and ρ_{dry} and ρ_{clay} are dry densities of bentonite and montmorillonite crystal (2.88 Mg/m^3), respectively (Fig. 2-7b). The parameter λ, assumed to be 0.05 here, is defined as d/a: the ratio of the distance d between two stacks along the edge-edge interface to the width of a stack along the basal plane a. Basal spacing $d_{(001)}$ of Na-montmorillonite was determined by XRD as 1.88 and 1.56 nm for ρ_{dry} = 0.9 Mg/m^3 [15] and 1.6 Mg/m^3 [5], respectively. Assuming that the number of clay sheets in a stack n was of 5-10[26], the interstitial pore size is calculated to be 6.0-11.1 nm for 0.9 Mg/m^3 and 1.2-1.4 nm for 1.35 Mg/m^3. Thus, the interstitial pore size decreases with increasing dry density. In addition, the fraction of interstitial pores has been evaluated to be 61% for 0.9 Mg/m^3 and 22% for 1.35 Mg/m^3, respectively[15]. These calculations suggest that the interlamellar space may become the main diffusion pathway at 1.35 Mg/m^3, while both the interlamellar and interstitial pore spaces may function as diffusion pathways at 0.9 Mg/m^3.

Diffusion alongside the basal plane of montmorillonite has a greater effect on bulk diffusivity than that alongside the edge surface. Deuterated water may migrate both horizontally and vertically in the case of diffusion normal to the preferred orientation (Fig. 2-7a). The activation energies should be different in the two directions, because interactions are with the basal and the edge surfaces, respectively. As the thickness of the montmorillonite stack is estimated to be 10-20 nm, while its width is at least 10-fold larger than its thickness, the diffusion along horizontal direction is considered the main process even when the deuterated water diffuses normal to the preferred orientation. Although the diffusion pathway is much more tortuous in the direction normal to the preferred orientation than in that parallel to the preferred orientation, the main diffusion process may be similar in both diffusional directions and the activation energy is therefore considered to show the isotropic behavior.

The slightly higher activation energy at the higher dry density can be attributed to a decrease in water mobility near the montmorillonite surface. Molecular dynamics calculations (MDs)[8,27] showed the distribution of a self-diffusion coefficient of water as a function of a distance from the surface. Water mobility within 1-2 nm from the surface is decreased to half of the water diffusivity similar to that in the bulk water around 5 nm from the surface; this phenomenon is referred to as the ‘‘iceberg effect’’ or ‘‘viscoelectric effect’’[8,21]. Using the same simulation at elevated temperatures of 298, 323, 343 and 373 K, the activation energy

near the surface is demonstrated to be 2-7 kJ/mol higher than that in regions further away from the surface (unpublished data). Assuming that the above effect applies to our system, all of the water in the pores of the bentonite may be under the iceberg effect at ρ_{dry} = 1.35 Mg/m^3, whereas only 50-60 vol.% of the pore water may be under the iceberg effect at ρ_{dry} = 0.9 Mg/m^3. Thus, the iceberg effect may increase the activation energy of D_e with increasing dry density. However, because the increase in the activation energy of diffusion near the montmorillonite surface may be small (2-7 kJ/mol by the MDs), the change in the activation energy of D_e would be small, as was the case, and thus may be considered to be insignificant.

2.4 Conclusion

To quantify the effects of temperature on the diffusivity of deuterated water (HDO) in compacted sodium bentonite, through-diffusion experiments were conducted at elevated temperatures ranging from 298 to 333 K. Kunipia F was compacted to a dry density of 0.9 or 1.35 Mg/m^3. The anisotropy of diffusivity was investigated both parallel and normal to the preferred orientation of the montmorillonite. The effective diffusion coefficient D_e of HDO was larger when the diffusional direction was parallel as opposed to normal to the preferred orientation for both dry densities. The magnitude of D_e and the anisotropy for HDO were in good accordance with previously reported results for tritiated water at room temperature. Activation energies of D_e were isotropic and increased with increasing dry density over the range of 19–25 kJ/mol. This relationship was considered to be due to both pore structure development and the high activation energy of water near the montmorillonite surface. In JNC (2000), the extrapolated D_e calculated by using Eq. (2-7) with the activation energy of 15 kJ/mol, which is the activation energy for diffusion of ions in bulk water, was used for safety assessment. Although the obtained activation energy (19-25 kJ/mol) was higher than that used in JNC (2000), the difference of diffusivity is confirmed to be small.

References

1) A. Muurinen, P. Pentilla-Hiltunen and J. Rantanen, “Diffusion mechanism of strontium and cesium in compacted bentonite,” *Mat. Res. Soc. Symp. Proc.*, 84, 803-812 (1987).
2) T. Kozaki, K. Inada, S. Sato, et al., “Diffusion mechanism of chloride ions in sodium montmorillonite,” *J. Contam. Hydrol.*, 47, 159-170 (2001).
3) Japan Nuclear Cycle Development Institute (JNC), *H12: Project to establish the technical*

basis for HLW disposal in Japan, Supporting report 3, Safety assessment of the geological disposal system, JNC Tech. Rep., JNC TN1410 2000-004, (2000).

4) T. Kozaki, H. Sato, A. Fujishima, et al., "Activation energy of cesium in compacted sodium montmorillonite," *J. Nucl. Sci. Technol.*, 33, 522-524 (1996).
5) K. Kozaki, A. Fujishima, S.Sato, et al., "Self-diffusion of sodium ions in compacted sodium montmorillonite," *Nucl. Technol.*, 121, 63-69 (1998).
6) T. Nakazawa, M. Takano, A. Nobuhara, et al., "Activation energies of diffusivity of tritium and electrical conduction in water-saturated compacted sodium montmorillonite," *Radioactive Waste Management and Environmental Remediation-ASME 1999*, (1999).
7) Y. H. Li and S. Gregory, "Diffusion of ions in sea water and in deep-sea sediments," *Geochim. Cosmoshim. Acta*, 38, 703-714 (1974).
8) Y. Ichikawa, K. Kawamura, M. Nakano, et al., "Unified molecular dynamics and homogenization analysis for bentonite behavior: current results and future possibilities," *Eng. Geol.*, 54, 21-32 (1999).
9) R. Pusch, O. Karnland, A. Muurinen, *Transport and microstructural phenomena in bentonite clay with respect to the behavior and influence of Na, Cu, and U*, SKB Technical report TR 89-34, Swedish Nuclear Fuel and Waste Management, Stockholm, (1989).
10) H. Sato, T. Ashida, Y. Kohara, et al., "Effect of dry density on diffusion of some nuclides in compacted sodium bentonite," *J. Nucl. Sci. Technol.*, 29, 873-882 (1992).
11) D. W. Oscarson, "Surface diffusion: is it an important transport mechanism in compacted clays?," *Clays Clay Miner.*, 42, 534-543 (1994).
12) J. W. Choi and D. W. Oscarson, "Diffusive transport through compacted Na- and Ca-bentonite," *J. Contam. Hydrol.*, 22, 189-202 (1996).
13) H. Ishikawa, K. Amemiya, Y. Yusa, et al., "Comparison of fundamental properties of Japanese bentonite as buffer material for waste disposal," *Proc. 9th Int. Clay Conf. Sci. Geol. Mem.*, 87, 107-115 (1990).
14) T. Shibutani, Y. Kohara, C. Oda, et al., *Physico-chemical characteristics of purified Na-smectite and protonation/deprotonation behavior of smectite surface in NaCl media*, JNC Tech. Rep., JNC TN8400 99-066, (1999) (in Japanese).
15) S. Suzuki, A. Fujishima, K. Ueno, et al., "Microstructural modeling of compacted sodium-bentonite and application of unified molecular dynamics/homogenization analysis

for diffusion process," *J. Clay Sci. Soc. Jpn.*, 41(2), 43-57 (2001) (in Japanese).

16) H. Sato, "The effect of pore structural factors on diffusion in compacted sodium bentonite," *Mat. Res. Soc. Symp. Proc.*, 663, 605-615 (2001).

17) J. M. Hollas, *Modern Spectroscopy, 3rd ed.*, Wiley, Chichester, (1996).

18) J. Crank, *The Mathematics of Diffusion, 2nd ed.*, Oxford Univ. Press, Oxford, UK, (1975).

19) T. B. Boving and P. Grathwohl, "Tracer diffusion coefficients in sedimentary rocks: correlation to porosity and hydraulic conductivity," *J. Contam. Hydrol.*, 53, 85-100 (2001).

20) P. T. Callaghan, "Pulsed field gradient nuclear magnetic-resonance as a probe of liquid state molecularorganization," *Aust. J. Phys.*, 37, 359-387 (1984).

21) R. J. Hunter and J. V. Leyendekkers, "Viscoelectric coefficient for water," *J. Chem. Soc. Faraday Trans.*, 1 (A204), 450-455 (1978).

22) Y. Nakashima, "Pulsed field gradient proton NMR study of the self-diffusion of H_2O in montmorillonite gel: effects of temperature and water fraction," *Am. Mineral.*, 86, 132-138 (2001).

23) Y. Nakashima, "Diffusion of H_2O in smectite gels: obstruction effects of bound H_2O layers," *Clays Clay Miner.*, 51, 9-22 (2003).

24) J. Brakel and P. M. Heertjes, "Analysis of diffusion in macroporous media in terms of a porosity, a tortuosity and a constrictivity factor," *Int. J. Heat Mass Transfer*, 17, 1093-1103 (1974).

25) P. N. Sen, C. Scala and M. H. Cohen, "A self-similar model for sedimentary rocks with application to the dielectric constant of fused glass beads," *Geophysics*, 46, 781-795 (1981).

26) R. Pusch, O. Karnland and H. Hökmark, *GMM—a general microstructural model for qualitative and quantitative studies of smectite clays*, SKB Technical report TR 90-43, Swedish Nuclear Fuel and Waste Management, Stockholm, (1990).

27) K. Kawamura and Y. Ichikawa, *Physical properties of clay minerals and water—by means molecular dynamics simulations*, Bull. Earthq. Res. Inst. Univ. Tokyo, 76, 311-320, (2001).

Table 1 Effective diffusion coefficients for HDO with respect to experimental temperature, dry density and diffusion direction

ρ_{dry} [Mg/m^3]	Diffusional direction	D_e [$\times 10^{-10}$ m^2/s]				Activation energy [kJ/mol]
		298 K	313 K	323 K	333 K	
0.9	P	2.8 ± 0.1	3.3 ± 0.0	4.8 ± 0.0	6.1 ± 0.1	19 ± 4
	N	1.6 ± 0.0	1.8 ± 0.0	2.6 ± 0.0	3.7 ± 0.1	21 ± 5
1.35	P	1.7 ± 0.0	2.2 ± 0.0	2.9 ± 0.0	4.6 ± 0.1	23 ± 5
	N	0.84 ± 0.03	0.95 ± 0.01	2.0 ± 0.0	2.2 ± 0.1	25 ± 7

Errors are from the least-squares fitting.

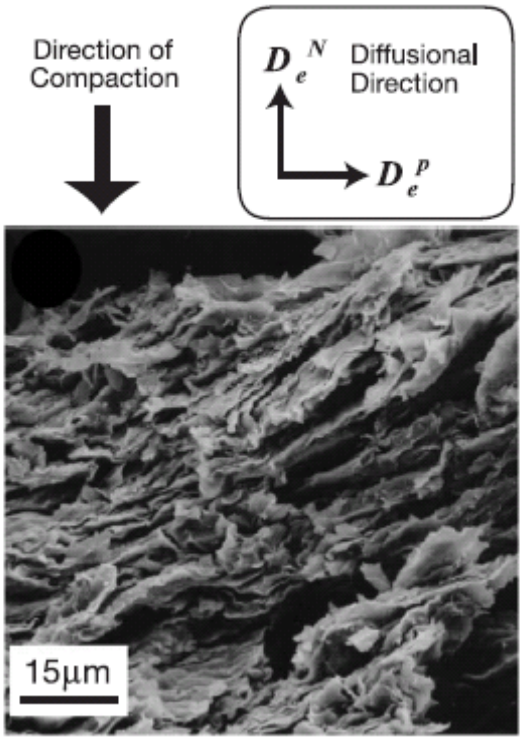

Fig. 2-1 Scanning electron micrograph (SEM) photograph of a cross section of compacted bentonite (saturated with solution and then freeze-dried). The preferred orientation of smectite flakes is normal to the direction of compaction.

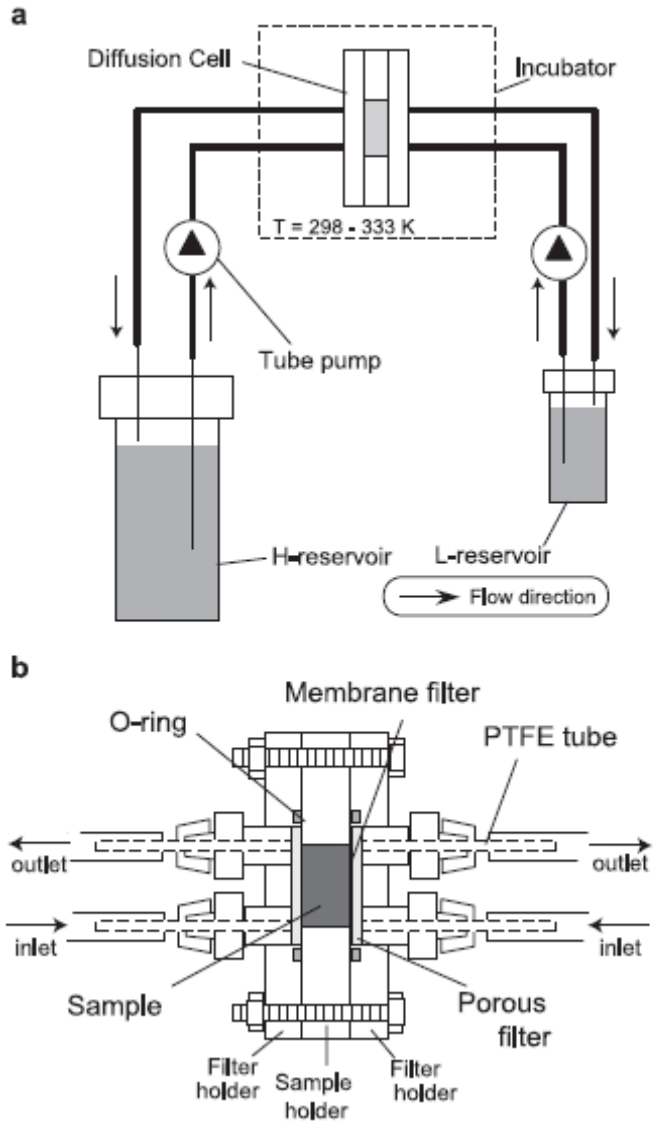

Fig. 2-2 (a) Schematic illustration of the flow-through diffusion system. The diffusion cell is placed in an incubator to maintain a constant temperature of 298, 313, 323 or 333 K, respectively. H- and L-reservoirs are high- and low-concentration reservoirs, respectively. (b) A cross section of the diffusion cell.

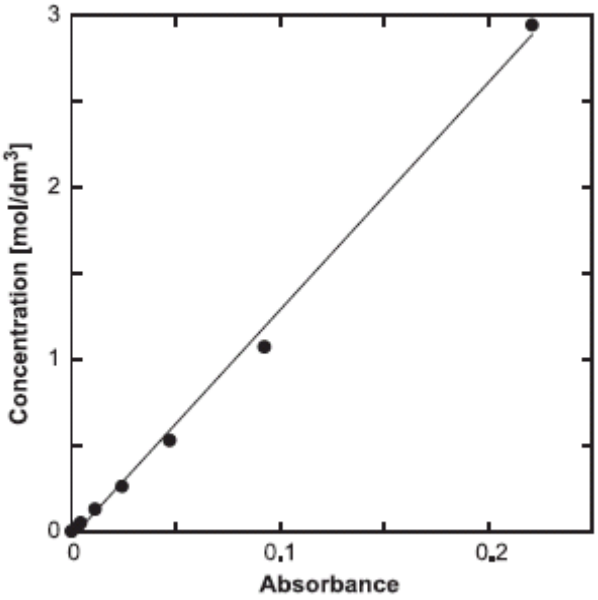

Fig. 2-3 The concentration of deuterated water plotted as a function of the height of the absorption peak at 2508 cm^{-1}.

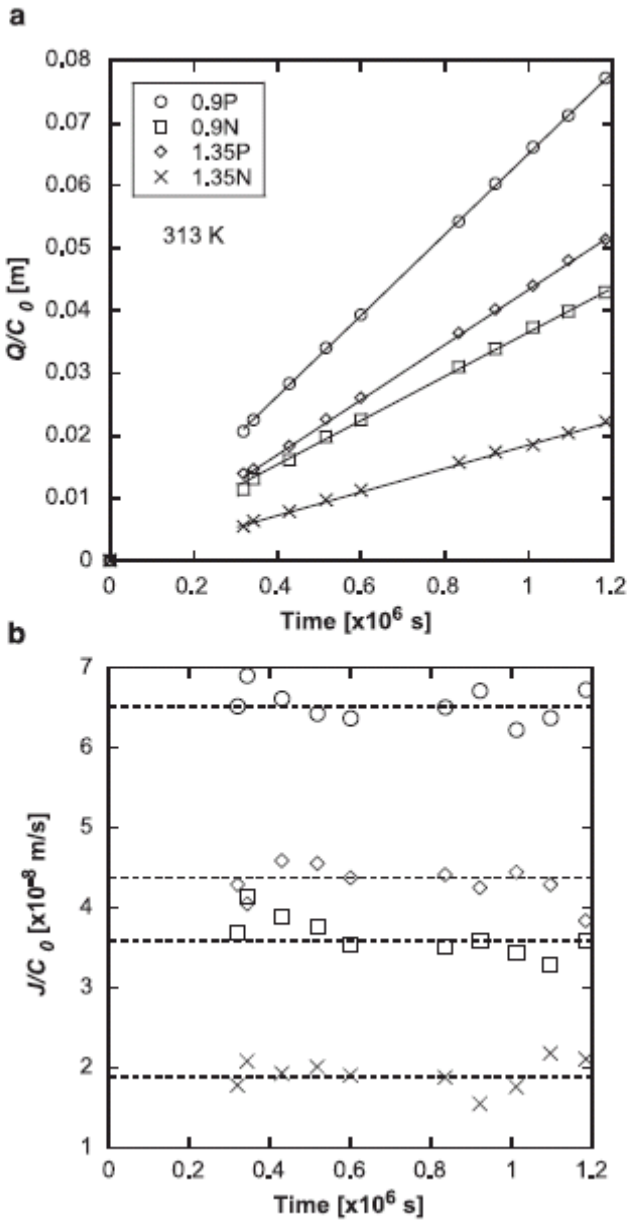

Fig. 2-4 (a) Typical break-through curves for deuterated water at a temperature of 313 K. ‘‘0.9’’ and ‘‘1.35’’ indicate the dry density, while ‘‘P’’ and ‘‘N’’ represent the diffusional direction. (b) The diffusive flux (Q/t) calculated at each time point.

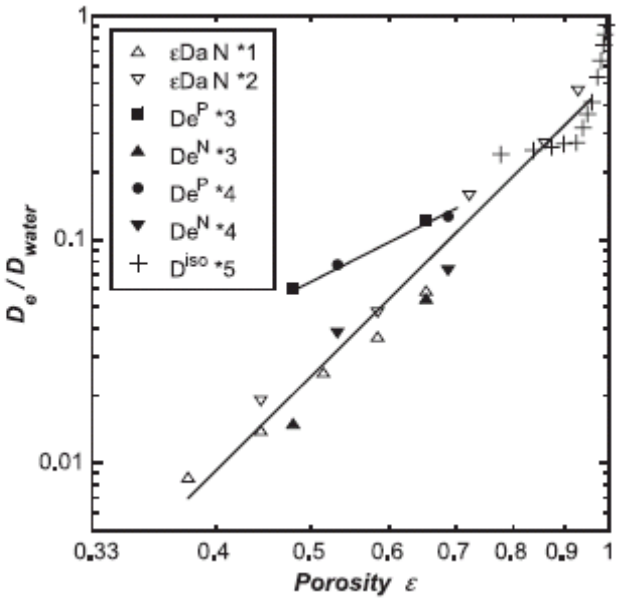

Fig. 2-5 Archie's plot of D_e of deuterated and tritiated water in compacted bentonite (Kunipia F) normalized by diffusivity of water molecule in bulk water (2.2×10^{-9} m^2/s) at room temperature. Porosity ε was calculated from the dry density (ρ_{dry}) and mineral density (ρ_{clay}) of Na-montmorillonite (2.88 g/cm^3). Solid lines were fitted by the least-square fitting of Eq. (2-5). (*1) Nakazawa et al. (1999)[6]; (*2) Sato et al. (1992)[10]; (*3) Sato (2001)[16]; (*4) this study; (*5) Nakashima (2001)[22].

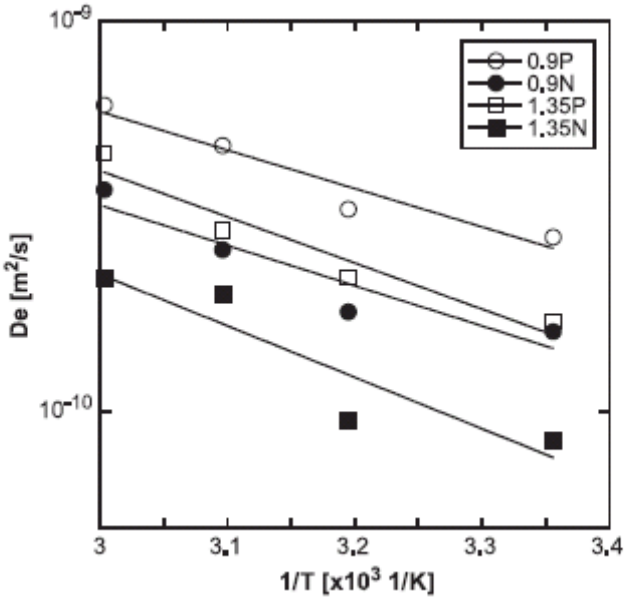

Fig. 2-6 Arrhenius plot of effective diffusion of deuterated water

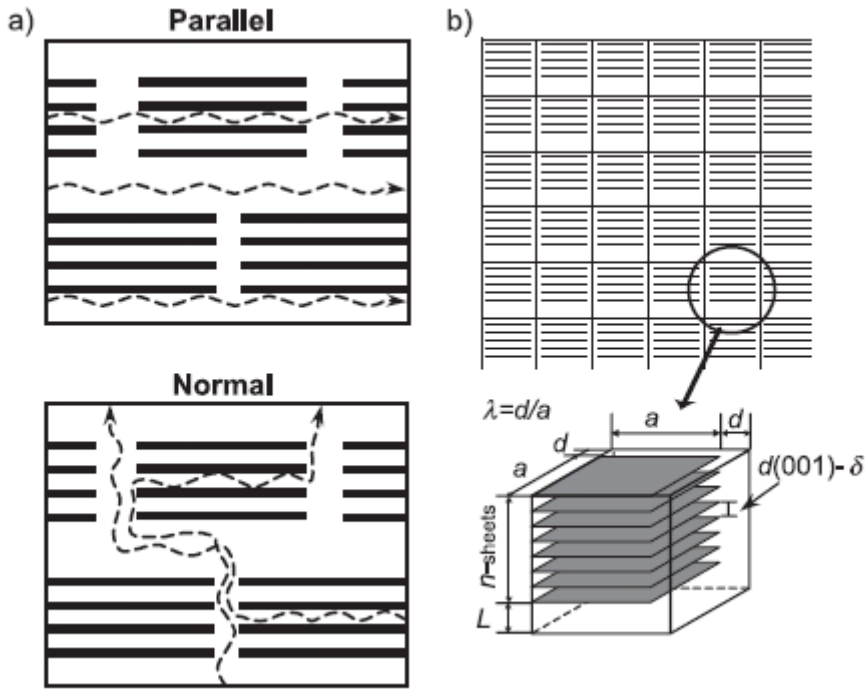

Fig. 2-7 (a) Illustrations of the microstructure of bentonite and diffusional pathways. (b) A microstructural model for compacted bentonite[15].

Chapter 3
Effect of sodium nitrate on diffusion of Cl^- and I^- in compacted bentonite

3.1 Introduction

The migration behavior of radionuclides has been widely investigated as part of the safety assessment of high-level radioactive waste (HLW)[2]. However, some phenomena specific to TRU waste, which influence migration behavior, must be taken into consideration for the safety assessment of TRU waste disposal. These include:

(1) The liquid concentrate from which some TRU waste is derived contains a large concentration of sodium nitrate (the nitrate concentration in porewater is 1.87×10^4 mol/m^3 when averaged over the waste in the entire disposal facility[1]).

(2) In TRU waste streams, the hulls and endpieces contain chlorine-36. Spent iodine filters contain high concentrations of iodine-129. As these radionuclides are not carried through to the vitrified reprocessing waste, they are not included in the safety assessment of HLW disposal.

(3) Hyperalkaline conditions in porewater within the engineered barriers (pH around 12.5 or so) are expected to persist for extensive periods, due to the leaching of the large quantities of cementitious materials used as conditioning and structural materials and as packaging.

As a site for the TRU repository has not yet been selected, the distribution of different types of waste within such a facility cannot be specified. Thus, although the wastes with highest concentrations of ^{36}Cl and ^{129}I do not contain nitrate, it is assumed that such nitrate will be dispersed throughout the entire engineered barrier system (EBS). Similarly different types of concrete and cement may be used for different purposes, but hyperalkaline conditions will occur throughout the EBS.

Diffusivities of Cl^- and I^- in compacted bentonite have been reported to increase with increasing NaCl concentration in the porewater (studies by Muurinen et al. (1989)[3] and Suzuki (2002)[4]). The increase in diffusivities of I^- has been also reported by Eriksen et al. (1996)[5]. Thus, increasing salinity of porewater is generally seen to increase the diffusivity of anions in compacted bentonite. Therefore, the concentration of sodium nitrate in porewater may be expected to be important in a safety assessment of TRU waste disposal. However, there is little available information on the effects of sodium nitrate on the diffusion of anions.

In this study, the effective diffusion coefficient of Cl^- and I^- in compacted bentonite will be determined as a function of $NaNO_3$ concentration, under hyper alkaline conditions, using a through-diffusion method.

3.2 Experimental

3.2.1 Materials

The bentonite used in the present study was Kunigel V1® (Kunimine Industries Co. Ltd.). Kunigel V1 consists of 46-49 wt% of smectite, 37-38 wt% of chalcedony and few wt% of minor minerals (plagioclase, calcite, dolomite, analcime and pyrite)[6]. The medium for the diffusion experiments was prepared by mixing Kunigel V1 with 0, 30 or 50 wt% of silica sand, with subsequent compaction to obtain a dry density of 1.6 Mg/m^3.

The tracer solutions were prepared with 5.0×10^{-5} mol/dm^3 Cl^- (0.94 MBq/dm^3 $^{36}Cl^-$) and 5.0×10^{-3} mol/dm^3 I^-; by dilution of $Na^{36}Cl$ solution (Amersham plc) or NaI solution prepared from non-radioactive NaI powder (Wako Pure Chemical Industries Co. Ltd.), respectively. The concentrations of $NaNO_3$ solutions were varied between 0.01, 0.5 and 5 mol/dm^3, while, additionally, 0.1 and 1 mol/dm^3 concentrations were used only for experiments of I^- with silica sand content of 30 wt%. The pH of the solutions was initially adjusted to 12.5 with NaOH solution.

In addition to these experiments, diffusion measurements were carried out with Kunipia F® (Kunimine Industries Co. Ltd.), which was a purified material consisting of over 95 wt% of smectite[6], were carried out at a dry density of 0.9 Mg/m^3 with 5 mol/dm^3 $NaNO_3$ concentration. The dry density of 0.9 Mg/m^3 for Kunipia F corresponds to the partial dry density of the smectite component of Kunigel V1 with silica sand content of 30 wt%, when compacted to a dry density of 1.6 Mg/m^3. The partial dry density was calculated from the following equation[7,8]:

$$\rho_{dm} = \frac{(1-f_s) f_m \rho_d}{1 - \left\{ \frac{(1-f_s)(1-f_m)}{\rho_{im}} + \frac{f_s}{\rho_s} \right\} \rho_d} \qquad (3\text{-}1)$$

Here ρ_{dm} is the partial dry density of smectite component, ρ_d is the dry density of Kunigel V1, ρ_{im} is the density of other minerals, ρ_s is the density of silica sand, f_s is the silica sand content

and f_m is the smectite content in Kunigel V1. In the calculations of ρ_{dm}, both ρ_{im} and ρ_s were assumed to be 2.7 Mg/m^3.

Figure 3-1 shows the through-diffusion cell. The acrylic resin cell consists of two solution reservoirs (50 cm^3 volume each), a sample holder and filters. One of the reservoirs contains tracer (designated as the high-concentration reservoir) and the other is initially tracer-free (designated as the low-concentration reservoir). The sample holder, also made of acrylic resin, contains a cylindrical sample compartment (20 mm in diameter and 10 mm in thickness). A membrane filter (about 0.1 mm in thickness, pore size 0.22 μm) is placed at each side of the bentonite sample, to avoid loss of material from the bentonite gel during the experiment. The membrane filter is supported by a porous plastic filter (2 mm in thickness and several hundreds of micrometer in pore size), which restricts the swelling pressure generated as the sample saturates and thus maintains density during the experiment.

3.2.2 Procedures

The bentonite was dried at 110^{o}C for more than 24 hours and compacted into the sample holders. To saturate the bentonite with $NaNO_3$ solution, the compacted bentonite was initially contacted with deionized water for more than two weeks under low pressure and then with $NaNO_3$ solutions for more than 5 weeks, by pouring appropriate solutions into both solution reservoirs. After saturation, the diffusion experiments were started by adding the tracer solution to the high-concentration reservoir. The tracer concentrations in the two reservoirs were periodically measured by taking a 0.5 ml (for $^{36}Cl^-$) or 0.4 - 0.1 ml (for I^-) aliquot for analysis. A 2π-gasflow counter (Aloka Co. Ltd., LBC-472-Q), was used to measure ^{36}Cl, after soaking the sampled solution onto filter paper. The iodine concentration was measured by ICP-AES (Shimadzu Corporation, ICPS-7500). The experiments using Cl^- were performed in a N_2 glove box (O_2 and CO_2 less than 1ppm, temperature 22.5 ± 2.5 ^{o}C) after compaction of bentonite. The experiments with I^- were performed under aerobic condition at 25.0 ± 1.0 ^{o}C.

After the breakthrough curve was obtained, the nuclide distribution in the compacted bentonite was determined. The bentonite sample was sliced into thin sections of 1 mm in thickness. To extract the tracers, each section was immersed into 4 ml of 1 mol/dm^3 NaCl (for the extraction of $^{36}Cl^-$) or 4 ml of 1 mol/dm^3 KCl (for I^-) for 7 to 14 days. A 0.5 ml aliquot of supernatant was taken from the solution without centrifuging, and radioactivity was measured by the 2π-gasflow counter for ^{36}Cl. The iodine concentration was measured by an ICP-AES

by taking a 1 ml sample of the supernatant after centrifugation. Differences in the experimental protocols were due to the inability to centrifuge samples in the radiation-controlled glove box.

3.2.3 Analytical method

The diffusive flux (J) in one dimension can be described with the effective diffusivity (D_e) using Fick's first law as the following equation[9]:

$$J = -D_e \frac{\partial C_p}{\partial x} \tag{3-2}$$

Here J is the diffusive flux in the direction of x (mol/m^2/s), D_e is the effective diffusion coefficient for diffusant (m^2/s) and C_p is the concentration of diffusant in the porewater of compacted bentonite (mol/dm^3). The D_e for each anion is determined from the break-through curves for steady state diffusion as indicated by the following equation:

$$D_e = -J \frac{L}{\Delta C_p} \tag{3-3}$$

Here L is the thickness of the bentonite sample (m) and ΔC_p is the concentration difference (mol/dm^3) in porewater between the two sides of the bentonite sample. The concentration of diffusant at each side of the bentonite sample is not simply assumed to be equal to the concentrations measured in the reservoirs, as the concentration drop through the filters could be significant. Therefore, ΔC_p is calculated considering the concentration gradient across the filter, using the following equation[4]:

$$\Delta C_p = C_L - C_H + 2J \frac{L_f}{D_e^f} \tag{3-4}$$

Here D_e^f is the effective diffusion coefficient of the filter (m^2/s), L_f is the filter thickness (m), C_H is the concentration of the high-concentration reservoir (mol/dm^3), and C_L is the concentration of the low-concentration reservoir (mol/dm^3). The average value of measured

tracer concentration in the high-concentration reservoir is used as the C_H value. The C_L is assumed to be 0 in the calculation of ΔC_p. The J is calculated by linear least-squares fitting to the break-through curves, when a steady state had been achieved. The D_e^f is determined by a diffusion experiment carried out without bentonite, using only the membrane-plastic filter assembly as the diffusive medium.

The diffusive flux can be also described using the apparent diffusion coefficient (D_a; m^2/s) as the following equation:

$$J = -D_a \frac{\partial C_b}{\partial x} \tag{3-5}$$

Here C_b is the concentration of diffusant per unit volume of compacted bentonite including porewater (mol/dm^3). The D_a is determined from the concentration gradient in compacted bentonite and the measured diffusive flux J at steady state, based on the following equation:

$$D_a = -J \frac{L}{\Delta C_b} \tag{3-6}$$

Here $\Delta C_b/L$ is the concentration gradient of diffusant in compacted bentonite ($mol/dm^3/m$), calculated by linear least-square fitting to the concentration profiles measured in bentonite samples.

As the C_b consists of the concentration of diffusant in porewater and the amount of diffusant sorbing on compacted bentonite per unit volume, the C_b is generally expressed as $C_b = (\varepsilon + \rho K_d)C_p$. Therefore, the relationship between D_e and D_a is expressed as the following equation[10]:

$$D_e = (\varepsilon + \rho K_d) D_a = \alpha D_a \tag{3-7}$$

Here ε is the porosity of compacted bentonite (dimensionless), ρ is the dry density of compacted bentonite (Mg/m^3) and K_d is the distribution coefficient of diffusant on compacted bentonite (m^3/Mg). The term ($\varepsilon + \rho K_d$) is defined as a capacity factor (α). The α was determined from the obtained D_e and D_a values based on the Eq.(3-7).

Reported errors contain propagation of measurement and other analytical uncertainties for individual samples.

3.3 Results

Break-through curves for Kunigel V1 with silica sand content of 30 wt% are shown in Fig. 3-2 and 3-3. The concentrations of Cl^- and I^- increase linearly as a function of time after 1-3x10^6 seconds, indicating that diffusion has reached a steady state. Steady state diffusion is confirmed by the linear concentration profiles measured directly in compacted bentonite (Fig. 3-4 and 3-5). The D_e, D_a and α values measured for Cl^- and I^- are listed in Tables 1 and 2. The D_e^f values used for the correction for the gradient over the filter are 3.0±0.1x10^{-10}, 2.6±0.3x10^{-9} and 7.3±0.5x10^{-9} m^2/s at 0.01, 0.5 and 5 mol/dm^3 $NaNO_3$ concentration for Cl^- and 3.9±1.0x10^{-10} m^2/s for I^-. The pH of the solutions decreased to about 12.0 by the end of the experiments with Cl^-, while decreases in pH to about 10.5 were found for some experiments with I^-, possibly due to the dissolution of CO_2 from the atmosphere.

Figure 3-6 shows the D_e values for Cl^- and I^- in Kunigel V1 with silica sand content of 30 wt%, plotted as a function of $NaNO_3$ concentration. The D_e values for each anion increase greatly with increase in $NaNO_3$ concentration from 0.01 to 0.5 mol/dm^3; thereafter the increase is more gradual.

3.4 Discussion

The measured D_e values for Cl^- and I^- increase with increasing $NaNO_3$ concentration, as shown in Fig. 3-6. Increase in the D_e values for anions has been reported in similar experiments using NaCl solution by Muurinen et al. (1989)[3] for MX-80 bentonite and Suzuki (2002)[4] for pure montmorillonite samples. The increase in the D_e values has been also reported by Eriksen et al. (1996)[5] for MX-80 bentonite. In compacted bentonite, anions are considered to be excluded from some pores by electric repulsion of negatively charged smectite surfaces. As such repulsion will decrease with increasing salinity of porewater, the pore space in which anions are free to diffuse is expected to increase with increasing salinity, resulting in the increases in the reported D_e values. The results presented here are also compatible with the increase in effective porosity for Cl^- and I^-, resulting from the concentrations of $NaNO_3$.

The effective porosity for non-sorbing diffusant can be estimated from the capacity factor,

α[10]. The α is generally expressed as ($\alpha = \varepsilon + \rho K_d$), which is originated from the relation of $C_b = (\varepsilon + \rho K_d)C_p$. Assuming that the K_d on the compacted bentonite is 0, α is identical to the total porosity ε. When the porosity to which Cl^- and I^- are accessible in porewater is decreased, the α becomes lower than ε. This α is equivalent to the effective porosity for diffusion of Cl^- and I^-. Figure 3-7 shows the α values derived for Kunigel V1 with silica sand content of 30 wt%, plotted as a function of $NaNO_3$ concentration. The α values for Cl^- and I^- are determined to be 0.043 and 0.041 respectively at 0.01mol/dm^3 $NaNO_3$ concentration, and then increase with increasing $NaNO_3$ concentration. At 5 mol/dm^3 $NaNO_3$ concentration, α of 0.20 for Cl^- and 0.24 for I^- are obtained. The α values for Cl^- and I^- are, thus, lower than the measured porosity ε (0.40±0.03). These low α values indicate that the effective porosity for diffusion of Cl^- and I^- is decreased, due to the anion exclusion from charged smectite surfaces. The increase in α is thus indicative of the increase in the effective porosity resulting from increasing $NaNO_3$ concentration. Similar tendencies are found for Kunigel V1 with sand contents of 0 and 50 wt%. Thus, a consistent decrease in anion exclusion can be seen in the present study, resulting from the increase in ionic strength caused by the $NaNO_3$ solution.

Figure 3-8 shows the logarithm of D_e values obtained in the present study for Cl^- and I^-, normalized by their diffusivities in bulk water (D_0), plotted as a function of the logarithm of measured α values. The D_0 values used in the calculation were 2.0×10^{-9} m^2/s for both Cl^- and I^- [11]. The D_e/D_0 values are found to increase in direct proportion to the α value in this log-log diagram. The relationship between the D_e/D_0 and α values can thus be expressed by the following equation:

$$\frac{D_e}{D_0} = \beta \alpha^m \qquad (3\text{-}8)$$

Here the β and the m are the parameters for the least-squares linear fit to the log-log transformed data. The least-squares fitting lines are also shown in Fig. 3-8. The parameters β and m are determined to be $\beta = 10^{-1.2 \pm 0.2}$, $m = 1.0 \pm 0.2$ for Kunigel V1 with no silica sand, $\beta = 10^{-0.8 \pm 0.2}$, $m = 1.2 \pm 0.2$ for 30 wt% sand and $\beta = 10^{-0.7 \pm 0.4}$, $m = 1.1 \pm 0.4$ for 50 wt%.

Suzuki et al. (2004)[12] has compiled D_e values for HTO and HDO, and found a similar relationship between log D_e values and the log ε of compacted bentonite. Nishiyama et al. (1990)[13] and Boving and Grathwohl (2001)[14] have reported similar relationships for I^- in a

variety of different rocks. Such relationships can generally be considered as an analogue to Archie's law, which describes the electrical conductivity of porous rocks as a function of fluid resistivity and porosity. The total porosity, ε, is equal to the effective porosity for the diffusion of HTO and HDO[4], since there is no exclusion from smectite surfaces for the neutral species. The anion exclusion effect is generally not considered for such diffusion of I^- in rocks, as the pore sizes involved are usually sufficiently large compared to the electrical field formed near the surface of minerals – and surface charges are lower than those of smectite – so that the effect is insignificant. However, the effective porosity for Cl^- and I^- in compacted bentonite is lower than ε due to the anion exclusion as shown in Fig. 3-7. In the present study, the D_e/D_0 values for anionic species are thus found to be proportional to the α values on the log-log diagram.

Figure 3-9 shows other relevant reported D_e/D_0 values for Cl^- and I^- plotted as a function of α values, together with those values obtained in the present study. By Muurinen et al. (1989)[3], α values were determined from both the concentration profiles in compacted bentonite as well as from the time-lag of breakthrough curve. In Fig. 3-9, the α values determined by time-lag method are plotted, because nonlinear concentration profiles were obtained in Murrinen et al. (1989)[3]. The D_e/D_0 values for Kunipia F obtained in the present study are plotted as "purified bentonite" data.

The reported D_e/D_0 values for each compacted bentonite are also correlative with the α values. The parameters β and m are determined to be $\beta = 10^{-0.6 \pm 0.1}$, $m = 1.5 \pm 0.1$ for MX-80 at a dry density of 1.2 Mg/m^3, $\beta = 10^{-1.0 \pm 0.1}$, $m = 1.3 \pm 0.1$ for MX-80 at a 1.8 Mg/m^3 and $\beta = 10^{-1.3 \pm 0.2}$, $m = 1.0 \pm 0.2$ for purified bentonite at a 0.9 Mg/m^3.

The least-square fitting lines for MX-80 at 1.8 Mg/m^3 and Kunipia F at 0.9 Mg/m^3 are lower than those for MX-80 at 1.2 Mg/m^3 and Kunigel V1 at 1.6 Mg/m^3 with silica sand contents of 0, 30 and 50 wt%. The best fit lines for Kunigel V1 at 1.6 Mg/m^3 become higher with the increasing silica sand content, as shown in Fig. 3-8. The diffusion pathway for anionic species in compacted bentonite for which lower fitting lines are obtained can be considered to be more tortuous, as lower D_e values are obtained even if the effective porosity for diffusion is determined to be equivalent. These results suggest that the tortuosity of the diffusion pathway for anionic species is affected by the kind of bentonite, the dry density and the silica sand content. The partial dry densities of the smectite component for MX-80 at 1.8 and 1.2 Mg/m^3 are about 1.6 and 1.0 Mg/m^3, respectively. The smectite partial densities for Kunigel V1 at 1.6

Mg/m^3 with silica sand contents of 0, 30 and 50wt% are about 1.1, 0.9 and 0.7 Mg/m^3, respectively. The fit lines thus tend to become lower with increasing smectite partial density. This might be expected if the pore structure becomes more complicated, and hence the tortuosity increases, with increasing smectite partial density.

The tortuosity of diffusion pathway appears dependent on the smectite partial density for compacted crude bentonite. However, this has to be related to the fact that the best least-squares fit for purified bentonite at 0.9 Mg/m^3 is lower than that for Kunigel V1 with 30 wt% sand, although the two compacted bentonites have the same smectite partial density. In purified bentonite, the orientation of smectite particles perpendicular to the direction of compaction has been reported to increase the tortuosity of diffusion pathway for HDO in this direction[12]. The lower fitting line for purified bentonite at 0.9 Mg/m^3 is thus considered to be due to an effect of the orientation of smectite particles.

The exponent m values lie in the range of 1.0 to 1.5. These m values are lower than those reported for HDO and HTO; 4.3 for compacted purified bentonite normal to the compaction orientation and 2.1 parallel to it[12]. Such m values higher than 1.0 indicate that the diffusion pathway become less tortuous with increasing effective porosity. Differences in the m values may be related to the geometry of the diffusion pathway in compacted bentonite. The effective porosity for HDO and HTO, assumed equal to the total porosity ε, is dependent on the dry density of compacted smectite. As the pore structure becomes more complicated with increasing dry density, the diffusion pathway becomes more tortuous. The higher m values for HDO and HTO are, therefore, a result of the large influence of changes in the pore structure of the compacted bentonite. In contrast, the increase in effective porosity for anionic species arises only from the decrease in anion exclusion effect, since the basic pore structure is not expected to change with the increasing salinity of porewater. For this reason, the lower m values of 1.0-1.5 obtained reflect the fact that the decrease in tortuousity of diffusion pathway with decreasing effective porosity caused by the decrease in anion exclusion is less significant.

The β value is determined to be in the range of 0.05-0.25 for all the compacted bentonites. The β would be expected to be 1 if the diffusivity of the tracer in the porewater is the same as that in the bulk water. In practice, the β has been treated as 1 in discussing the diffusion behavior in rocks[14-16], as the porewater of rocks can be regarded as the bulk water due to the large pore sizes. A β value less than 1 suggests that anion diffusivity in the porewater of

compacted bentonite is around 5-25% of that in the bulk water, possibly due to the "structuring" of dipolar water caused by the electrical field resulting from the charged smectite surfaces.

3.5 Conclusions

The effective diffusion coefficients (D_e) for Cl^- and I^- in compacted bentonite were obtained for 0.01 - 5 mol/dm^3 $NaNO_3$ solutions under hyperalkaline conditions. The obtained D_e values for Cl^- and I^- increased from around 10^{-12} to 10^{-11} m^2/s with increasing $NaNO_3$ concentration. The capacity factor (α) values, which are equal to the effective porosity for diffusion of anions, also increased with increasing $NaNO_3$ concentration, suggesting that the increases in the D_e values were caused by a decrease in anion exclusion. The D_e/D_0 values for Cl^- and I^-, which are the normalized D_e values by their diffusivities in bulk water (D_0), were found to increase in proportion to the α values on a log-log plot, although similar relationships between the log D_e and log ε was found for neutral species in compacted bentonite and for anionic species in porous rocks. This relationship between the log D_e/D_0 and the log α is considered to arise from the lower effective porosity than ε in compacted bentonite due to anion exclusion.

References

1) Japan Nuclear Cycle Development Institute and The Federation of Electric Power Companies, *Progress report on disposal concept for TRU waste in Japan*, JNC TY1400 2000-002, (2000).
2) Japan Nuclear Cycle Development Institute (JNC), *H12: Project to establish the technical basis for HLW disposal in Japan, Supporting report 3, Safety assessment of the geological system*, JNC TN1410 2000-004, (2000)
3) A. Muurinen, P. Penttila-Hiltunen and K. Uusheimo, "Diffusion of chloride and uranium in compacted sodium bentonite," *Mat. Res. Soc. Symp. Proc.*, 127, 743-748 (1989).
4) S. Suzuki, *Study on diffusion behavior of nuclide in buffer material*, JNC TN8400 2002-006, Japan Nuclear Cycle Development Institute (JNC), (2002), (in Japanese).
5) T. E. Eriksen and M. Jansson, *Diffusion of I^-, Cs^+ and Sr^{2+} in compacted bentonite – Anion exclusion and surface diffusion*, SKB Tech. rep. TR 96-16, Swedish Nuclear Fuel and Waste Management Co., (1996).

6) M. Ito, M. Okamoto, M. Shibata, et al., *Mineral composition analysis of bentonite*, PNC TN8430 93-003, Japan Nuclear Cycle Development Institute (JNC), (1993), (in Japanese).
7) Y. Kuroda, K. Idemitsu, H. Furuya, et al., "Diffusion of technetium in compacted bentonites in the reducing condition with corrosion products of iron," *Mat. Res. Soc. Symp. Proc.*, 465, 909-916 (1997).
8) H. Sato and S. Miyamoto, *A study on diffusion and migration of lead in compacted bentonite – the effects of dry density, silica sand content and temperature on diffusion and migration of Pb-210 in sodium bentonite-*, JNC TN8400 2001-018, Japan Nuclear Cycle Development Institute (JNC), (2001).
9) J. Crank, *The mathematics of diffusion, 2nd Ed.*, Pergamon Press, Oxford, 44, (1975).
10) K. Skagius and I. Neretnieks, "Porosities and diffusivities of some nonsorbing species in crystalline rocks," *Water Resour. Res.*, 22(3), 389-398 (1986).
11) Y. Marcus, *Ion Properties*, Marcel Dekker, Inc., New York, (1997).
12) S. Suzuki, H. Sato, T. Ishidera, et al., "Study on anisotropy of effective diffusion coefficient and activation energy for deuterated water in compacted sodium bentonite," *J. Contam. Hydrol.*, 68, 23-37 (2004).
13) K. Nishiyama, S. Nakashima, R. Tada, et al., "Diffusion of an ion in rock pore water and its relation to pore characteristics," *Mining Geology*, 40(5), 323-336 (1990), (in Japanese).
14) T. B. Boving and P. Grathwohl, "Tracer diffusion coefficients in sedimentary rocks: correlation to porosity and hydraulic conductivity," *J. Contam. Hydrol.*, 53, 85-100 (2001).
15) A. Polak, R. Nativ and R. Wallach, "Matrix diffusion in northern Negev fractured chalk and its correlation to porosity," *J. Hydrol.*, 268, 203-213 (2002).
16) R. A. Berner, *Early Diagenesis*, Princeton University Press, New Jersey, (1980).

Table 1 Effective diffusion coefficients (D_e), apparent diffusion coefficient (D_a) and capacity factor α for Cl^-

Bentonite	Dry density (Mg/m^3)	Silica sand (wt%)	$NaNO_3$ (mol/dm^3)	D_e ($10^{-11}m^2/s$)	D_a ($10^{-10}m^2/s$)	α
Kunigel V1	1.6	0	0.01	0.41 ± 0.01	1.7 ± 0.1	0.024 ± 0.002
	1.6	0	0.5	1.8 ± 0.2	1.9 ± 0.2	0.095 ± 0.015
	1.6	0	5	2.2 ± 0.4	1.0 ± 0.2	0.22 ± 0.06
	1.6	30	0.01	0.77 ± 0.03	1.8 ± 0.3	0.043 ± 0.007
	1.6	30	0.5	3.2 ± 0.3	2.4 ± 0.2	0.13 ± 0.02
	1.6	30	5	3.2 ± 0.3	1.6 ± 0.2	0.20 ± 0.03
	1.6	50	0.01	1.4 ± 0.1	2.7 ± 0.2	0.052 ± 0.005
	1.6	50	0.5	5.2 ± 0.1	4.0 ± 0.3	0.13 ± 0.01
	1.6	50	5	4.0 ± 0.3	2.4 ± 0.2	0.17 ± 0.02
Kunipia F	0.9	0	5	3.2 ± 0.2	1.3 ± 0.1	0.25 ± 0.02

Table 2 Effective diffusion coefficients (D_e), apparent diffusion coefficient (D_a) and capacity factor α for I^-

Bentonite	Dry density (Mg/m^3)	Silica sand (wt%)	$NaNO_3$ (mol/dm^3)	D_e ($10^{-11}m^2/s$)	D_a ($10^{-10}m^2/s$)	α
Kunigel V1	1.6	0	0.01	0.35 ± 0.01	1.3 ± 0.2	0.027 ± 0.004
	1.6	0	0.5	2.0 ± 0.1	1.8 ± 0.2	0.11 ± 0.01
	1.6	0	5	3.8 ± 0.6	1.7 ± 0.1	0.22 ± 0.04
	1.6	30	0.01	0.65 ± 0.03	1.6 ± 0.1	0.041 ± 0.003
	1.6	30	0.1	2.0 ± 0.2	2.5 ± 0.4	0.080 ± 0.015
	1.6	30	0.5	4.1 ± 0.4	2.9 ± 0.2	0.14 ± 0.02
	1.6	30	1	4.7 ± 1.1	2.5 ± 0.3	0.19 ± 0.05
	1.6	30	5	6.6 ± 2.1	2.7 ± 0.4	0.24 ± 0.09
	1.6	50	0.01	2.0 ± 0.2	1.8 ± 0.3	0.11 ± 0.02
	1.6	50	0.5	5.7 ± 1.2	3.8 ± 0.3	0.15 ± 0.03
	1.6	50	5	6.3 ± 1.6		
Kunipia F	0.9	0	5	5.3 ± 0.9	1.2 ± 0.1	0.44 ± 0.08

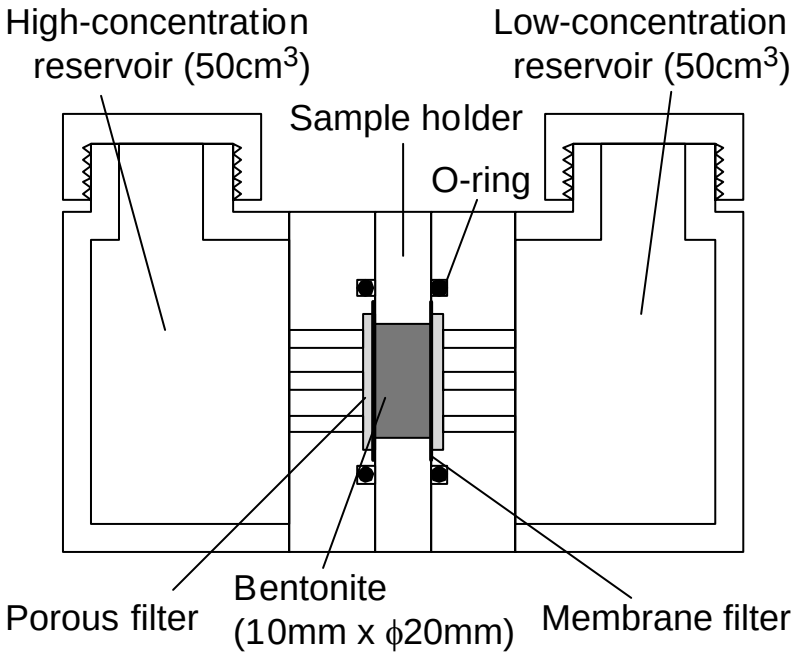

Fig. 3-1 Schematic illustration of the through-diffusion cell

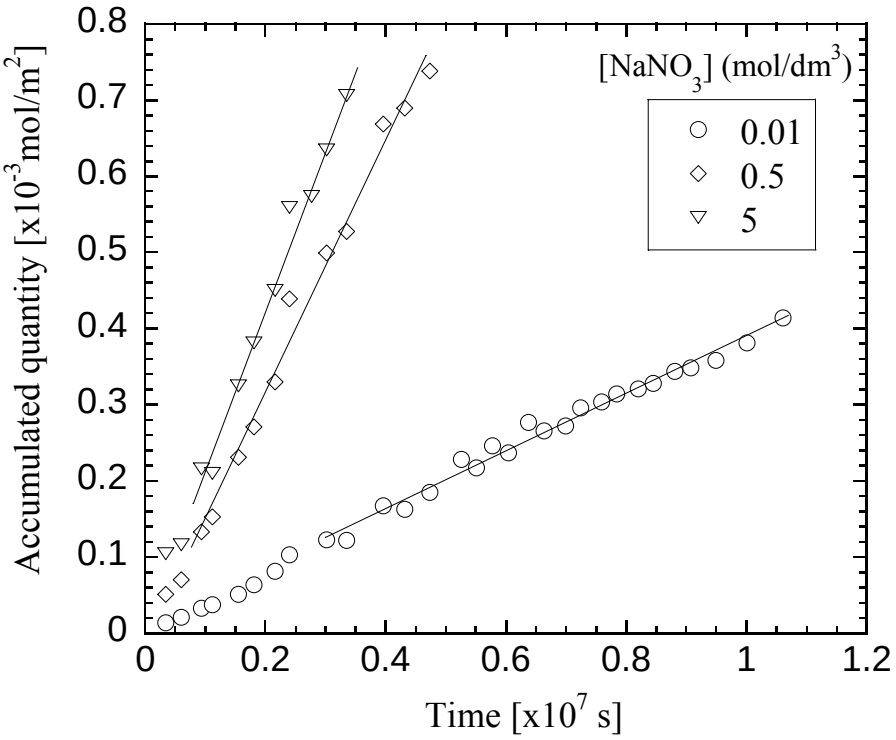

Fig. 3-2 Break-through curves of Cl^- for Kunigel V1 with 30 wt% silica sand

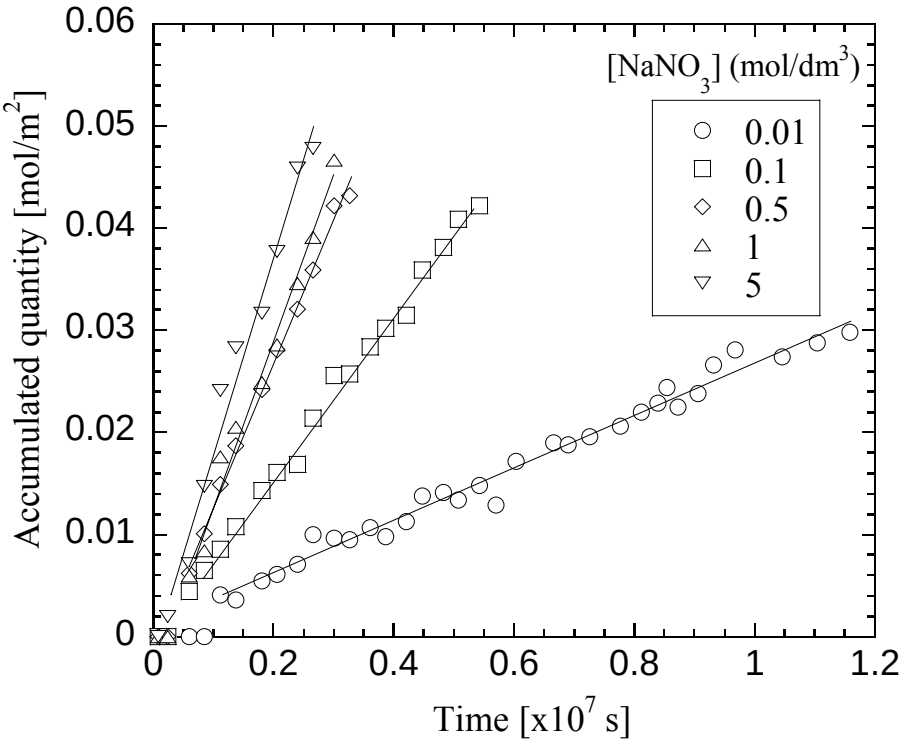

Fig. 3-3 Break-through curves of I^- for Kunigel V1 with 30 wt% silica sand

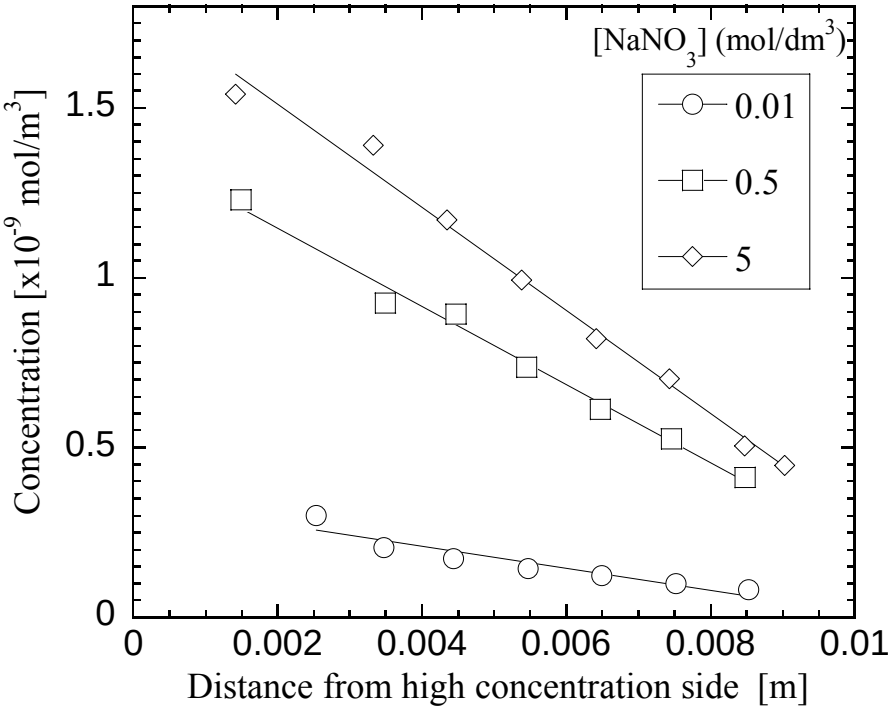

Fig. 3-4 Concentration profiles of Cl^- for Kunigel V1 with 30 wt% silica sand

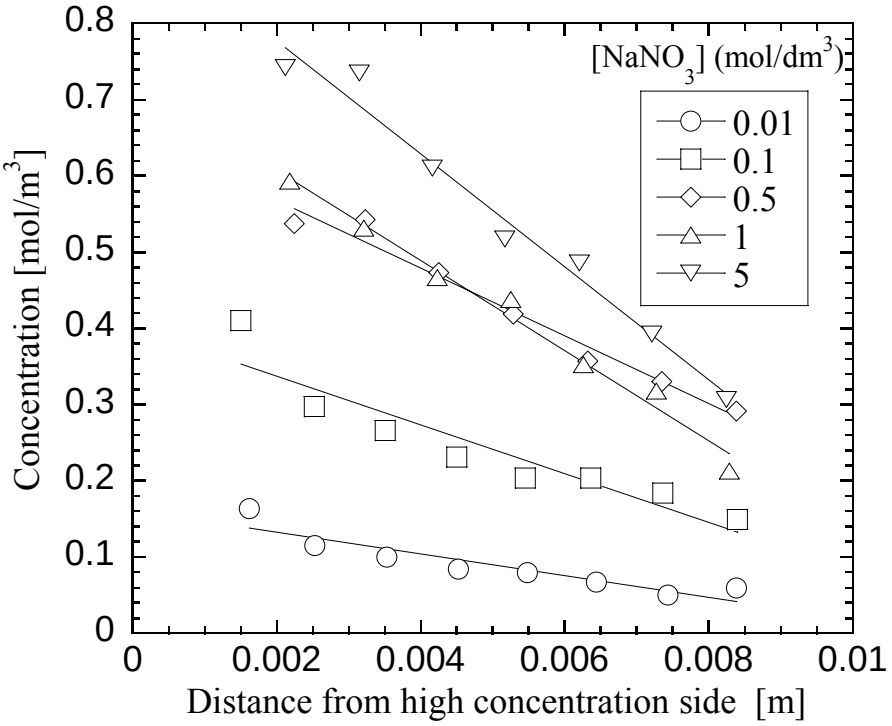

Fig. 3-5 Concentration profiles of I^- for Kunigel V1 with 30 wt% silica sand

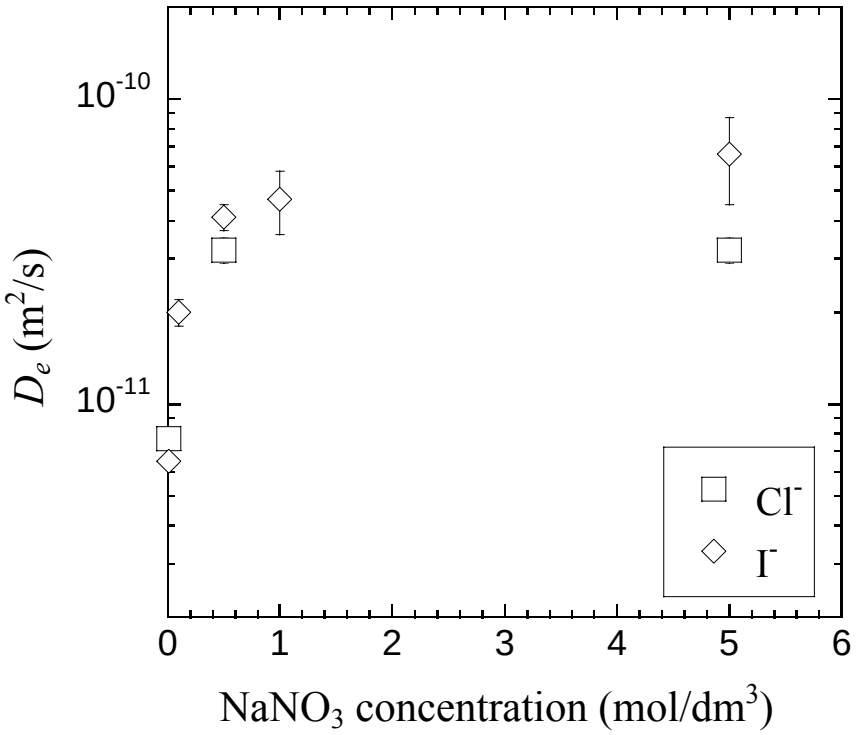

Fig. 3-6 $NaNO_3$ concentration influence on D_e values for Kunigel V1 with 30 wt% silica sand

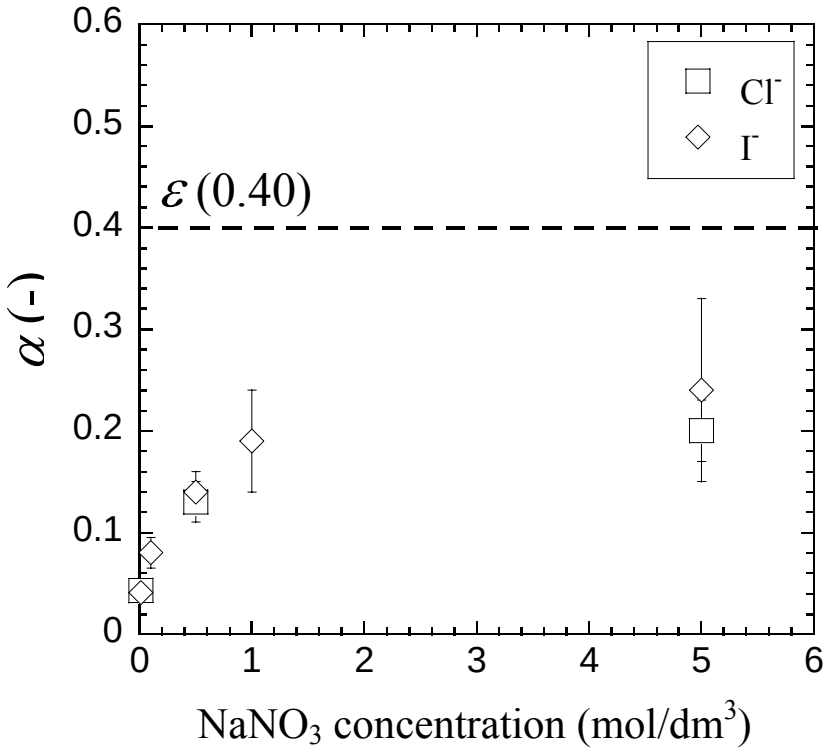

Fig. 3-7 $NaNO_3$ concentration influence on α values for Kunigel V1 with 30 wt% silica sand

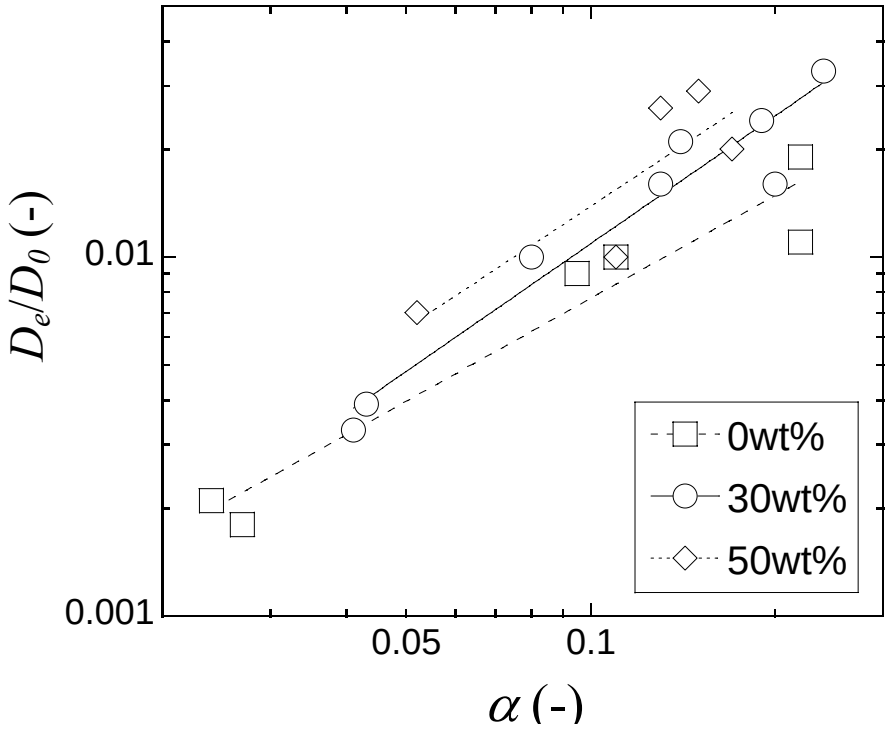

Fig. 3-8 D_e/D_0 values for Cl^- and I^- as a function of determined α values

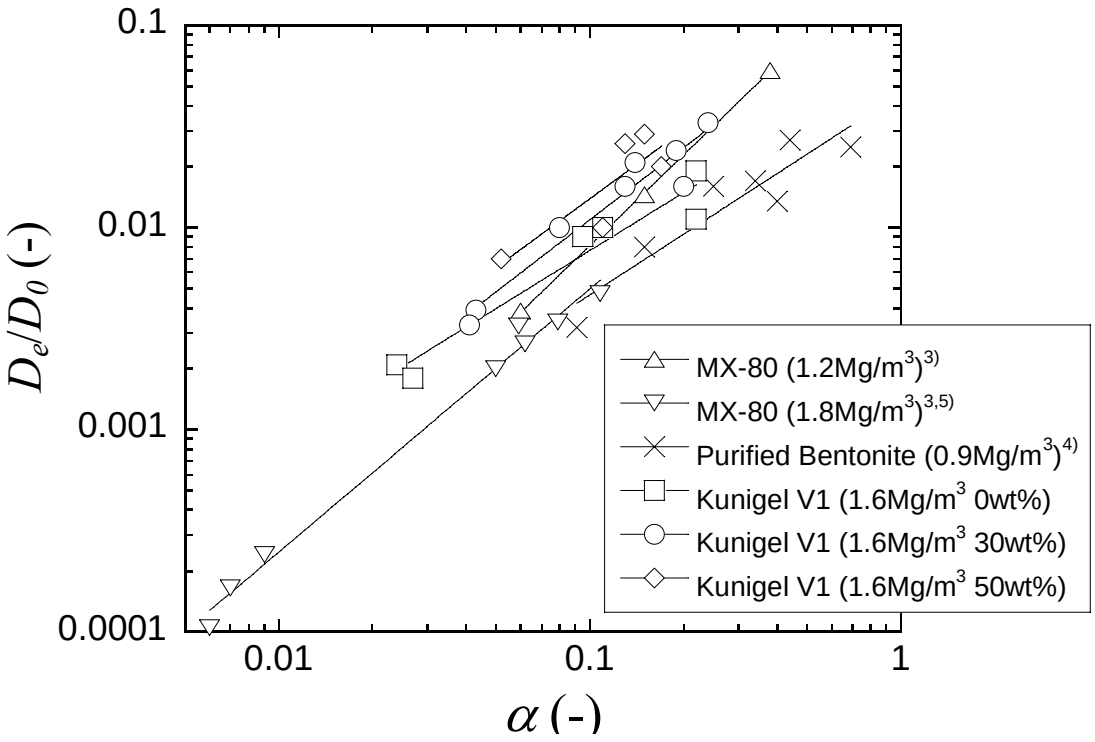

Fig. 3-9 Literature D_e/D_0 values for Cl^- and I^- as a function of α

Chapter 4
Corrosion of carbon steel in compacted bentonite and its effect on neptunium diffusion under reducing condition

4.1 Introduction

Extensive studies have been available for understanding carbon steel corrosion behavior in aqueous media under anaerobic conditions. However, only a few publications have been concerned with carbon steel corrosion in a porous media such as compacted bentonite[1-5]. Within the multi-barrier system, corrosion is expected to be a more complex process than in aqueous media. It can be influenced not only by the chemistry of pore solution such as pH, redox potential, and anions present, but also by the corrosion products of carbon steel and the transport capability of buffer for these corrosion products, including the gas phase generated.

Related to radionuclide migration in the bentonite, the corrosion of carbon steel may physically or chemically affect it. Corrosion may affect the chemistry of the pore solution and thus result in changes in the migration behavior of radionuclides. Furthermore, corrosion products may also influence the migration by filling into the pore. It may also induce buffer alteration, which may result in changes of some crucial properties such as sorption capability relevant to requirements as the buffer of repository. However, these effects haven't been considered in the current safety assessment of geological disposal[6].

This study concerns two relevant aspects: (a) corrosion of carbon steel in the presence of water-compacted bentonite and corrosion products preformed under aerobic conditions; and (b) its effect on neptunium diffusion under reducing condition, known as a crucial constituent of the conditions relevant to repository.

4.2 Methods

4.2.1 Materials and preparation of specimens

Carbon steel specimens were prepared from carbon steel (SM41B) disks, 25 mm in diameter and 4 mm in thickness. Firstly, the disk was wet-polished with 400-, 800-grade silicon carbide (SiC) grinding papers. Secondly, it was assembled in the electrochemical apparatus as illustrated in Fig. 4-1 in aerobic conditions. The apparatus consisted of electrochemical cell and potentiostat/galvanostat, connected to a personal computer used for data acquisition. The electrochemical cell consisted of an acrylic resin vessel and three electrodes: Pt counter

electrode, Fe working electrode and Ag/AgCl reference electrode. An area of 20 mm in diameter of the disk was exposed to 0.1 mol/l NaCl electrolyte for corrosion. This corrosion procedure was adopted for simulating a practical circumstance. The possible practical circumstance can be considered that: (a) before overpack is transported into a repository, overpack corrosion may occur during the period of closure preparation due to exposure to atmosphere; (b) even during the primarily stage of post-closure of repository, aerobic corrosion will also occur by consuming oxygen trapped in the repository after closure; and eventually; (c) anaerobic corrosion occurs and a reducing condition is expected to be created. After electrochemical corrosion, the disk was disassembled from the electrochemical cell, and then, dried in a desiccator at 25^{o}C. A series of the carbon steel disks were prepared by this means. These corrosion products formed electrochemically were analyzed by XRD (Shimadzu, model XRD.XD-D1) in a thin-film mode with Cu-Kα radiation worked at 40 kV and 30 mA under aerobic conditions. These corrosion products were appointed as the pre-formed corrosion products to distinguish the corrosion products generated under reducing corrosions later.

Typical Japanese sodium bentonite, Kunigel-V1, was used. It contained approximately 95wt.% of montmorillonite. Its mineral composition and chemical composition were given elsewhere[7]. The bentonite powder was compacted into a 20-mm-diameter, 20-mm-high cylinder in various compaction dry densities, to be served as a bentonite specimen. The dry densities were 0.8, 1.4, 1.6, and 1.8 Mg/m^3. These bentonite cylinders were named V0.8, V1.4, V1.6 and V1.8, corresponding to the densities. It was set in a column illustrated in Fig. 4-2, to be water-saturated under reducing conditions. The column mainly consisted of the upper and lower lids, and sample holder. The bentonite cylinder was sandwiched between two porous ceramic filterss (25 mm in diameter and 4 mm in thickness). Two holes on both sides of the upper and lower lids allowed water to soak into the bentonite specimen. The whole column was first soaked in deionized water, then was moved into a 5×10^{-3} mol/l $Na_2S_2O_4$ soaking solution for 1 month to be water-saturated in a glove box purged with purified nitrogen gas with less than 1 ppm oxygen, with typical level of 0.1 ppm. Such a glove box was appointed as low-oxygen glove box. The redox potential of the soaking solution was kept in the range of -200 to -400 mV (vs. SHE) and pH 6.5-7.5.

4.2.2 Corrosion experiment

Corrosion experiment of carbon steel was designed to simulate overpack corrosion and migration of its corrosion products under reducing conditions established after a certain long time of post-closure of repository. It was performed by allowing the carbon steel specimen to come into contact with the bentonite specimen under reducing conditions by using a column similar to that shown in Fig. 4-2 in the low-oxygen glove box. The upper lid was temporarily disassembled. The top ceramic filter was replaced by the carbon steel specimen with its pre-corroded surface towards the bentonite specimen. The column, partly disassembled, was then reassembled and again immersed in soaking solution to allow corrosion of carbon steel for a certain period.

4.2.3 Diffusion experiment of neptunium

Diffusion experiment of neptunium was performed with and without carbon steel using the same type of the column shown in Fig. 4-2. In the case of diffusion without carbon steel, after water-saturation of the bentonite specimen, the upper lid was temporarily disassembled. The top ceramic filter was removed from the upper lid and 25-50 mm^3 of neptunium- 237 tracer was spiked on the top surface of the bentonite specimen. In the case of diffusion with carbon steel, neptunium tracer was spiked after the carbon steel specimen corroded for a certain period as described in section 4.2.2.

4.2.4 Analyses

For the corrosion experiment, after a certain corrosion time schedule, the apparatus shown in Fig. 4-2 was disassembled. The carbon steel specimen was observed firstly by taking photographs, and then, the bentonite specimen was cut into slices of 0.1-2.0 mm in thickness. During this procedure, photographs of transverse section of each slice were taken. The slices were analyzed by wet-XRD (Rigaku, RINT-TTR modification) to identify the corrosion products after the corrosion experiment. The slices were placed in a specially designed vacuum vessel after being taken in the low-oxygen glove box, and then, transported into another low-oxygen glove box for obtaining X-diffraction patterns. The wet-XRD was also equipped in a low-oxygen glove box and was capabilities of relative humidity control in the range of 10–90% at 25^oC and of temperature control up to 70^oC. Such a system ensured a relatively high reliability of analysis through avoiding oxidation and moisture loss of the

specimen analyzed.

For the diffusion experiment of neptunium, a similar procedure was carried out. The neptunium concentration in each slice was measured by alpha spectrometer and high-resolution inductively coupled plasma-mass spectrometry (ICP-MS). The oxidation states of neptunium were investigated by thenoyltrifluoroacetone in xylene (TTA-xylen) extraction technique.

4.3 Results and discussion

4.3.1 Observation of carbon steel and bentonite

Observed results of the carbon steel and the bentonite specimens are illustrated typically in Fig. 4-3.

Firstly, on the carbon steel, before contacting with the bentonite specimen, the surfaces of the pre-corroded carbon steel specimens could be categorized into three groups: (a) most of them appeared as uniform porous thin, powdery, orange layers, the red-rust, as shown as photograph No. a1 in Fig. 4-3; (b) several of them, however, were coated by uniform black layers due to a relatively long immersion time after potentiostatic corrosion procedure (see photograph No. b1); and (c) the remaining contained a black layer below a loosely adherent orange rust layer on the exterior (see photograph No. c1). XRD analyses of these corrosion products showed that the red-rust was a mixture of $Fe(OH)_2$/$Fe(OH)_3$ and FeOOH, and the black layers were maghemite (Fe_2O_3). After coming into contact with the bentonite for a certain time under reducing conditions, the colors of all these surfaces became dark-green, as shown in photographs No. a2, b2 and c2 in the same figure.

Next, the colors of transverse sections of the bentonite showed interesting scenery: a dark-green color appeared on the interfacial surface (see photographs No. a3, b3 and c3) and on the first transverse section shown as photographs No. a4, b4 and c4, which was mostly adjacent to the carbon steel specimen; then, it changed from the dark-green to a red/yellowish-brown, from the interface to the bentonite specimen interior (from photograph series No. 4); and finally, color reverted to the original one of the bentonite, the pale-gray (the last photograph in each group in Fig. 4-3), at a certain depth towards the bentonite interior.

Additionally, it was noticed that cracks were obvious on some transverse sections as shown in Fig. 3(a). These cracks did not appear on transverse sections in the range of either the interface or the opposite end of the bentonite, closer to the interface. Typical visible range of

the cracks was 0.2–2.0 mm in depth. Beyond this range, it disappeared.

4.3.2 Corrosion processes

When the carbon steel specimen came into contact with the bentonite specimen, the pre-formed corrosion products observed, red-rust or black meghemite, were thrust into the bentonite due to external pressure. At the same time, pore water permeated to contact it. Portions of the pre-formed corrosion products reacted with the pore water permeated. Possible reactions were given by the following according to thermodynamic predictions using thermodynamic data[8].

For the carbon steel specimens in group (a), the following reactions may occur:

$$FeO(OH) + 3H^+ + e^- = Fe^{2+} + 2H_2O, \qquad logK = 17.9 \quad (4\text{-}1)$$

$$3FeO(OH) + H^+ + e^- = Fe_3O_4 + 2H_2O, \qquad logK = 3.80 \quad (4\text{-}2)$$

For those in group (b), maghemite may react as:

$$2Fe_2O_3 + 4H^+ + 2e^- = Fe^{2+} + Fe_3O_4 + 2H_2O, \qquad logK = 14.80 \quad (4\text{-}3)$$

$$2Fe_2O_3 + 2H^+ + 2e^- = Fe(OH)_2 + Fe_3O_4, \qquad logK = 2.42 \quad (4\text{-}4)$$

Additionally, meghemite may also convert to FeO(OH) and/or $Fe(OH)_3$ due to moisture by reactions given as:

$$Fe_2O_3 + H_2O = FeO(OH), \qquad logK = 86.09 \quad (4\text{-}5)$$

$$Fe_2O_3 + 3H_2O = 2Fe(OH)_3, \qquad logK = 12.28 \quad (4\text{-}6)$$

Theoretically, these reactions may progress until the initial corrosion products are exhausted or the equilibrium is achieved. However, only a fraction of these pre-formed corrosion products reacts due to limited reaction area in the bentonite pore situation, differing from an aqueous case. Consequently, the corrosion products change their forms to a mixture of the

preformed corrosion products and the new one. Such mixtures result in the red/yellowish-brown visually on the transverse sections of bentonite specimen, as a consequence of these reactions.

Pore water permeates through the pre-formed corrosion products, anaerobic corrosion of carbon steel may occur according to thermodynamic prediction and is proved partly by the color changes of the carbon steel described above. It may be interpreted by electrochemical reactions, which are made up of anodic and cathodic reactions:

$$\text{Anodic reaction: } Fe \rightarrow Fe^{2+} + 2e^- \quad (4\text{-}7)$$

$$\text{Cathodic reaction: } 2H_2O + 2e^- \rightarrow 2OH^- + H_2(g) \quad (4\text{-}8)$$

Firstly, the iron dissolves as Fe^{2+}, and the electrons released by anodic reaction is captured by H_2O. The general reaction may be written as:

$$Fe + 2H_2O = Fe(OH)_2 + H_2(g) \quad (4\text{-}9)$$

The concentration of ferrous ion increased in the vicinity of the carbon steel specimen and is finally controlled by the solubility product of ferrous hydroxide, $Fe(OH)_2$. Ferrous hydroxide is relatively insoluble and stable in the absence of oxygen (reducing condition) at low temperature range. Nevertheless, it would be transformed to magnetite as given in the following due to intrinsic thermodynamic instability:

$$3Fe(OH)_2 = Fe_3O_4 + 2H_2O + H_2(g) \quad (4\text{-}10)$$

In general, magnetite would be formed due to the nature of the thermodynamic stability preferred from a long time standpoint. Therefore, the following reaction can also be considered in the present study:

$$3Fe + 4H_2O = Fe_3O_4 + 4H_2(g) \quad (4\text{-}11)$$

The dark-green color observed on the interface is regarded as indicative of $Fe(OH)_2$ and Fe_3O_4, or their mixture. To further prove their presence, XRD analyses were performed on

several carbon steel specimens with dark-green corrosion products and on several bentonite slices colored typically. Unfortunately, neither magnetite nor ferrous hydroxide were identified, although oxidation of ferrous iron was avoided by using the XRD analyzer equipped in the low-oxygen glove box. This resulted, possibly from the total amount of $Fe(OH)_2$ and/or Fe_3O_4 in the bentonite, which was too limited to be analyzed by the XRD.

Besides $Fe(OH)_2$ and Fe_3O_4, siderite and green rusts are also the possible forms of corrosion products under anaerobic conditions depending on various solution chemistries. But it is unlikely in the present study. The pore water chemistry of the bentonite was predicted by modeling given by Ochs et al. (1999)[9]. Based on this model, the concentrations of anions CO_3^{2-}, Cl^-, or SO_4^{2-} are estimated to be 4.2×10^{-5}, 2.5×10^{-3} and 6.1×10^{-3} mol/l, respectively, in the present study. Siderite may be formed by:

$$Fe^{2+} + CO_3^{2-} = FeCO_3, \qquad \log K = 10.45 \quad (4\text{-}12)$$

Such low concentration of CO_3^{2-} in the present study would be unlikely to form siderite. This will be discussed again later, combining concentration of ferrous ion. Green rusts are known as Fe(II)-Fe(III) hydroxy compounds containing anions such as CO_3^{2-}, Cl^-, or SO_4^{2-}. The redox potential, Eh, of green rust containing CO_3^{2-}, GR1(CO_3^{2-}), could be thermodynamically predicted by the following reaction reported by Drissi et al. (1995)[10].

$$5Fe(OH)_2 + HCO_3^- + 2H_2O = Fe^{II}_4Fe^{III}_2(OH)_{12}CO_3\cdot 2H_2O + H^+ + 2e^- \quad (4\text{-}13)$$

$$Eh[GR1(CO_3^{2-})] = -0.32 - 0.0296\log[HCO_3^-] - 0.0296pH \quad (4\text{-}14)$$

Making an assumption of equilibrium between $[CO_3^{2-}]$ and $[HCO_3^-]$, the range of redox potential, Eh[GR1(CO_3^{2-})], is then -269 to -328 mV in the present study. This potential value is consistent with the measured redox potential (-200 to -400 mV) of soaking solution. However, it seems unlikely due to the very low concentration of carbonate, and competition between the other anions, whose concentrations are about two orders of magnitude higher than $[CO_3^{2-}]$. Refait et al. (1997)[11] have mentioned that formation of GR1(CO_3^{2-}) would be completely avoided if the initial $[CO_3^{2-}]$ is under 0.005 mol/l in their work on iron aqueous corrosion. The redox potential, Eh, of green rust containing SO_4^{2-}, GR2(SO_4^{2-}), could be thermodynamically predicted in the reaction given by Génin et al. (1996)[12].

$$6Fe(OH)_2 + SO_4^{2-} + 2H_2O = Fe^{II}_4Fe^{III}_2(OH)_{12}SO_4 \cdot 2H_2O + 2e^- \quad (4\text{-}15)$$

$$Eh[GR2(SO_4^{2-})] = -0.55 - 0.0296\log[SO_4^{2-}] \quad (4\text{-}16)$$

Substituting the concentration of SO_4^{2-} in Eq. (4-16), the potential of Eh[GR2(SO_4^{2-})] is -484 mV. This value is not in the range of the value measured in the present study. Furthermore, green rust GR1(Cl^-) is also unlikely if the above two green rusts could not be formed, based on the different affinity of green rust compounds to these anions, which is in the sequence of $CO_3^{2-} > SO_4^{2-} > Cl^-$, reported by Miyata (1983)[13].

Even though no powerful evidence such as XRD pattern is available to identify the corrosion products, the occurrence of anaerobic carbon steel corrosion described in Eqs. (4-9) and (4-10) could also be well supported by hydrogen generation, another form of the products. There is no doubt that hydrogen gas is generated. The cracks were observed clearly for some bentonite specimens with relatively high dry densities, as shown as Fig. 4-3(a). The cracks revealed the gas generation. In bentonite, hydrogen gas dissolvs in the pore water and dissipates by diffusion. However, if the rate of hydrogen generation exceeds the diffusive transport rate, accumulative hydrogen pressure becomes higher than the pore water pressure, then a free gas phase can be formed. When the free gas pressure locally exceeds the swelling pressure, gas transport pathways could be created. The hydrogen gas is possibly transported via an interconnected network of microcracks formed by tensile rupture of the clay under high gas pressure. The interconnected network pathways, the cracks, are obvious in Fig. 4-3(a). The cracking appears close to the interface, where hydrogen gas generate primarily.

According to the discussion above, the general processes of the carbon steel corrosion could be: (a) portions of the pre-formed corrosion products are thrust into the bentonite due to an external pressure, and pore water permeates the pre-formed corrosion products layer; (b) a fraction of the pre-formed corrosion products reacts with the water permeated by the mechanism of hydration and/or reduction; and (c) the water permeats through the pre-formed corrosion products layer and comes into contact with metallic iron, and then, the anaerobic corrosion occurrs.

4.3.3 Effect on neptunium diffusion

Neptunium profiles were obtained and plotted as a function of $x/t^{0.5}$ as shown in Fig. 4-4 for

the diffusion experiment with and without carbon steel. In Fig. 4-4, x is penetration depth in bentonite, and t is the experimental period. All the profiles consist of two slopes, a steep and a gradual. The steep expresses a slow fraction and the gradual a fast one. Based on diffusion theory in porous media, assuming two independent diffusion terms, apparent diffusion coefficients of iron could be obtained by fitting the experimental data to the following equation given in our previous study[7].

$$C = C_{0f} erfc\left(\frac{x}{2\sqrt{D_{af}t}}\right) + C_{0s} erfc\left(\frac{x}{2\sqrt{D_{as}t}}\right) \qquad (4\text{-}17)$$

where D_{af} and D_{as} are apparent diffusion coefficient of the fast and the slow fraction, respectively, and C_{0f}, C_{0s} are the corresponding boundary concentrations; 'erfc' is the error function complement. The diffusion coefficients are plotted as a function of dry density, as shown in Fig. 4-5. The fast apparent diffusion coefficient of neptunium, D_{af}, is determined to be in the order of 10^{-13}-10^{-12} m^2/s, and the slow one in the order of 10^{-15}-10^{-14} m^2/s, corresponding to the diffusivity of Np(V) and Np(IV), respectively. The different values of the diffusion coefficients suggest that neptunium diffusivity under reducing conditions is approximately two orders of magnitude lower than under oxidizing conditions.

Interfacial concentrations of the fast fraction are obviously lower in the diffusion with carbon steel than that without, as shown in Fig. 4-4. It is estimated from each profile and given in Table 1, showing approximately two orders of magnitude lower in the diffusion with carbon steel than that without. This result reveals that the presence of carbon steel causes the decrease in the total amount of neptunium diffused into the bentonite. To further understand the effect of the corrosion of carbon steel, neptunium oxidation states were investigated to the diffusion both with and without carbon steel. Neptunium oxidation states were analyzed by TTA-xylen extraction techniques. The total amount of neptunium and the amount of tetravalent neptunium were measured. The results showed that tetravalent neptunium, Np(IV), accounted for 99% of the total neptunium in the bentonite in the diffusion with carbon steel, and only 63% in that without. It should be noticed that both the diffusion with and without carbon steel were performed under the reducing condition, which was proved by the redox potential measured in soaking solution. The redox potential was in the range of -200 to -400

mV (vs. SHE) during all experimental periods. Different percentages of the tetravalent suggested that the corrosion of carbon steel under anaerobic conditions maintained strong reducing condition, even more effective than strong chemical reductant, $Na_2S_2O_4$. The strong reducing condition kept most tetravalent neptunium from being oxidized to be pentavalent neptunium, thus effectively restraining migration of neptunium in the bentonite.

Comparing the diffusion coefficients obtained in the diffusion with and without carbon steel, no significant difference could be observed, as shown in Fig. 4-5. This reveals no significant effect of the corrosion products on the diffusion coefficient in the present study. Because the diffusion coefficient would be decreased if sorption increased due to the presence of the corrosion products, based on the theory of diffusion in porous media, it may be considered that the sorption capability of the corrosion products accumulated on the interface is much less than that of the bentonite, known as a satisfying sorbent. Additionally, the layer of the corrosion products is extremely thin, in general typically less than 2 mm, as shown in Fig. 4-3. Such a thin layer is considered unlikely to cause change in the sorption property, especially in the presence of bentonite. However, generally, it is still noticed that the diffusion coefficients for the fast fraction were slightly higher in the diffusion with carbon steel than that without. It might be considered as some relation with migration of the microbubbles of hydrogen gas, but not clear at the moment in the present study.

4.4 Conclusions

Corrosion of carbon steel and its effect on neptunium diffusion were studied by the corrosion experiment and the neptunium diffusion experiment under conditions with consideration for constituents of the repository. Corrosion of carbon steel maintained strong reducing conditions to keep most neptunium in a low oxidation state, the tetravalent, thus effectively restrained migration of neptunium in the bentonite. The apparent diffusion coefficient of the tetravalent neptunium was approximately two orders of magnitude lower than that of the pentavalent. No meaningful effect of the corrosion products on neptunium diffusion coefficient, possibly due to its extremely low sorption capability compared to the bentonite and the limitation of the total amount of the corrosion products. This result means that the effect of corrosion on the radionuclide migration, especially redox-sensitive radionuclides in the buffer, should be considered for a reliable safety assessment of geological disposal.

References

1) T. Fukuda and M. Akashi, "Effect of [HCO_3^-+CO_3^{2-}] on corrosion crevice repassivation potential of carbon steel in simulated bentonite environment," *Mat. Res. Soc. Symp. Proc*., 412, 597-602 (1996).
2) A. Honda, T. Teshina, K. Tsurudome, et al., "Effect of compacted bentonite on the corrosion behavior of carbon steel as geological isolation overpack," *Mat. Res. Soc. Symp. Proc.*, 212, 287-294 (1991).
3) A. Honda, N. Taniguchi, H. Ishikawa, et al., *Experimental research on corrosion behavior of carbon steel in anaerobic condition*, *PNC Tech. Rev.*, 104, 125-134 (1997), (in Japanese).
4) Y. Kojima, T. Hioki and S.Tsujikawa, "Simulation of the state of carbon steel n years after disposal with n years of corrosion product on its surface in a bentonite environment," *Mat. Res. Soc. Symp. Proc.*, 353, 711-718 (1995).
5) N. Taniguchi, A. Honda and H. Ishikawa, "Experimental investigation of passivation behavior and corrosion rate of carbon steel in compacted bentonite," *Mat. Res. Soc. Symp. Proc.*, 506, 495-501 (1998).
6) Japan Nuclear Cycle Development Institute (JNC), *Second progress report on research and development for the geological disposal of HLW in Japan. H12: Project to establish scientific and technical basis for HLW disposal in Japan (Project Overview Report)*, JNC TN1410 2000-001, (2000).
7) K. Idemitsu, S. Yano, X. Xia, et al., "Diffusion behavior of iron corrosion products in buffer materials," *Mat. Res. Soc. Symp. Proc.*, 713, 113–120 (2002).
8) J. I. Drever, *The geochemistry of natural waters, surface and groundwater environmentals. Appendix II: Standard-State, Thermodynamic Data for Some Common Species. Appendix III: Equilibrium constants at 258C and Enthalpies of reaction for selected reactions, (third edition)*, Prentice Hall, Upper Saddle River, NJ 07458, 413-422 (1998).
9) M. Ochs, B. Lothenbach, M.Shibata, et al., *Bentonite porewater chemistry*, JNC TN8400 99-075, (1999).
10) S. H. Drissi, Ph. Refait, M. Abdelmoula, et al., "The preparation and thermodynamic properties of Fe(II)-Fe(III) hydroxide-carbonate (green rust 1); pourbaix diagram of iron in carbonate-containing aqueous media," *Corros. Sci.*, 37, 2025-2041 (1995).
11) Ph. Refait, S. H. rissi, J. Pytkiwicz, et al., "The anionic species competition in iron

aqueous corrosion: role of various green rust compounds," *Corros. Sci.*, 39, 1699-1710 (1997).

12) J. M. R. Génin, A. A. Olowe, Ph. Refait, et al., "On the stoichiometry and pourbaix diagram of Fe(II)-Fe(III) hydroxysulphate or sulphate-containing green rust: 2. An electrochemical and Mössbauer spectroscopy study," *Corros. Sci.*, 38, 1751-1762 (1996).

13) S. Miyata, "Anion-exchange properties of hydrotalcite-like compounds," *Clays Clay Miner.*, 31, 305-311 (1983).

Table 1 Interfacial concentrations of neptunium diffused as the fast fraction in the diffusion with and without carbon steel

Name of specimen	With carbon steel (Bq/g-Bentonite)	Without carbon steel (Bq/g-Bentonite)
V0.8	2.3×10^{-1}	5.6×10^{0}
V1.4	8.9×10^{-2}	3.6×10^{-1}
V1.6	-	2.4×10^{0}
V1.8	5.2×10^{-2}	2.7×10^{1}

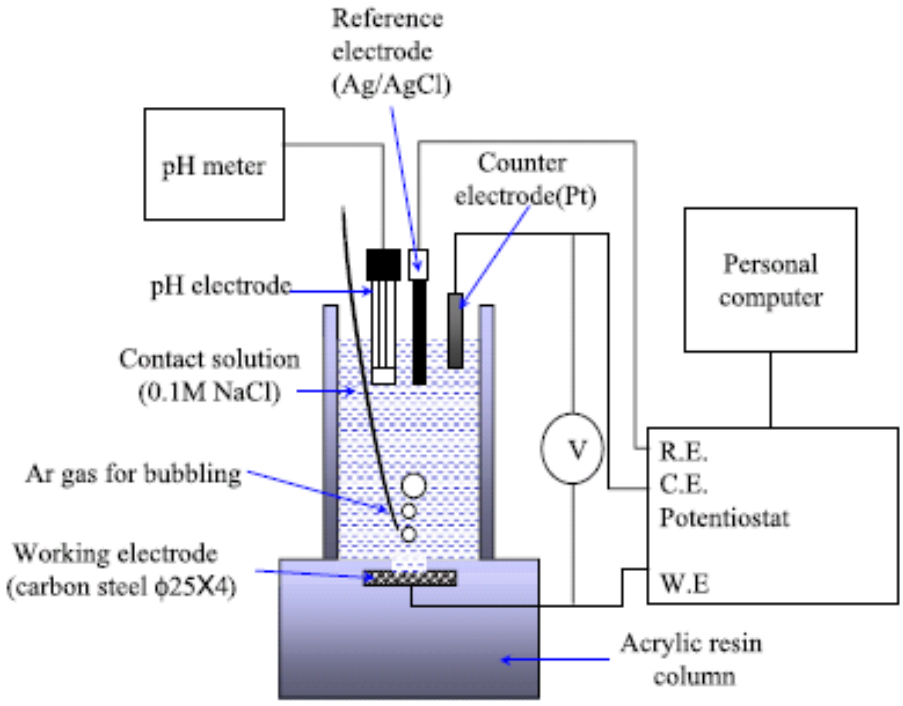

Fig. 4-1 Electrochemical apparatus used for preparation of carbon steel specimens.

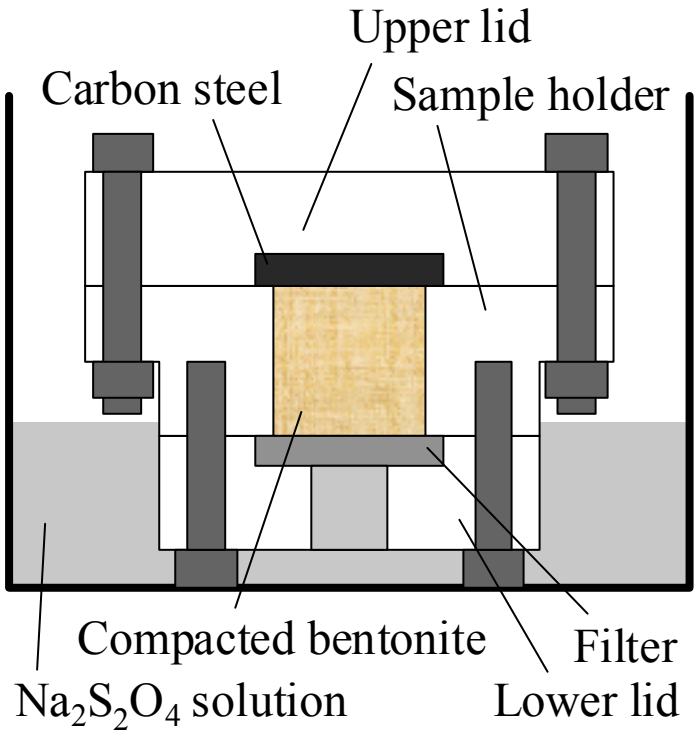

Fig. 4-2 Schematic of apparatus used for preparation of bentonite specimens.

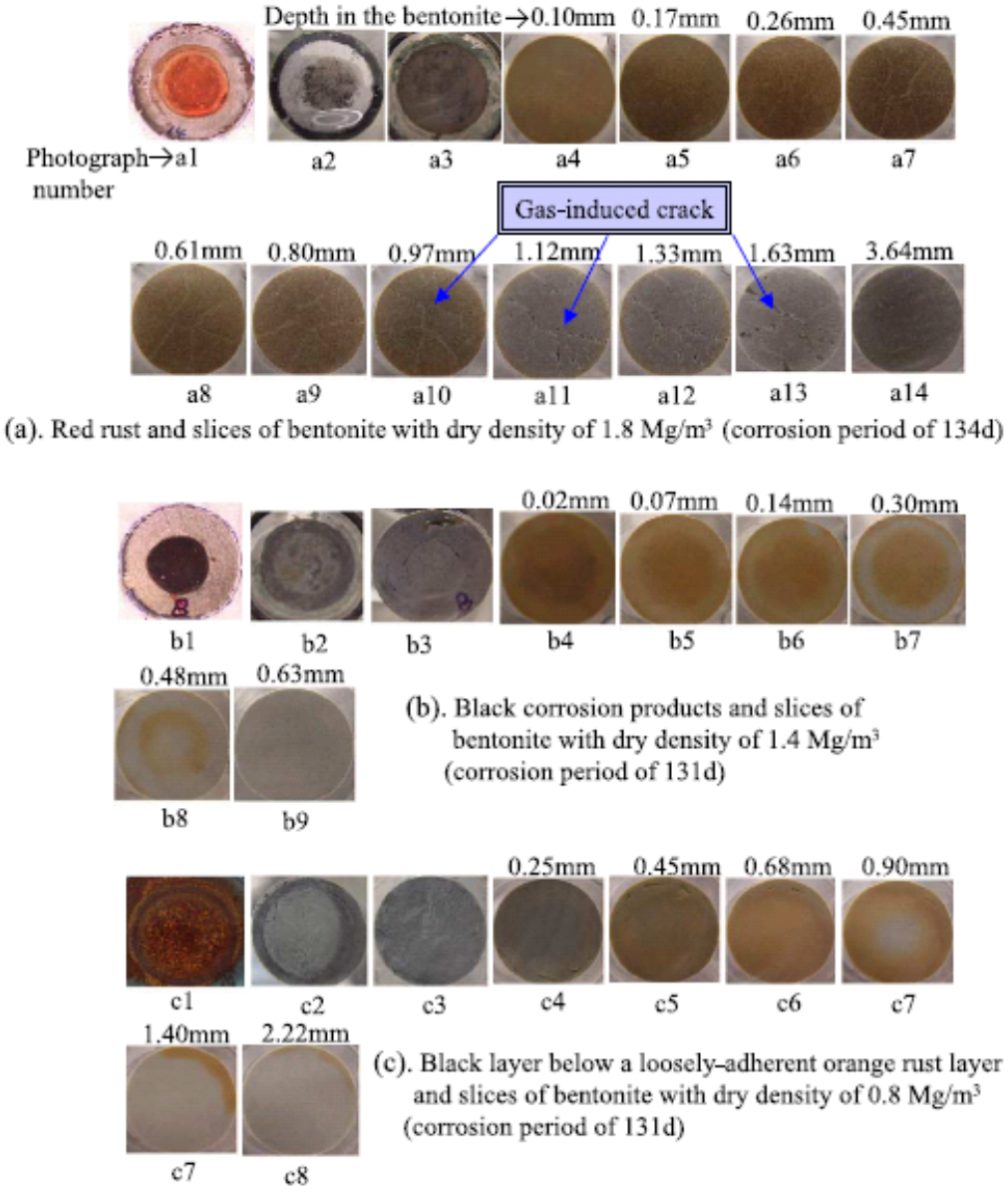

Fig. 4-3 Typical photographs illustrating the changes in color of the carbon steel before and after making contact with the bentonite specimen, and of the transverse sections of the bentonite after the corrosion experiment. To view this figure in color, please see the on-line version of the paper.

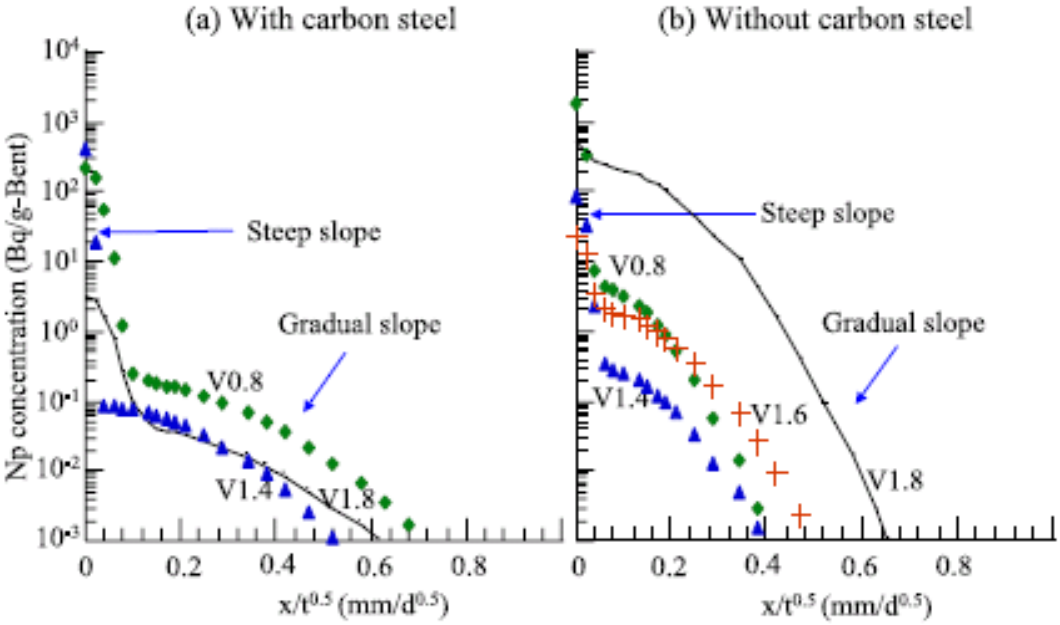

Fig. 4-4 Neptunium profiles in the bentonite specimens with dry density of 0.8, 1.4, 1.6 and 1.8 Mg/m^3 in the diffusion (a) with carbon steel, and (b) without carbon steel, plotted as a function of $x/t^{0.5}$ (the profile in bentonite specimen with dry density of 1.6 mg/m^3 was not shown in (a) due to breakage of the specimen during slicing).

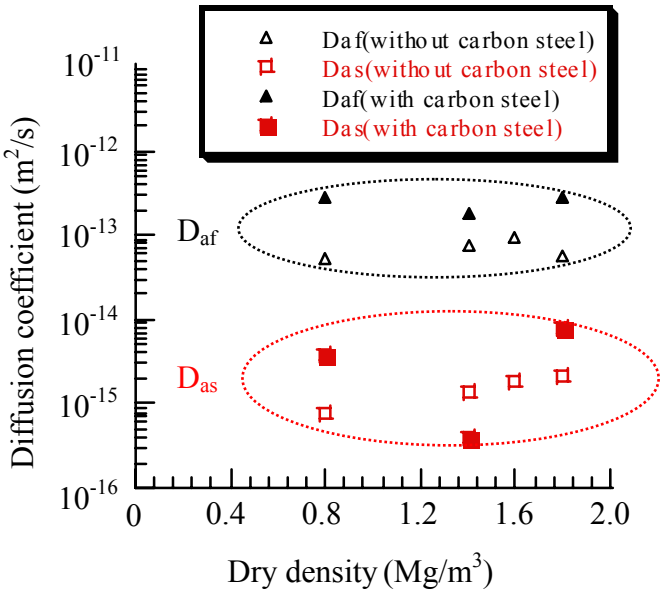

Fig. 4-5 Apparent diffusion coefficients of neptunium obtained from the diffusion with and without carbon steel, plotted as a function of dry density of bentonite.

Chapter 5
Corrosion products from carbon steel formed in compacted bentonite under reducing conditions

5.1 Introduction

Corrosion products have been reported to affect the diffusion behavior of radionuclides in compacted bentonite[2-10]. The corrosion products can affect the sorption of radionuclides onto the buffer materials[1], the porosity of buffer[8], the diffusion pathways and reduction of radionuclides[2-7,9,10]. In order to estimate the effects of the corrosion products, characterization of the corrosion products from carbon steel in compacted bentonite is important. The corrosion product thermodynamically stable under expected geological conditions in a repository is magnetite or siderite for groundwater containing high-concentrations of CO_3^{2-} ion[1]. In previous experimental studies, Honda et al. reported that magnetite was identified on the carbon steel both in artificial, low-salinity groundwater and in artificial sea water at 80°C under low-oxygen conditions[11]. Considering corrosion of carbon steel in the presence of compacted bentonite, Taniguchi et al. reported the formation of siderite on carbon steel placed in compacted bentonite at 80°C under low oxygen conditions[12]. Kozaki et al. has reported that the corrosion product formed on pure iron film placed in compacted bentonite was either hydroxide or oxide[13]. Thus, iron hydroxide or oxide has been presumed to exist on the carbon steel surface in the presence of compacted bentonite as corrosion products. However, as there is little analytical method to obtain the direct evidence of the existence of these minerals, the kind of minerals formed on the carbon steel surface is still unclear. In addition, although the corrosion products formed on the carbon steel surface has been investigated, the corrosion products present in the pore space of compacted bentonite, and which could directly affect the sorption of radionuclides and dissolution of corrosion products in compacted bentonite, has not been identified. Furthermore, exchange between the Fe^{2+} ions derived from the corrosion products and cations in the smectite interlayers in compacted bentonite may occur[1]. The swelling of Fe^{2+}-adsorbed smectite (Fe-smectite) is known to be less than that of Na-smectite[14]. The sorption and diffusion behavior of radionuclides in Fe-smectite has also been reported to be different than in Na-smectite[15]. Idemitsu et al. carried out migration experiments on corrosion product movement by electromigration from carbon steel into compacted bentonite and pointed out the possibility of alteration to Fe-smectite from the

observation that the concentration of Na in compacted bentonite decreased with increasing Fe concentration in a 2 to 1 the ratio[16]. Sasamoto et al. reported that the presence of Fe-smectite was indicated in bentonite powder which had been immersed in deionized water with iron powder for 6 years at room temperature[17]. In a natural analog study by Kamei et al, alteration to Fe-smectite was observed near an iron support which had been in contact with Na-smectite for about 2000 days in a bentonite mine[14]. However, there is no experimental study on alteration of smectite to Fe-smectite contained in compacted bentonite due to the presence of corrosion products in simulated repository conditions.

In this study, corroded carbon steel was placed in contact with compacted bentonite under reducing conditions. The carbon steel was corroded electrochemically under aerobic conditions in order to simulate the corrosion of overpack, which would occur due to exposure to atmosphere before the transportation of the overpack into a repository. The corrosion products distributed in the compacted bentonite were investigated by selective dissolution analysis[18,19], to estimate the crystallinity of Fe-bearing compounds. The valence of Fe in the corrosion products was spectrophotometrically determined. Furthermore, the alteration of smectite to Fe-smectite contained in compacted bentonite was analyzed by X-ray diffraction (XRD). From these analyses, the corrosion products of carbon steel in compacted bentonite were determined.

5.2. Experimental

5.2.1 Materials

The carbon steel used in this study was SM41B. The carbon steel coupons were 25 mm diameter and 4 mm thickness. In an actual disposal circumstance, corrosion of overpack material will occur under aerobic conditions due to exposure to the atmosphere prior to repository closure. Aerobic corrosion will also occur post-closure by consumption of oxygen trapped in the repository. Taking into consideration the possibility of aerobic corrosion, the surfaces of carbon steel coupons were corroded electrochemically under aerobic conditions in 0.1 mol/dm^3 NaCl electrolyte. The corrosion products were identified by XRD as $Fe(OH)_2$, $Fe(OH)_3$, FeOOH and magnetite. The detailed procedures of electrochemical corrosion are described in 4.2.1.

The bentonites used were Kunigel V1® and Kunipia F® (Kunimine Industries Co. Ltd.). Kunigel V1 consisted of 46 to 49 wt% smectite, 37 to 38 wt% chalcedony and a few wt% of

minor minerals, plagioclase, calcite, dolomite, analcime and pyrite[20]. Kunipia F consisted of over 95 wt% smectite[20]. The Kunigel V1 was compacted to dry densities of 0.8, 1.4, 1.6 and 1.8 Mg/m^3, while Kunipia F was compacted to 1.2 Mg/m^3. The dry density of 1.2 Mg/m^3 for Kunipia F corresponded to the partial dry density of the smectite component of Kunigel V1 compacted to 1.6 Mg/m^3 [21].

The acrylic resin column shown in Fig. 4-2 was used. The column consists of upper and lower lids, a sample holder between lids and a filter. The sample holder has a cylindrical compartment (20 mm diameter and 20 mm length), in which bentonite is compacted and held for the duration of the experiment. The carbon steel coupons are positioned in the upper lid in direct contact with the compacted bentonite. The lower lid has an opening through which solution is allowed to soak into the compacted bentonite. A porous ceramic filter, 25 mm in diameter and 4 mm in thickness, is positioned between the hole in the lower lid and compacted bentonite to restrict leakage of bentonite.

5.2.2 Procedures

The bentonite was dried at 110^{o}C for more than 24 hours, and then compacted into the sample holder of the column. The column was initially immersed under low pressure in deionized, degassed water, degassed in an N_2 glove box, in order to saturate the compacted bentonite and then in 0.005 mol/dm^3 $Na_2S_2O_4$ solution for more than 1 month. In the saturation period, a temporary lid similar to the lower lid with an opening and a filter was used as an upper lid in order to saturate the compacted bentonite by completely immersing the columns in solution. After saturation in 0.005 mol/dm^3 $Na_2S_2O_4$ solution, the carbon steel coupon in the upper lid was set in contact with compacted bentonite. The column was re-immersed in 0.005 mol/dm^3 $Na_2S_2O_4$ solution. The Eh and pH of the solution were kept in the range from -200 to -400 mV and 6.5 to 7.5, respectively. The columns for Kunigel V1 compacted to 0.8, 1.4, 1.6 and 1.8 Mg/m^3 were immersed for 1342, 1362, 1552 and 1414 days, respectively. For Kunipia F, the column analyzed by selective dissolution was immersed for 1352 days, while the column used for XRD analysis was immersed for 1498 days. After the columns were immersed for the experimental periods, the compacted bentonite was sliced into transverse sections 0.2 to 0.6 mm thick. The sections were analyzed by selective dissolution analysis for Fe content[18,19]. The valence of iron in each section was determined spectrophotometrically. The procedures for selective dissolution analysis and valence analysis

are described in Section II.3. During the slicing of compacted bentonite, photographs of each transverse section were taken. For the column of Kunipia F used for XRD analysis, fractions from selected sections were dried and ground into powder. The bentonite powders were pressed onto silicone plates and analyzed by XRD (Rigaku Corporation, rint 2100) using CuKα radiation to measure the basal spacings of smectite. In the XRD analysis, the relative humidity was controlled at 10% intervals in the range from 0 to 100%. The XRD analysis was carried out only for Kunipia F. All procedures after compaction of bentonite were carried out in an N_2 glove box, in which the concentrations of O_2 and CO_2 were maintained lower than 1 ppm, at 22.5 ± 2.5 ^oC in temperature.

5.2.3 Procedures for selective dissolution and valence analyses

After slicing, the compacted bentonite sections were placed into polyethylene centrifuge tubes. To extract Fe^{2+} and Fe^{3+} from the pore water of compacted bentonite, 6 ml of 1 mol/dm^3, NH_4Cl solution prepared with deionized water, degassed in an N_2 glove box, was added to the tubes. The tubes were shaken until any bentonite lumps dispersed. If bentonite lumps did not disappear, the bentonite was dispersed using an ultrasonic washer. After shaking for 24 hours, the tubes were centrifuged for 10 minutes at 3000 rpm by a centrifuge (Hettich, EBA20) and then 2 ml aliquots of supernatant from each section were diluted to 10 ml by 0.01 mol/dm^3 HCl solution. The concentration of Fe in the diluted supernatants was measured by ICP-AES (Shimadzu Corporation, ICPS-7500). In addition, 1 ml aliquots of supernatant in two spectrophotometric cells were diluted to 10 ml with degassed deionized water. One of the spectrophotometric cells was used to measure the concentration of bivalent Fe in the diluted supernatant by spectrophotometer (Hach Company, DR2010) using the reagent for bivalent Fe analysis (Hach Company, Iron Ferrous Reagent). The other cell was used to measure the total concentration of Fe using the reagent for total Fe analysis (Hach Company, Iron (Total) Reagent). In cases where the total concentration of Fe was higher than the upper detection limit of the spectrophotometer, the supernatant was further diluted to the detectable concentration. After the concentrations were measured, the residual supernatant was removed. This extraction using 1 mol/dm^3 NH_4Cl solution was repeated three times.

After the NH_4Cl extraction, 10 ml of sodium oxalate solution adjusted to pH 3.5 was added to the centrifuge tubes and then the tubes were heated at 80^{o}C for 30 minutes with periodic shaking. After heating, 1.5 ml of saturated NaCl solution was added to the tube. The tubes

were centrifuged for 10 minutes at 3000 rpm. After centrifuging, the concentration of Fe in the supernatant was measured by ICP-AES. The concentrations of bivalent Fe and the total concentration of Fe were also measured by the spectrophotometer. The measurements by ICP-AES and spectrophotometer were carried out using the same procedures as those in the NH_4Cl extraction. After the concentrations were measured, the residual supernatant was removed. The extraction using sodium oxalate solution was repeated until the total concentration of Fe in supernatant measured by spectrophotometer was less than 0.005 mol/dm^3, because the maximum extractable concentration of Fe by the oxalate extraction was judged to be about 0.005 mol/dm^3. The sodium oxalate solution was prepared by adding 0.15 mol/dm^3 oxalate solution to 0.15 mol/dm^3 sodium oxalate solution until the pH was 3.5. The 0.15 mol/dm^3 oxalate solution and 0.15 mol/dm^3 sodium oxalate solution were prepared from deionized water degassed in an N_2 glove box. The oxalate extraction method was used to extract amorphous, non-crystalline or poorly ordered Fe oxides[18,19].

After the oxalate extraction, 10 ml of dithionite-citrate-bicarbonate (DCB) solution was added to the centrifuge tubes. The tubes were heated at 80^{o}C for 5 minutes and then 0.15 g of $Na_2S_2O_4$ powder was added to the tubes. After this procedure was repeated three times, the tubes were heated again for 5 minutes. After heating, 1.5 ml of saturated NaCl solution was added and the tubes were centrifuged for 10 minutes at 3000 rpm. The concentration of Fe in the supernatant was measured by ICP-AES using the same procedures as for the other extractions. After the measurement by ICP-AES, the residual supernatant was removed. The measurements by spectrophotometer were not applied to the DCB extraction, because reduction of Fe by $Na_2S_2O_4$ powder occurred during DCB extraction. The DCB solution was prepared by mixing 0.3 mol/dm^3 sodium citrate solution and 1 mol/dm^3 sodium hydrogen carbonate solution. The mixing ratio of sodium citrate solution and sodium hydrogen carbonate solution was 8 to 1. DCB extraction is used to extract Fe oxides of varying crystallinity[18,19].

After DCB extraction, 6 ml of 1 mol/dm^3 HCl solution was added to the centrifuge tubes in order to extract comparatively well crystallized Fe compound. The tubes were shaken for about 24 hours and then centrifuged for 10 minutes at 3000 rpm. After centrifuging, the concentration of Fe in the supernatant was measured by ICP-AES.

5.3 Results

Figure 5-1 shows photographs of transverse sections of Kunigel V1 compacted to 1.6 Mg/m^3. The sections of compacted bentonite were dark-green adjacent to the carbon steel (< 0.61 mm). The color changed from dark-green to brown with increasing distance from the carbon steel (0.61 to 2.23 mm) and finally changed from brown to pale-gray (> 2.23mm), the original color of compacted Kunigel V1. Similar color changes were observed on the transverse sections for Kunigel V1 compacted to 0.8, 1.4 and 1.8 Mg/m^3. The colors of transverse sections for Kunipia F compacted to 1.2 Mg/m^3 also changed from dark-green to brown and then from brown to pale-yellow, the original color of compacted Kunipia F. In the sections 1.80-3.97 mm from the steel, cracks were observed. The cracks first appeared on the brown transverse sections and continued to several mm depth after the color of transverse sections changed from brown to pale-gray. The large cracks visible in the lower left in the photographs at 3.24 and 3.97 mm are considered to be artifacts, formed when the compacted bentonite was sliced. Cracks were only observed in Kunigel V1 compacted to 1.4, 1.6 and 1.8 Mg/m^3. No cracks appeared for Kunigel V1 compacted to 0.8 Mg/m^3 nor in Kunipia F compacted to 1.2 Mg/m^3.

Figures 5-2 to 5-6 show the results of selective dissolution analysis for Kunigel V1 compacted to 0.8, 1.4, 1.6, 1.8 Mg/m^3 and for Kunipia F compacted to 1.2 Mg/m^3, respectively. The concentration profiles of Fe obtained from the NH_4Cl, oxalate, DCB and HCl extractions are expressed as Fe-NH_4Cl, Fe-Oxalate, Fe-DCB and Fe-HCl, respectively. Fe-Total indicates the sum of concentrations of Fe obtained from these four extractions. The vertical axis is the concentration of Fe contained in unit weight of bentonite. In cutting the compacted bentonites into sections, Kunigel V1 compacted to 1.4, 1.6 and 1.8 Mg/m^3 was found to be stiff at brown colored section. It was often difficult to cut the brown colored bentonite into thin sections, because the bentonite chipped easily into fragments while being cut. Therefore, detailed Fe profiles were not obtained between 2.2 to 5.5 mm for Kunigel V1 compacted to 1.4 Mg/m^3 and between 0.9 to 3.3 mm for 1.8 Mg/m^3 Kunigel V1. Most of the corrosion products in compacted bentonite were extracted by the NH_4Cl and oxalate extractions, while DCB and HCl extractions hardly extracted any corrosion products. In the NH_4Cl extraction process, the concentration of Fe did not appreciably decrease although the extraction of 1 mol/dm^3 NH_4Cl solution was repeated three times.

Figures 5-7 to 5-11 show the results of valence analysis for Kunigel V1 compacted to 0.8,

1.4, 1.6, 1.8 Mg/m^3 and for Kunipia F compacted to 1.2 Mg/m^3, respectively. The concentration profiles of bivalent and trivalent Fe are expressed as Fe(II) and Fe(III), respectively. The concentrations of Fe(II) were determined by multiplying the concentration obtained from ICP-AES by the ratio of Fe(II) concentration to total Fe concentration obtained from spectrophotometrical analysis. The concentrations of Fe(III) were determined by subtracting the concentrations of Fe(II) from the concentration of Fe obtained from ICP-AES. The concentration profiles of Fe(II) and Fe(III) were obtained from the results of NH_4Cl and oxalate extractions. The Fe extracted by DCB and HCl extractions was negligible. High concentrations of Fe(II) were found adjacent to the carbon steel and then the concentration decreased sharply. The concentration of Fe(III) in Kunigel V1 compacted to 1.4, 1.6 and 1.8 Mg/m^3 was almost constant to about 3 mm from the carbon steel and then decreased. The concentration of Fe(III) in Kunipia F was also constant to about 0.8 mm from the steel. For Kunigel V1 compacted to 0.8 Mg/m^3, Fe(III) concentration adjacent to the carbon steel was low. The ratio of Fe(II) to Fe(III) was highest adjacent to the carbon steel and decreased with increasing distance from the steel. The transverse sections in which high concentrations of Fe(II) were detected were dark-green, while the sections in which Fe(III) was dominant were brown. The distance at which the color of transverse sections changed from dark-green to brown was in good agreement with the distance at which Fe(III) became dominant. Most of the Fe obtained from the NH_4Cl extraction was Fe(II), while Fe(III) was only extracted by oxalate extraction.

Figure 5-12 to 5-14 shows the XRD profiles of dark-green, brown and pale-yellow sections of Kunipia F compacted to 1.2 Mg/m^3 in the range from 0 to 100 % relative humidity (RH). The dark-green and brown sections dominantly contained Fe(II) and Fe(III), respectively. In the pale-yellow colored section, Fe was barely extracted. In the pale-yellow section, the diffraction peaks occurred at about 9.2^o in the range from 0 to 20% RH, and then occurred at 7.3^o to 7.6^o in the range from 40 to 60%. At 70% RH or above, the peaks occurred at about 6.1^o. The basal spacings calculated from the diffraction peaks are about 9.6 Å, 11.6 to 12.1 Å and about 14.5 Å in the range from 0 to 20%, 40 to 60% and 70 to 100% RH, respectively. The basal spacing of smectite at the pale-yellow section thus increases with increasing RH in distinct steps. This variation of basal spacing is similar to the reported variation of Na-smectite[22,23]. The profiles of dark-green and brown sections were similar to that of pale-yellow section.

5.4 Discussion

5.4.1 Corrosion products formed in compacted bentonite

In the selective dissolution analysis, NH_4Cl extraction can extract Fe^{2+} and Fe^{3+} from the pore water of compacted bentonite. Oxalate extraction is able to extract amorphous, non-crystalline or poorly ordered Fe oxides. The DCB and HCl extractions are able to extract Fe oxides of varying crystallinity and comparatively well crystallized Fe compounds, respectively[18,19]. In this study, most of the corrosion products were extracted by NH_4Cl and oxalate extractions, while Fe compounds extracted by DCB and HCl extractions were negligible. In addition, the Fe extracted by NH_4Cl extraction was mainly Fe(II). Most Fe(III) was extracted by oxalate extraction. These results suggested that the corrosion products distributed into the compacted bentonite from carbon steel were Fe^{2+} and amorphous, non-crystalline or poorly ordered Fe compounds. The corrosion products had scarcely crystallized within 3-4 years at room temperature in compacted bentonite.

The Fe(II) compounds extracted by oxalate extraction are considered to be $Fe(OH)_2$, $FeCO_3$ and green rust. However, $FeCO_3$ and green rust would have difficulty forming in pore spaces of compacted bentonite, because the concentrations of anions were expected to be quite low[13]. Therefore, the Fe(II) compound extracted by oxalate extraction was considered to be amorphous, non-crystalline or poorly ordered $Fe(OH)_2$. The Fe(III) compound extracted by oxalate extraction was also considered to be amorphous, non-crystalline or poorly ordered $Fe(OH)_3$ from a similar consideration. The colors of $Fe(OH)_2$ and $Fe(OH)_3$ are dark-green and brown, respectively. These colors were consistent with those observed on the transverse sections of compacted bentonite.

The analysis of valence indicated that $Fe(OH)_2$ was distributed adjacent to the carbon steel. $Fe(OH)_2$ decreased steeply within about 1 mm from carbon steel for Kunigel V1 compacted to 1.4, 1.6 and 1.8 Mg/m^3 and for Kunipia F. For Kunigel V1 compacted to 0.8 Mg/m^3, $Fe(OH)_2$ also decreased steeply within 2.5 mm. In this study, as the Eh of pore water was kept in the range of -200 to -400 mV, the carbon steel is considered to corrode by the following reaction[13]:

$$Fe + 2H_2O = Fe(OH)_2 + H_2 . \qquad (5\text{-}1)$$

The profiles of $Fe(OH)_2$ in compacted bentonite are considered to be the results of distribution of $Fe(OH)_2$ generated on the surface of carbon steel. The cracks observed in transverse sections of Kunigel V1 compacted to 1.4, 1.6 and 1.8 Mg/m^3 were possibly the effect of H_2 gas generated by the corrosion reaction expressed in Eq. (5-1) as discussed in Section 4.3.1 and 4.3.2. For Kunigel V1 compacted to 0.8 Mg/m^3 and Kunipia F compacted to 1.2 Mg/m^3, the H_2 gas generated on the surface of carbon steel is considered to diffuse through the compacted bentonites, and therefore no cracks appeared on the transverse section of compacted bentonite.

The valence analyses indicated that a considerable amount of $Fe(OH)_3$ was contained in the compacted bentonite. In this study, as the Eh in pore water was maintained in the range from -200 to -400 mV, minor amounts of Fe(II) would have been oxidized to Fe(III). Therefore, the $Fe(OH)_3$ in the compacted bentonite originated from the distribution of corrosion products which had been produced by electrochemical corrosion on the surface of the steel under aerobic conditions before the coupons were set in contact with compacted bentonite. These results indicated that $Fe(OH)_3$ in compacted bentonite was not easily reduced to $Fe(OH)_2$, although the Eh of pore water was maintained in the range from -200 to -400 mV for 3 to 4 years. The concentration of Fe^{3+} in pore water was considered to be extremely low because of the low solubility of $Fe(OH)_3$ so that little Fe^{3+} was reduced to Fe^{2+}. Therefore, the reduction of $Fe(OH)_3$ is considered to be quite slow.

The $Fe(OH)_3$ was found to be distributed further into the bentonite than $Fe(OH)_2$. The concentrations of $Fe(OH)_3$ in Kunigel V1 compacted to 1.4, 1.6 and 1.8 Mg/m^3 were almost constant until about 3 mm from the carbon steel and then they decreased. The concentration in Kunipia F compacted to 1.2 Mg/m^3 was also almost constant until about 0.8 mm from the steel. For Kunigel V1 compacted to 0.8 Mg/m^3, $Fe(OH)_3$ distributed until about 18 mm, and besides, a decrease in concentration of $Fe(OH)_3$ in the neighborhood of carbon steel was found. These profiles of $Fe(OH)_3$ were not clearly dependent on the distance from carbon steel. The formation of these profiles might be explained by decrease of pH in pore water immediately after the carbon steel was set in contact with compacted bentonite. The decrease of pH allowed the aerobic Fe(III) corrosion products to dissolve in the pore water and then Fe^{3+} ions migrated into the compacted bentonite. The Fe^{3+} precipitated due to increased pH, as the pH of pore water was buffered by bentonite and the H^+ was released out of the column. The decrease in pH might be caused by HCl, which was a residue of electrical corrosion, on

the surface of carbon steel.

5.4.2 Alteration to Fe-smectite

The concentration of Fe obtained by NH_4Cl extraction was $3.6x10^{-4}$ mol/g for Kunipia F compacted to 1.2 Mg/m^3 adjacent to the carbon steel. This value is comparable to about 60% of $1.18x10^{-3}$ eq/g for Kunipia F[20]. If all of the Fe obtained from NH_4Cl extraction existed as Fe^{2+} ions in the pore water of compacted bentonite, a considerable proportion of the cations in smectite interlayers in Kunipia F should exchange with Fe^{2+}, that is alteration to Fe-smectite. The kind of cation in smectite interlayer is known to affect the variation of basal spacing as a function of RH [22,23]. The basal spacing of Ca^{2+}-adsorbed smectite, which is a representative of smectite absorbing bivalent cations in the interlayers, has been reported to be about 11.6 Å at 0% RH and gradually increase from 14.5 to 16.0 Å in the range from 30 to 80% [23]. However, the basal spacing of smectite in dark-green section, in which high concentration of Fe(II) was obtained from NH_4Cl extraction, was about 9.6 Å in the range from 0 to 20% RH, and then increased to 11.6 to 12.1 Å in the range from 40 to 60%. This variation of basal spacing in dark-green section was similar to that in pale-yellow section, in which the alteration to Fe-smectite was not observed. In the XRD profiles of dark-green section, there is no diffraction peak at about 7.6^o, which corresponds to the basal spacing of 11.6 Å, at 0% RH as shown in Fig. 5-12. The diffraction peak at 5.5^o to 6.1^o, which corresponds to the basal spacing of 14.5 to 16.0 Å, was not found in the range from 40 to 60%. Thus, Fe-smectite was not detected by the XRD analyses. In the NH_4Cl extraction process, although the extraction of 1 mol/dm^3 NH_4Cl solution was repeated three times, remarkable decreases in concentration of Fe did not occur. The Fe obtained from NH_4Cl extraction was mainly Fe(II). The Fe(II) compound formed in compacted bentonite was considered to be $Fe(OH)_2$ from the results of oxalate extraction. Therefore, most of the Fe(II) obtained from NH_4Cl extraction was considered to be derived from the dissolution of $Fe(OH)_2$. The concentration of Fe^{2+} absorbing at the interlayer of smectite was considered to be quite low. The alteration of smectite to Fe-smectite in compacted bentonite, thus, does not easily occur due to the corrosion products in the pore spaces of compacted bentonite at room temperature.

This difficulty of alteration to Fe-smectite is possibly caused by the sufficiently lower concentration of Fe^{2+} than Na^+ in pore water of compacted bentonite. The reaction equation describing the replacement of Fe^{2+} on the Na-smectite surface and ion selectivity coefficients

K_{GT} are expressed by the following equations[14]:

$$2\mathrm{XNa} + \mathrm{Fe}^{2+} = \mathrm{X_2Fe} + 2\mathrm{Na}^{+} \qquad K_{GT} = \frac{2[\mathrm{X_2Fe}^{2+}][\mathrm{CEC}]\{\mathrm{Na}^{+}\}^2}{[\mathrm{XNa}^{+}]^2\{\mathrm{Fe}^{2+}\}} \qquad (5\text{-}2)$$

where $[X_2Fe^{2+}]$ and $[XNa^{+}]$ are the concentration of Fe^{2+} and Na^{+} sorbed on the smectite surface respectively, $\{Fe^{2+}\}$ and $\{Na^{+}\}$ are the activities of Fe^{2+} and Na^{+} ions in pore water, respectively, and [CEC] is the cation exchange capacity for compacted bentonite. The activities of Fe^{2+} and Na^{+} can be assumed to be the concentration of Fe^{2+} and Na^{+}, respectively. Assuming that $[XNa^{+}]$ is equal to [CEC] because of low concentration of replaced Fe^{2+} on the smectite, the ratio of Fe-smectite to CEC is expressed by the following equation:

$$\frac{2[\mathrm{X_2Fe}^{2+}]}{[\mathrm{CEC}]} = \frac{K_{GT}[\mathrm{Fe}^{2+}]}{[\mathrm{Na}^{+}]^2} \qquad (5\text{-}3)$$

The concentration of Na^{+} in pore water of compacted bentonite is assumed to be equal to that in the immersion solution of 0.01 mol/dm^3. K_{GT} was reported to be 0.06 ± 0.00 for ionic strength of 0.001 and 1.85 ± 0.29 for ionic strength of 0.05 [14]. In this study, the concentration of Fe^{2+} is controlled by the solubility of $Fe(OH)_2$ based on the following equation:

$$\mathrm{Fe(OH)_2} + 2\mathrm{H}^{+} = \mathrm{Fe}^{2+} + 2\mathrm{H_2O} \quad \mathrm{LogK}=12.9^{18)}. \qquad (5\text{-}4)$$

The pH of pore water in compacted bentonite adjacent to the carbon steel is considered to increase due to the dissolution of $Fe(OH)_2$. Therefore, H^{+} is considered to diffuse from the immersion solution to the pore water near carbon steel through compacted bentonite. In contrast, Fe^{2+} is considered to diffuse through compacted bentonite into the solution. Assuming that the diffusion of H^{+} and Fe^{2+} reached a steady state, the diffusive fluxes of H^{+} and Fe^{2+} can be expressed by the following equations:

$$J_{H^+} = D_e^{H^+}\frac{[\mathrm{H}^{+}]_{im}}{L} \qquad J_{Fe^{2+}} = D_e^{Fe^{2+}}\frac{[\mathrm{Fe}^{2+}]}{L} \qquad (5\text{-}5)$$

Here J_{H^+} and $J_{Fe^{2+}}$ are the diffusive fluxes of H^+ from the immersion solution into the pore water near carbon steel in compacted bentonite and that of Fe^{2+} into immersion solution, respectively; $D_e^{H^+}$ and $D_e^{Fe^{2+}}$ are the effective diffusion coefficients of H^+ and Fe^{2+} in compacted bentonite, respectively; $[H^+]$ is the concentration of H^+ in immersion solution and $[Fe^{2+}]$ is the concentration of Fe^{2+} in the pore water of compacted bentonite adjacent to the carbon steel. In Eq. (5-5), the concentration of H^+ in the pore water adjacent to the carbon steel is assumed to be sufficiently lower than that in the immersion solution. The concentration of Fe^{2+} in the immersion solution is assumed to be 0. As J_{H^+} is equal to $2J_{Fe^{2+}}$ at a steady state, $[Fe^{2+}]$ can be expressed by the following equation:

$$[Fe^{2+}] = \frac{D_e^{H^+}}{2D_e^{Fe^{2+}}}[H^+]_{im} \qquad (5\text{-}6)$$

Although $D_e^{H^+}$ and $D_e^{Fe^{2+}}$ have been rarely reported, the $D_e^{H^+}$ is considered to be several times higher than $D_e^{Fe^{2+}}$ from the difference between their diffusivities in bulk water. The pH of the immersion solution is 6.5 to 7.5. Therefore, $[Fe^{2+}]$ can be estimated to be about 1.0×10^{-6} mol/dm^3. The ratio of replaced Fe-smectite can be estimated to be a few % from Eq. (5-3). As the concentration of Fe^{2+} derived from the dissolution of corrosion products is, thus, sufficiently lower than that of Na^+ in pore water of compacted bentonite, the alteration of smectite to Fe-smectite rarely occurred.

5.5 Conclusions

Carbon steel, which had previously been corroded electrochemically under aerobic conditions, was left in contact with compacted bentonite under reducing conditions for 3 to 4 years at room temperature. The compacted bentonite was cut into sections and Fe distribution was investigated by selective dissolution analysis, to estimate the crystallinity of Fe-bearing compounds. The valences of Fe in compacted bentonite were also investigated spectrophotometrically. The corrosion products distributed into the compacted bentonite were considered to be amorphous, non-crystalline or poorly ordered $Fe(OH)_2$ and $Fe(OH)_3$. Furthermore, the alteration of smectite to Fe-smectite due to the corrosion products in compacted Kunipia F was analyzed by XRD. From XRD profiles, alteration of smectite to

Fe-smectite was minor.

References

1) Japan Nuclear Cycle Development Institute (JNC), *H12: Project to establish the technical basis for HLW disposal in Japan, Supporting report 3, Safety assessment of the geological system*, JNC TN1410 2000-004, (2000).
2) B. Torstenfelt, K. Andersson, H. Kipatsi, et al., "Diffusion Measurements in Compacted Bentonite," *Mat. Res. Soc. Symp. Proc.*, 11, 295-302 (1982).
3) B. Torstenfelt, H. Kipatsi, K. Andersson, et al., "Transport of Actinides through a Bentonite Backfill," *Mat. Res. Soc. Symp. Proc.*, 11, 659-668, (1982).
4) Y. Albinsson, R. Forsyth, G. Skarnemark, et al., "Leaching/Migration of UO_2-fuel in Compacted Bentonite," *Mat. Res. Soc. Symp. Proc.*, 176, 559-565 (1990).
5) Y. Albinsson, B. Christiansen-S□tmark, I. Engkvist et al., "Transport of Actinides and Tc through a Bentonite Backfill Containing Small Quantities of Iron or Copper," *Radiochim. Acta* 52/53, 283-286 (1991).
6) K. Idemitsu, Y. Tachi, H. Furuya, et al., "Diffusion of Uranium in Compacted Bentonites in the Reducing Condition with Corrosion Products of Iron," *Mat. Res. Soc. Symp. Proc.*, 412, 683-690 (1996).
7) Y. Kuroda, K. Idemitsu, H. Furuya et al., "Diffusion of Technetium in Compacted Bentonites in the Reducing Condition with Corrosion Products of Iron," *Mat. Res. Soc. Symp. Proc.*, 465, 909-916 (1997).
8) K. Idemitsu, Y. Tachi, H. Furuya et al., "Diffusion of Cs and Sr in Compacted Bentonites under Reducing Conditions and in the Presence of Corrosion Products of Iron," *Mat. Res. Soc. Symp. Proc.*, 506, 351-358 (1998).
9) H. Ramebäck, M. Skålberg, U. B. Eklund, et al., "Mobility of U, Np, Pu, Am and Cm from Spent Nuclear Fuel into Bentonite Clay," *Radiochim. Acta* 82, 167-171 (1998).
10) K. Idemitsu, X. Xia, T. Ichishima, et al., "Diffusion of Plutonium in Compacted Bentonites in the Reducing Condition with Corrosion Products of Iron," *Mat. Res. Soc. Symp. Proc.*, 608, 261-266 (2000).
11) A. Honda, N. Taniguchi, H. Ishikawa et al., "Experimental Research on Corrosion Behavior of Carbon Steel in Anaerobic Condition," *PNC Tech. Rev.*, 104, 125-134 (1997), (in Japanese).

12) N. Taniguchi, A. Honda, M. Kawasaki, et al., *The Assessment of Corrosion Type and Corrosion Rate of Carbon Steel in Compacted Bentonite*, JNC TN8400 99-003, Japan Nuclear Cycle Development Institute (JNC), (1999), (in Japanese).

13) T. Kozaki, Y. Imamura, J. Takada, et al., "Corrosion of Iron and Migration of Corrosion Products in Compacted Bentonite," *Mat. Res. Soc. Symp. Proc.*, 353, 329-336 (1995).

14) G. Kamei, C. Oda, S. Mitsui, et al., "Fe(II)-Na Ion Exchange at Interlayers of Smectite: Adsorption-desorption Experiments and a natural Analogue," *Eng. Geol.*, 54, 15-20 (1999).

15) N. Kozai, Y. Adachi, S. Kawamura et al., "Characterization of Fe-montmorillonite: A Simulant of Buffer Materials Accommodating Over pack Corrosion Product," *J. Nucl. Sci. Tech.*, 38(12), 1141-1143 (2001).

16) K. Idemitsu, S. Yano, X. Xia, et al., "Migration Behavior of Iron Ion in Compacted Bentonite under Reducing Condition by using Electromigration," *Mat. Res. Soc. Symp. Proc.*, 757, 657-664 (2003).

17) H. Sasamoto, T. Suyama and M. Shibata, *Laboratory Experiment of Iron-Bentonite Interaction*, JNC TN8400 2003-047, Japan Nuclear Cycle Development Institute (JNC), (2004), (in Japanese).

18) J. W. Stucki, B. A. Goodman and U. Schwertmann, *Iron in Soils and Clay Minerals*, D. Reidel Publishing Company, Dordrecht, Holland, 83, (1988).

19) N. Yoshinaga, C. Mizota and M. Nakai, "An Analytical Method for Noncrystalline Clay Constituents in Soils: Selective Chemical Dissolution - Difference IR Absorption Spectroscopy," *J. Clay Sci. Soc. Jpn.*, 23(1), 31 (1983), (in Japanese).

20) M. Ito, M. Okamoto, M. Shibata, et al., *Mineral composition analysis of bentonite*, PNC TN8430 93-003, Japan Nuclear Cycle Development Institute (JNC), (1993), (in Japanese).

21) Y. Kuroda, K. Idemitsu, H. Furuya, et al., "Diffusion of technetium in compacted bentonites in the reducing condition with corrosion products of iron," *Mat. Res. Soc. Symp. Proc.*, 465, 909-916 (1997).

22) T. Iwasaki and T. Watanabe, "Distribution of Ca and Na Ions in Dioctahedral Smectites and Interstratified Dioctahedral Mica/Smectites," *Clays Clay Miner.*, 36(1), 73-82 (1988).

23) T. Sato, T. Watanabe and R. Otsuka, "Effects of Layer Charge, Charge Location, and Energy Change on Expansion Properties of Dioctahedral Smectites," *Clays Clay Miner.*, 40(1), 103-113 (1992).

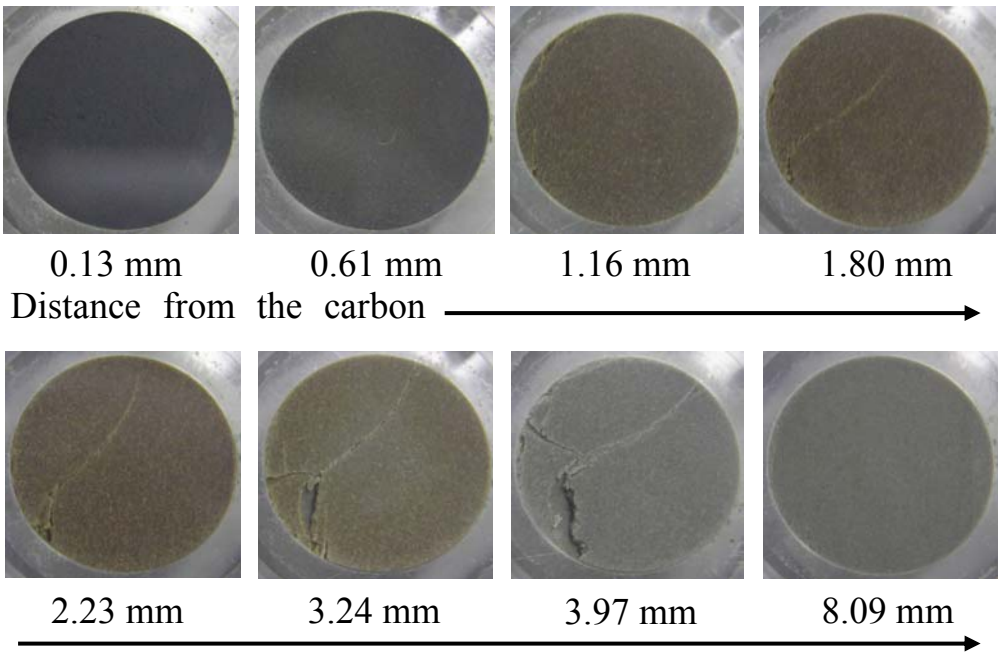

Fig. 5-1 Photographs of transverse sections of Kunigel V1 compacted to 1.6 Mg/m^3 (The large cracks visible in the lower left in the photographs at 3.24 and 3.97 mm are considered to be artifacts, formed when the compacted bentonite was sliced.)

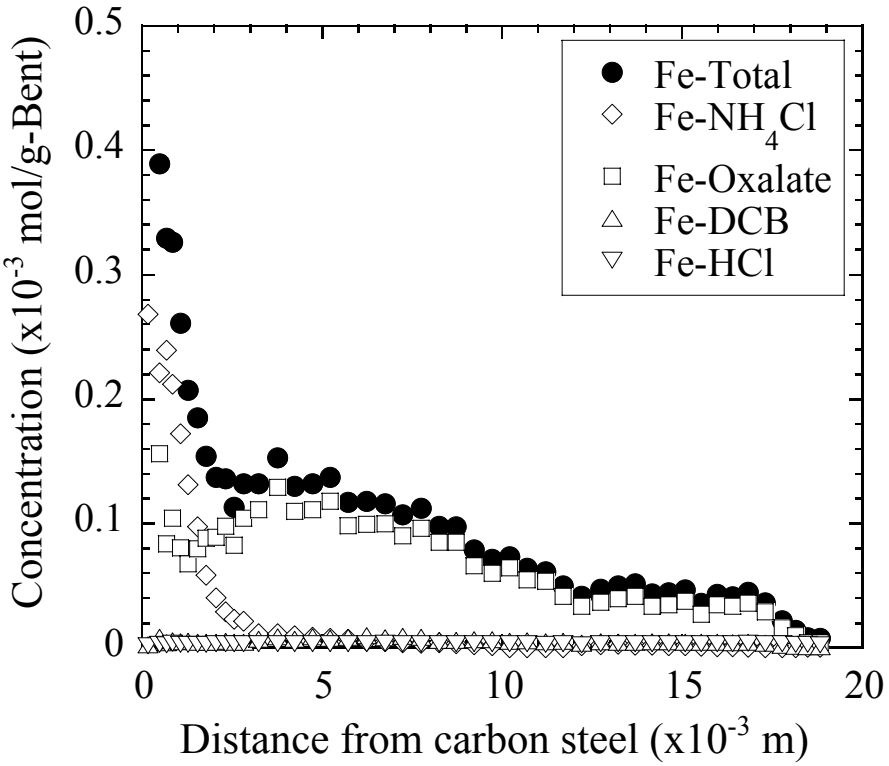

Fig. 5-2 Results of selective dissolution analysis for Kunigel V1 compacted to 0.8 Mg/m^3

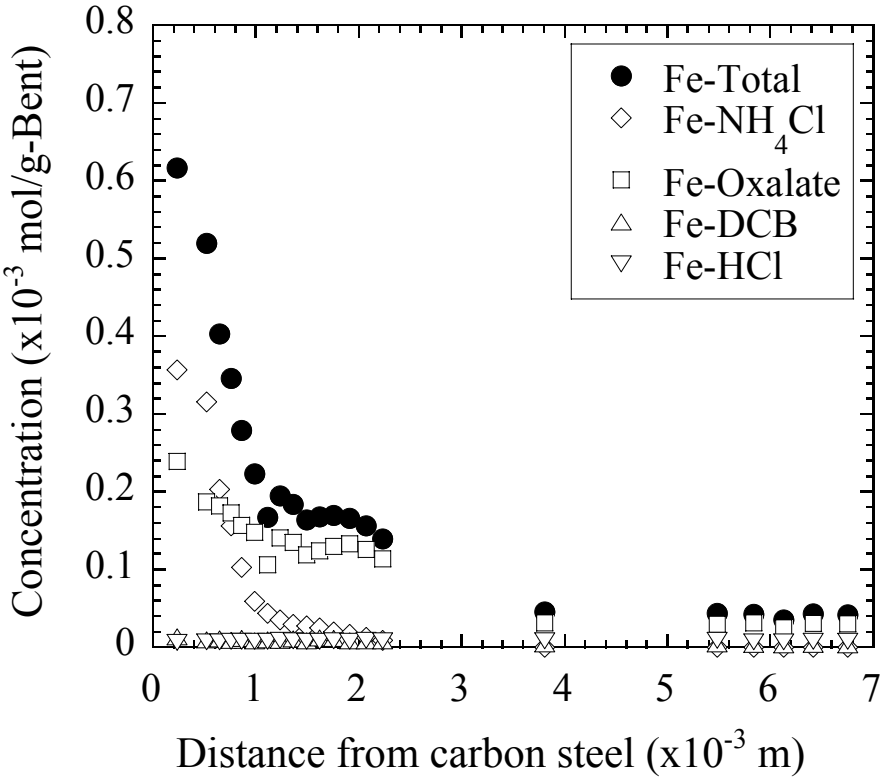

Fig. 5-3 Results of selective dissolution analysis for Kunigel V1 compacted to 1.4 Mg/m^3

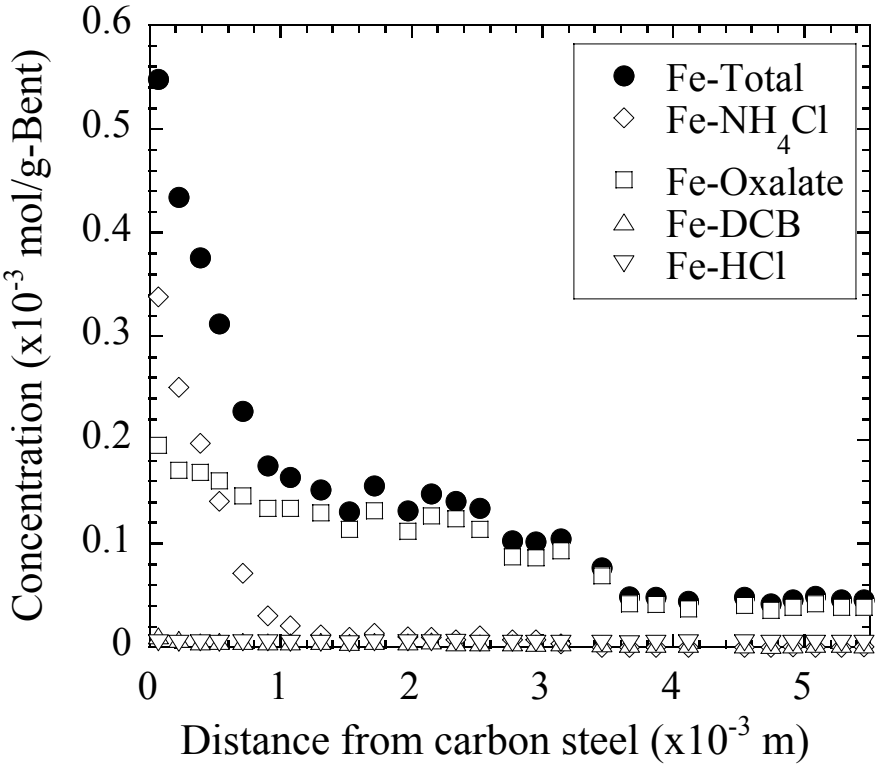

Fig. 5-4 Results of selective dissolution analysis for Kunigel V1 compacted to 1.6 Mg/m^3

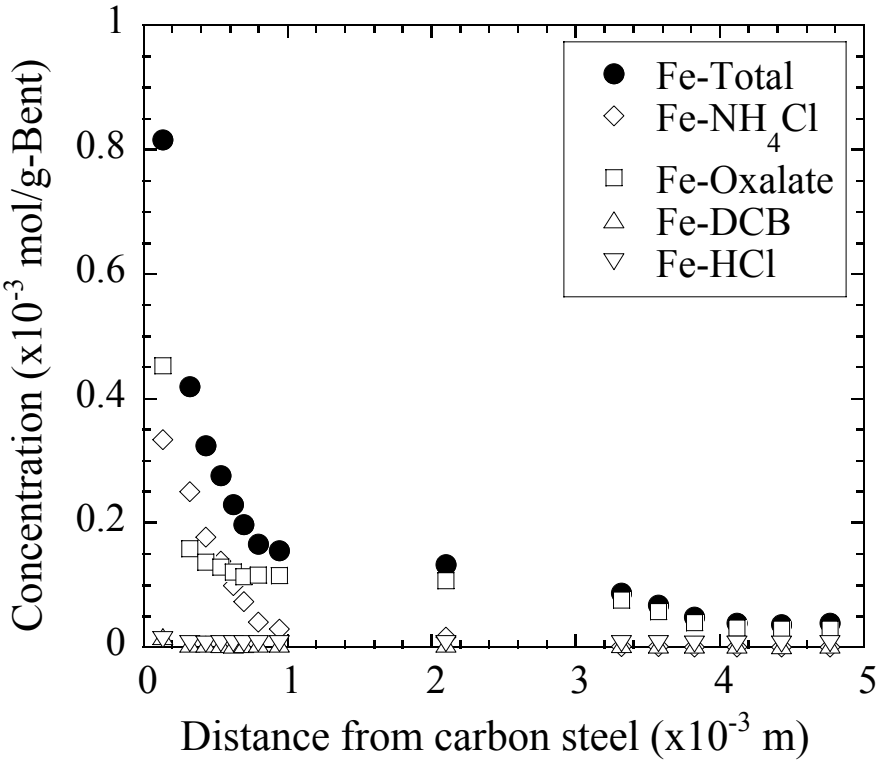

Fig. 5-5 Results of selective dissolution analysis for Kunigel V1 compacted to 1.8 Mg/m^3

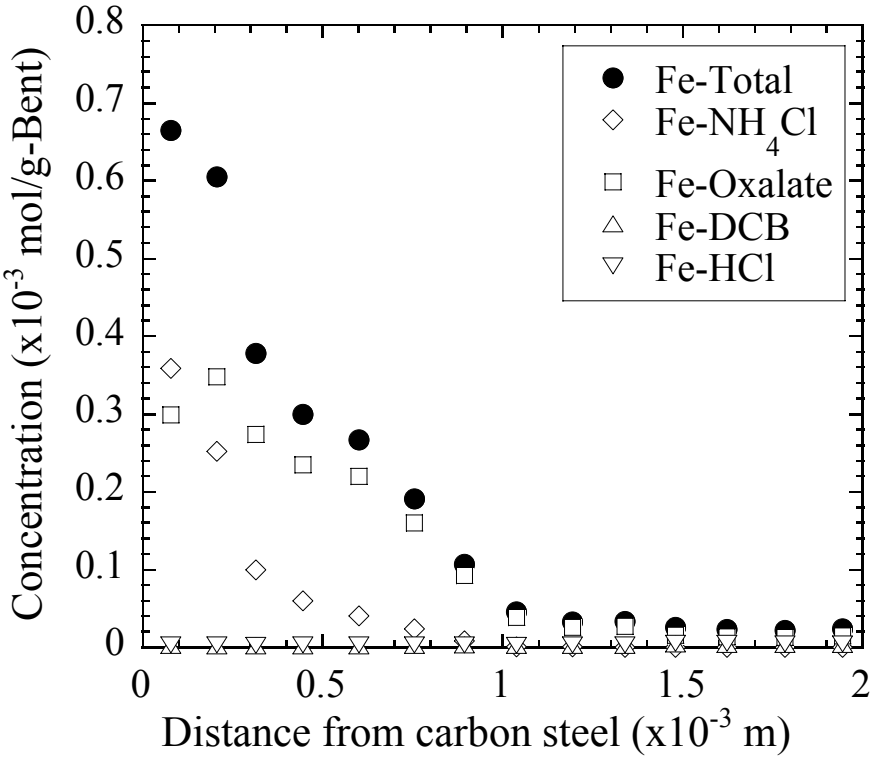

Fig. 5-6 Results of selective dissolution analysis for Kunipia F compacted to 1.2Mg/m^3

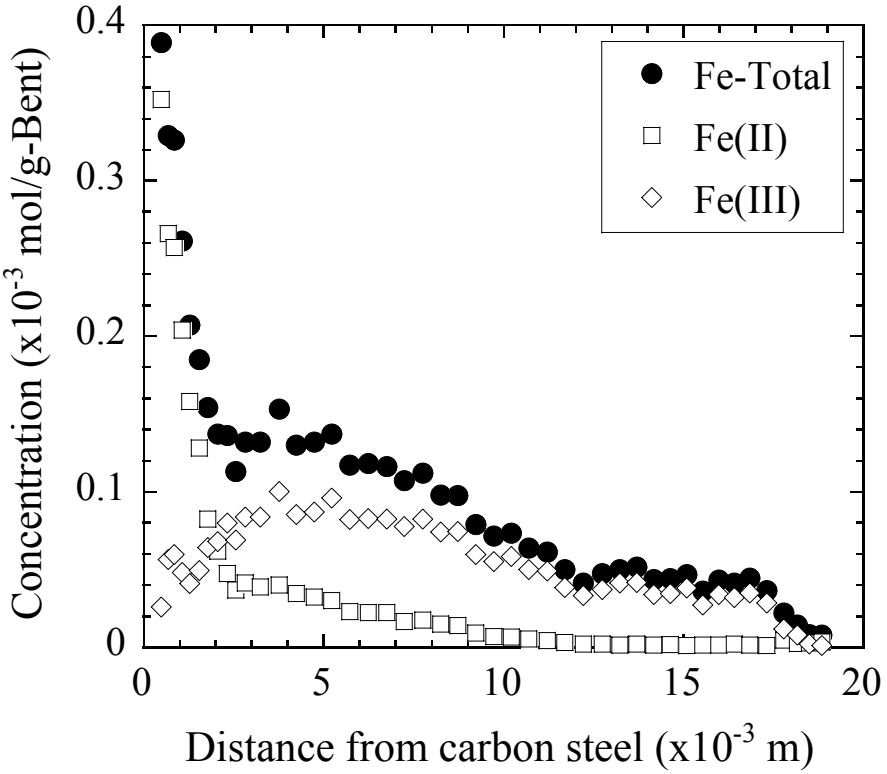

Fig. 5-7 Results of valence analysis for Kunigel V1 compacted to 0.8 Mg/m^3

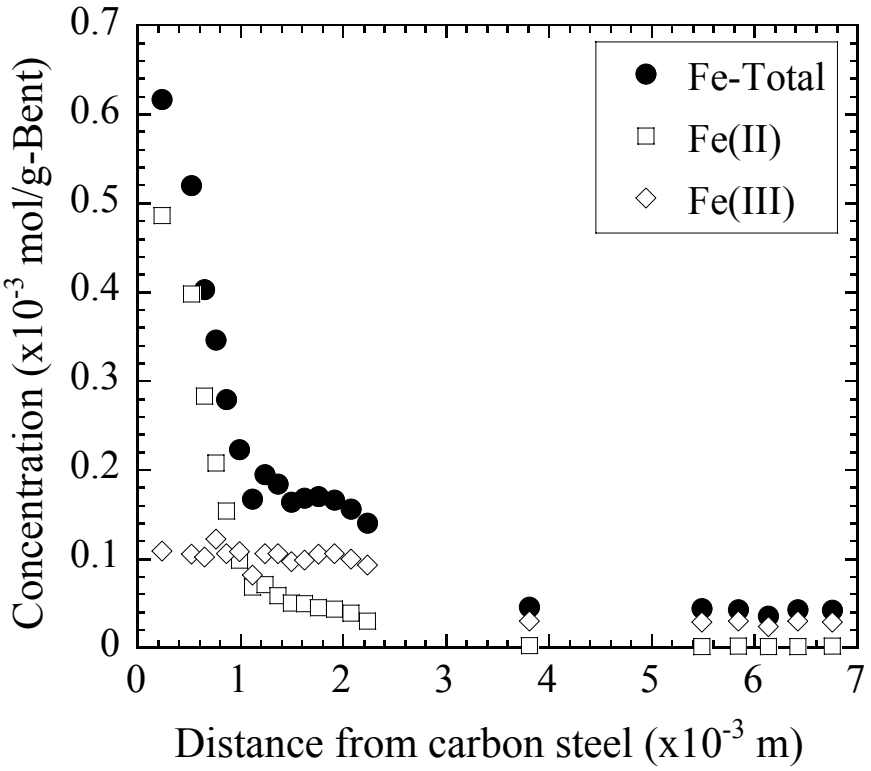

Fig. 5-8 Results of valence analysis for Kunigel V1 compacted to 1.4 Mg/m^3

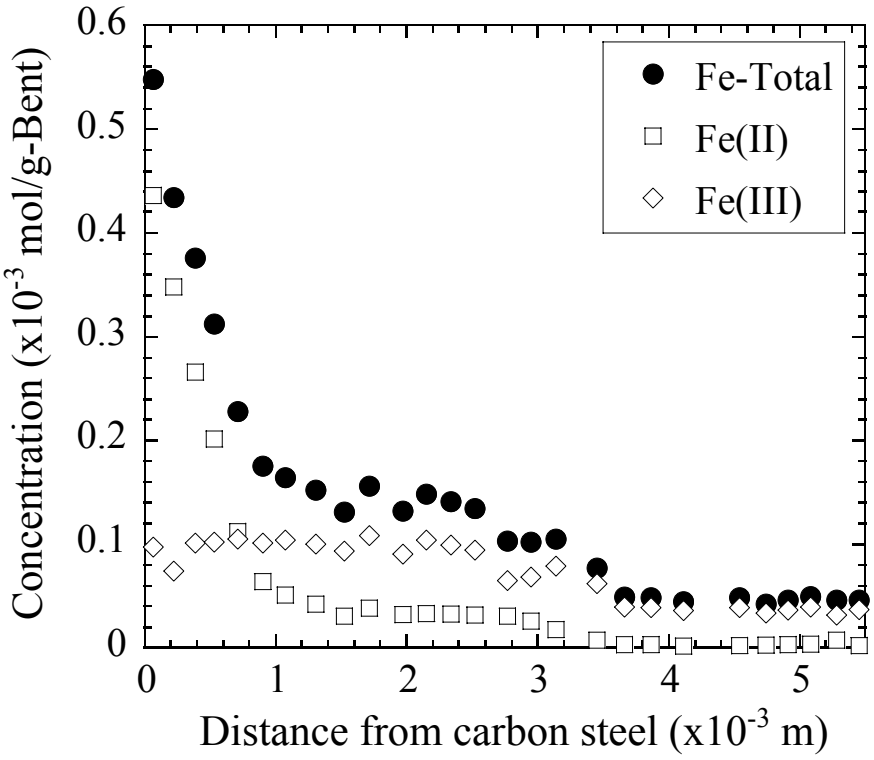

Fig. 5-9 Results of valence analysis for Kunigel V1 compacted to 1.6 Mg/m^3

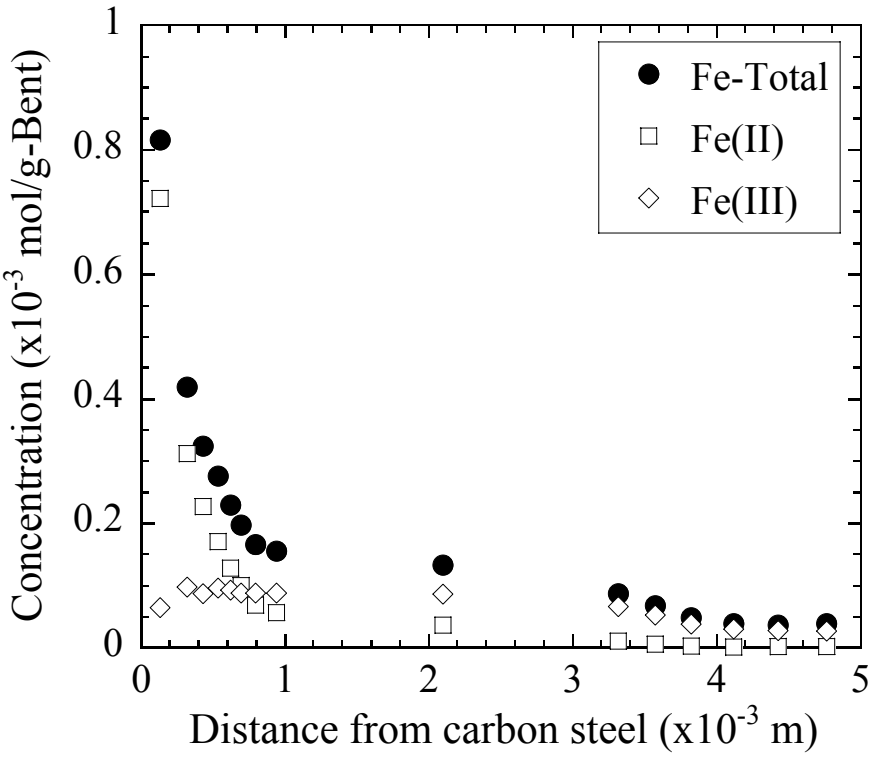

Fig. 5-10 Results of valence analysis for Kunigel V1 compacted to 1.8 Mg/m^3

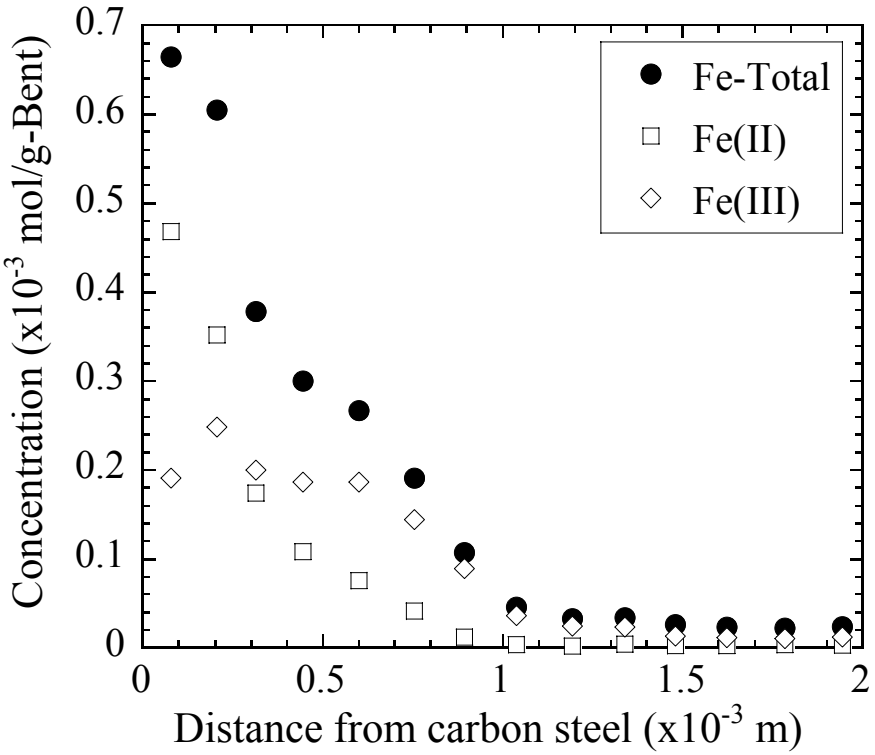

Fig. 5-11 Results of valence analysis for Kunipia F compacted to 1.2 Mg/m^3

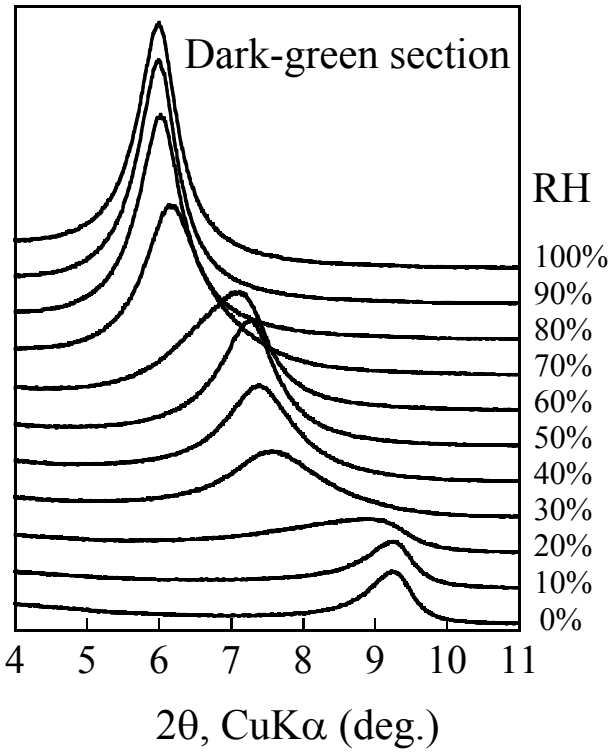

Fig. 5-12 XRD profiles of dark-green section of Kunipia F compacted to 1.2 Mg/m^3 in the range from 0 to 100 % RH

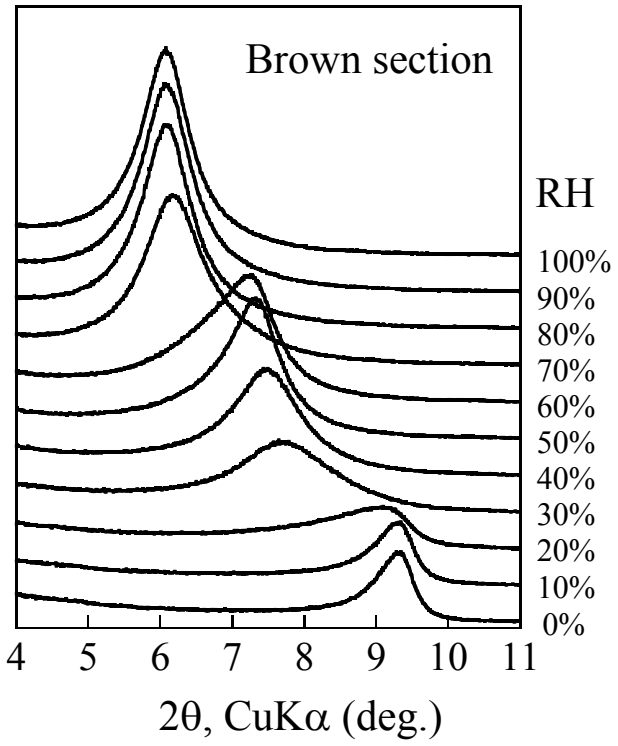

Fig. 5-13 XRD profiles of brown section of Kunipia F compacted to 1.2 Mg/m^3 in the range from 0 to 100 % RH

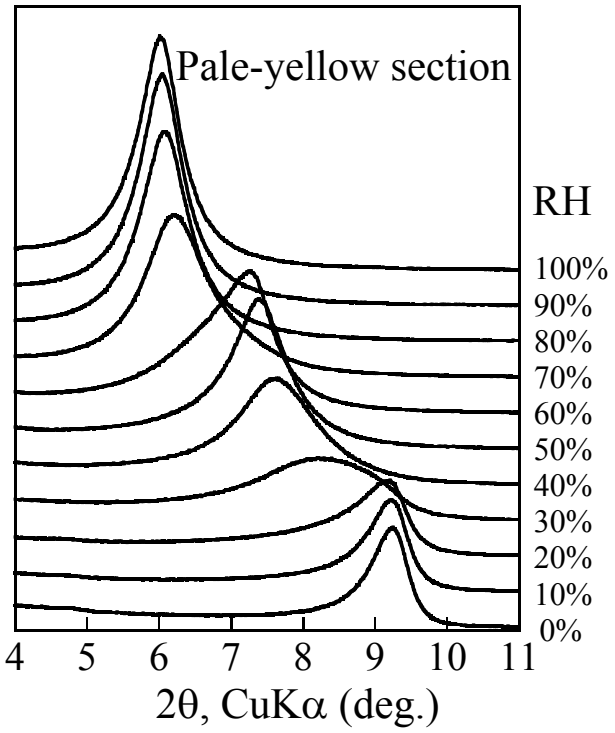

Fig. 5-14 XRD profiles of pale-yellow section of Kunipia F compacted to 1.2 Mg/m^3 in the range from 0 to 100 % RH

Chapter 6
Montmorillonite alteration in compacted bentonite in contact with carbon steel for ten years

6.1 Introduction

Smectite, which is a major component of bentonite, might be altered to other minerals by interactions with the corrosion products. Such an alteration could result in loss of swelling and self-healing capacity. After the overpack has a mechanical failure due to the corrosion, the radionuclides contained in vitrified waste will dissolve into the groundwater and diffuse through the compacted bentonite[1)]. The diffusion and sorption behaviours of radionuclides are affected not only by the alteration of smectite but also by the corrosion products migrating into compacted bentonite. Further, the corrosion products affect the chemical composition and redox potential of pore water in compacted bentonite.

The stability of smectite has been reported to be affected by the presence of metal Fe and Fe oxides in aqueous solutions. Lantenois et al. (2005)[2)] has investigated the interaction between metal Fe and a variety of natural and synthetic smectite samples at 80^{o}C by batch experiments and has reported that smectite was destabilized to form newly formed 1:1 phyllosilicate phases (odinite and crondstedtite) under basic pH conditions. Wilson et al. (2006)[3)] has investigated the stability of Na-montmorillonite between 80 and 250^{o}C and reported that Fe-rich smectite, whose swelling property was lower than the montmorillonite starting material, and berthierine was identified at 250^{o}C. Guillaume et al. (2003)[4)] has reported that the alteration of montmorillonite to chlorite and saponite were identified in batch experiments performed at 300^{o}C in the presence of metallic Fe and magnetite powder in low-salinity solutions. Guillaume et al. (2004)[5)] has reported that the alteration of montmorillonite to high-charge trioctahedral Fe^{2+}-rich smectite was found by batch experiments in the presence of magnetite and hematite in low-salinity solutions at 300^{o}C. However, all these experiments were performed by the batch method. The alteration of smectite in compacted bentonite when it is placed in contact with carbon steel, which represents the simulated condition in a nuclear repository, has not been studied experimentally.

The corrosion product that is thermodynamically stable under expected geological conditions in a repository is magnetite or siderite for groundwater containing high-concentrations of CO_3^{2-} ion[1)]. In chapter 5, the corrosion products formed in compacted

bentonite is identified to be amorphous, non-crystalline or poorly ordered $Fe(OH)_2$ and $Fe(OH)_3$. Ferrous hydroxide possibly increases the concentration of Fe^{2+} in the pore water of compacted bentonite and affects the sorption behaviour of radionuclides. Ferrous hydroxide is considered to crystallize on the thermodynamically stable minerals in the long term. However, such crystallization has not been confirmed by experimental studies. Therefore, the mineralogical evolution of ferrous hydroxide in compacted bentonite should be investigated experimentally by long-term corrosion experiment.

In this study, carbon steel was placed in contact with compacted bentonite under anaerobic conditions for ten years at 80°C. The compacted bentonite was analyzed by X-ray diffraction (XRD) in order to investigate the presence of newly formed phyllosilicates resulting from the alteration of montmorillonite due to its interaction with corrosion products. The oriented samples prepared from the powder of compacted bentonite were analyzed by XRD in order to identify the clay minerals contained in compacted bentonite. The possibility of montmorillonite alteration was also discussed from the cation exchange capacity (CEC) of compacted bentonite. The corrosion products distributed in compacted bentonite were investigated by selective dissolution analysis[6], to estimate the crystallinity of Fe-bearing compounds. The valence of Fe in the corrosion products was spectrophotometrically determined. From these analyses, the corrosion products of carbon steel in compacted bentonite were determined.

6.2 Experimental

6.2.1 Materials

The carbon steel used in this study was SM400B, which is one of the candidate overpack materials. The carbon steel coupons measured 30 × 30 × 2 mm. Each carbon steel coupon was wet-polished with 800-grade grinding papers. The composition of SM400B is listed in Table 1.

The bentonites used were Kunipia F® and Kunigel V1® (Kunimine Industries Co. Ltd.). Kunipia F consists of over 95 wt% montmorillonite[7]. Kunigel V1 consists of 46 to 49 wt% montmorillonite, 37 to 38 wt% chalcedony and a few wt% of minor minerals, i.e., plagioclase, calcite, dolomite, analcime and pyrite[7]. Kunipia F and Kunigel V1 were compacted to dry densities of 1.8 Mg/m^3.

Simulated sea water (SW), simulated sea water containing a high concentration of carbonate

(SWC) and low-saline solution (LS) were used in the experiment. The composition of the SW is listed in Table 2. The SWC was prepared by adding $NaHCO_3$ to the SW until the concentration of $NaHCO_3$ was 0.1 mol/dm^3. The LS contained 2.5×10^{-3} mol/dm^3 of $NaHCO_3$ and NaCl. The initial pHs of the SW, SWC and LS were 7.9, 8.7 and 9.1, respectively. These solutions were prepared from deionized water degassed in an N_2 glove box, in which the concentrations of O_2 and CO_2 were maintained lower than 1 ppm.

Figure 6-1 schematically shows the titanium column used in this study. The column consists of upper and lower lids and a sample holder between the lids and filters. The sample holder has a cylindrical sample compartment (diameter, 42 mm and thickness, 14 mm), in which carbon steel coupon is placed and bentonite is compacted. The carbon steel coupons are positioned at the centre of the compacted bentonite. A ceramic filter is placed on each side of the bentonite sample in order to avoid loss of material from the bentonite during the experiment. The upper and lower lids have an opening through which the solution is allowed to soak into the compacted bentonite. The column was completely immersed in the solution during the experiment.

6.2.2 Procedures

The carbon steel coupon and bentonite was compacted within the cylindrical compartment of the column, and then the column was immersed in the experimental solution. The column was immersed for ten years in an N_2 glove box. The column into which Kunipia F was compacted was immersed in SW at 80^{o}C. The columns into which Kunigel V1 was compacted were immersed in SW, SWC and LS at 80^{o}C. After ten years, the column was frozen in liquid nitrogen following which the compacted bentonite was removed from the column. The frozen compacted bentonite was removed from the carbon steel coupon by a hammer. The compacted bentonite was sliced into sections from the surface in contact with carbon steel. The sections were analyzed by XRD in order to identify the newly formed phyllosilicates. The CEC of each section was analyzed. The corrosion products in compacted bentonite were analyzed by selective dissolution analysis for Fe content[6]. The valence of Fe in each section was determined spectrophotometrically. The procedures for XRD, CEC and selective dissolution and valence analyses are described in Sections 6.2.3, 6.2.4 and 6.2.5, respectively. All procedures after the compaction of bentonite were performed in an N_2 glove box.

6.2.3 Procedures for XRD analysis

The compacted bentonite was sliced into sections having thickness ranging from 0.2 to 1.0 mm. The sections were dried at room temperature and then ground into powder. The bentonite powders were pressed onto silicone plates and analyzed by XRD (Rigaku Corporation, rint 2100). In the XRD analysis, the relative humidity was controlled at 10% intervals in a range from 0 to 100% in order to measure the basal spacings of clay minerals.

The bentonite powder was dispersed in deionized water. After the dispersed solution was left for a few minutes, the supernatant of the solution was taken and a small amount of the supernatant was dropped on silicone plates. The silicone plates were dried at room temperature for 24 h. The basal spacings of clay minerals in these oriented samples were analyzed by XRD. Furthermore, 20% of ethylene glycol solution was dropped on the oriented sample and the sample was dried for 24 h at room temperature. The oriented samples with ethylene glycol (EG) treatment were also analyzed by XRD. The clay minerals were identified from the difference in the basal spacings between the oriented samples with EG treatment and that with no EG treatment. The XRD analysis was performed using CuKα radiation at 40kV and 300mA.

6.2.4 Cation exchange capacity (CEC) analysis

The compacted bentonite was sliced into sections weighing 0.1 to 0.4 g. The sliced sections were dried at room temperature for 24 h, and then placed into polyethylene centrifuge tubes. To remove the corrosion products, 0.1 mol/dm^3 HCl solution was added to the tubes. Immediately after the HCl solution was added, the tubes were shaken and centrifuged for 10 min at 6000 rpm by a centrifuge (Hettich, EBA20), and then the supernatant was removed. After the pretreatment of HCl solution, 1 mol/dm^3 NH_4Cl solution was added to the tubes in order to saturate the cation exchange site with NH_4^+. After shaking for 24 h, the tubes were centrifuged for 10 min at 6000 rpm and then the supernatant was removed. The NH_4Cl treatment was repeated three times. To extract the residual NH_4Cl from the bentonite, 8 ml of 80% ethanol was added to the tubes. The tubes were centrifuged for 10 min at 6000 rpm and then the supernatant was removed. Washing by using 80% ethanol was repeated four times. After the washing, 4 ml of 0.5 mol/dm^3 KCl solution was added to the tubes. After shaking for 24 h, the tubes were centrifuged for 10 min at 6000 rpm and then 200 μl aliquots of supernatant from each section were diluted to 1000 ml by deionized water. The concentration

of NH_4^+ in the diluted supernatants was measured by a chromatograph (Toso Corporation, 2010). The CEC of bentonite was calculated from the concentration of NH_4^+. KCl treatment was repeated until no NH_4^+ was detected.

6.2.5 Procedures for selective dissolution and valence analyses

The compacted bentonite was sliced into sections weighing 0.05 to 0.2 g. After the slicing, the compacted bentonite sections were placed in polyethylene centrifuge tubes. NH_4Cl and oxalate extraction were carried out in order to extract Fe^{2+} and Fe^{3+} from the pore water of compacted bentonite and to extract amorphous, non-crystalline or poorly ordered Fe oxides, respectively. The procedures of NH_4Cl and oxalate extraction are described in Section 5.2.3.

After the oxalate extraction, 6 ml of 1 mol/dm^3 HCl solution was added to the centrifuge tubes in order to extract a comparatively well crystallized Fe compound. The tubes were shaken for approximately 24 h and then centrifuged for 10 min at 3000 rpm. After centrifuging, the concentration of Fe in the supernatant was measured by ICP-AES. The concentrations of bivalent Fe and the total concentration of Fe were also measured by the spectrophotometer. The measurements by ICP-AES and spectrophotometer were carried out by using the same procedures as those in the NH_4Cl extraction. The extraction using HCl solution was repeated until the total concentration of Fe in the supernatant measured by the spectrophotometer became identical to that obtained by HCl extraction from the bentonite not used for the experiment.

6.3 Results

Figure 6-2 show a photograph of the surface in contact with carbon steel coupon and the sections of Kunipia F immersed in SW. The sections of Kunipia F were dark green adjacent to the carbon steel. The dark-green colour becomes pale with increasing distance from the carbon steel. A similar colour change was found in the Kunigel V1 immersed in SW, SWC and LS.

Figure 6-3 shows the XRD patterns of powdered Kunipia F measured at 30^{o}C, 0% relative humidity. The patterns of (a), (b) and (c) correspond to the sample at 1.1 mm from the carbon steel, at 0.5 mm from the carbon steel and adjacent to the carbon steel, respectively. In the case of the pattern at a distance of 1.1 mm from the carbon steel, in which any Fe was hardly detected, a peak was found at approximately 9.3^o, and labelled as M001 in Fig. 6-3. This peak

corresponds to 001 reflection of montmorillonite in Kunipia F, of which the basal spacing is approximately 9.5 Å. The peaks labelled M are considered to be the integral series of the 001 reflection. M020 peak corresponds to 020 reflection of montmorillonite. Q peak corresponds to quarts. On the other hand, in the XRD pattern for Kunipia F adjacent to the carbon steel, the peak labelled G at approximately 10.8^{o} is found in addition to the M001 reflection. This peak is also found in the pattern at 0.5 mm from carbon steel, in which approximately 2×10^{-4} mol/g-Bent of Fe was extracted. Furthermore, there are small peaks labelled L in the pattern adjacent to the carbon steel. In the XRD analysis for the Kunipia F powder adjacent to the carbon steel, the relative humidity was controlled at 10% intervals in the range from 0 to 100% in order to measure the basal spacings. In the Kunipia F powder adjacent to the carbon steel, the diffraction peak at approximately 9.3^{o} was not shifted for relative humidity from 0 to 10%. However, the diffraction peak shifted at 7.0^{o} to 7.4^{o} in the range from 30 to 60%, and then the peak occurred at approximately 6.1^{o} at 70% relative humidity or above. Thus, the 001 reflection of montmorillonite was confirmed to be the swelling behaviour. However, the diffraction peak at approximately 10.8^{o} was not shifted by the increasing relative humidity, indicating no swelling ability.

Figure 6-4 shows the XRD patterns of powdered Kunigel V1 measured at 30^{o}C, 0% relative humidity. The patterns of (a), (b), (c) and (d) correspond to the sample not used for the experiment, the sample adjacent to the carbon steel immersed in SW, in SWC and in LS, respectively. The peaks labelled M001 at approximately 9.3^{o} corresponds to the 001 reflection of montmorillonite in Kunigel V1. The peaks labelled M are considered to be the integral series of the 001 reflection. M020 peak corresponded to the 020 reflection of montmorillonite. Q peak corresponds to quarts. In the XRD patterns of Kunigel V1, the peak labelled G at approximately 10.8^{o} is rarely found.

Figure 6-5 shows the XRD patterns of oriented samples prepared from the Kunipia F powder adjacent to the carbon steel. The XRD patterns of oriented samples before and after EG treatment are shown in the upper and lower patterns, respectively. In the pattern before EG treatment, peaks at 9.1^{o} and 10.8^{o} are found. The peak at 9.1^{o} observed in the XRD pattern before EG treatment is shifted at 5.5^{o} after EG treatment. Thus, the swelling behaviour of the 001 reflection of montmorillonite is also found in the pattern of the oriented sample with EG treatment. The swelling behavior of montmorillonite with EG treatment is also found in the XRD patterns of Kunigel V1 immersed in SW, SWC and LS.

Figures 6-6 to 6-9 show the results of CEC and selective dissolution analyses for Kunipia F, Kunigel V1 immersed in SW, SWC and LS, respectively. The concentration profiles of Fe obtained from the NH_4Cl, oxalate and HCl extractions are expressed as Fe-NH_4Cl, Fe-Oxalate and Fe-HCl, respectively. Fe-Total indicates the sum of concentrations of Fe obtained from these three extractions. Symbol × shows the CEC of compacted bentonite. The vertical axis is the concentration contained in unit weight of bentonite. Most of the corrosion products in compacted bentonite were extracted by the NH_4Cl and oxalate extractions, while HCl extractions hardly extracted any corrosion products. In the NH_4Cl extraction process, the concentration of Fe did not appreciably decrease although the extraction of 1 mol/dm^3 NH_4Cl solution was repeated three times.

Figures 6-10 to 6-13 show the results of the valence analysis of Kunipia F, Kunigel V1 immersed in SW, SWC and LS, respectively. The concentration profiles of bivalent and trivalent Fe are expressed as Fe(II) and Fe(III), respectively. The concentrations of Fe(II) were determined by multiplying the concentration obtained from ICP-AES by the ratio of Fe(II) concentration to total Fe concentration obtained from spectrophotometrical analysis. The concentrations of Fe(III) were determined by subtracting the concentrations of Fe(II) from the concentration of Fe obtained from ICP-AES. Most of the Fe extracted from the compacted bentonite was Fe(II). Most of the Fe obtained from the NH_4Cl extraction was Fe(II), while only Fe(III) was extracted by oxalate extraction.

6.4 Discussion

6.4.1 Alteration of montmorillonite in Kunipia F

A peak labelled G at approximately 10.8^o was found in the XRD pattern for powdered Kunipia F adjacent to the carbon steel, as shown in Fig. 6-3. This peak was also found in the pattern at 0.5 mm from the carbon steel from which approximately 2×10^{-4} mol/g-Bent of Fe was extracted. However, this peak was not found in the pattern at 1.1 mm distance from carbon steel in which any Fe was hardly detected. Therefore, the peak labelled G at approximately 10.8^o correspond to the Fe compound formed in the pore space of Kunipia F by the corrosion of carbon steel or to the newly formed phyllosilicates resulting from the alteration of montmorillonite due to the interaction with corrosion products.

The basal spacings of 1:1 phyllosilicates are known to be approximately 7 Å for serpentine minerals and most of the kaorin minerals or 10 Å for halloysite[8]. The basal spacing of 2:1

phyllosilicates are known to be 9.3 Å or above[8]. The peak at approximately 10.8° corresponds to the basal spacing of approximately 8.2 Å. This basal spacing is different from those of the 1:1 and 2:1 phyllosilicates. For the experiment carried out at 80°C by a batch method, Lantenois et al. (2005)[2] reported that smectite altered to odinite and crondstedite due to the interaction with metal Fe. The basal spacings of odinite and crondstedite were reported to be approximately 7 Å, which was different from that of approximately 8.2 Å found in this study. Therefore, the peak at approximately 10.8° does not correspond to the newly formed 1:1 or 2:1 phyllosilicates. If the montmorillonite in Kunipia F is altered to other minerals, the CEC of Kunipia F should be decreased. However, the CEC of Kunipia F adjacent to the carbon steel hardly decreased as shown in Fig. 6-6. Consequently, the results of XRD and CEC analyses indicate that the peaks at approximately 10.8° found in the XRD patterns at 0.5 mm from carbon steel and adjacent to the carbon steel in Fig. 6-3 correspond to the corrosion products formed in Kunipia F. The alteration of montmorillonite in Kunipia F due to the interaction with corrosion products was not observed in this study.

6.4.2 Corrosion products formed in Kunipia F

The Fe compounds under anaerobic conditions are considered to be Fe oxide or hydroxide, siderite and green rust as indicated in Section 4.3.2. Green rust, or Fe(II)-Fe(III) hydroxy compounds, consists of positively charged hydroxide sheets containing anions such as CO_3^{2-}, SO_4^{2-} or Cl^- at the interlayers. Two types of stacking for the hydroxide sheets, a rhombohedral Green rust (GR1) and a hexagonal Green rust (GR2), have been reported. For GR1(Cl^-), which consists of rhombohedral hydroxide sheets containing Cl^- at the interlayer, 003 reflection has been reported to be at approximately 8 Å[9]. For the experiment of Kunipia F, SW was used for the immersion solution. SW contained 5.6×10^{-1} mol/dm^3 of Cl^-, which was two orders of magnitude higher than the concentration of HCO_3^- and SO_4^{2-} as listed in Table 2. Therefore, it is unlikely that green rust containing CO_3^{2-} or SO_4^{2-} forms at the interlayer. Furthermore, the 003 reflection has been reported to be at approximately 11.8° for CuKα radiation for the green rust containing CO_3^{2-} or SO_4^{2-} at the interlayer[10], which is quite different from the peak observed in this study. These results suggest that the peak at approximately 10.8° found in the XRD patterns at 0.5 mm from carbon steel and adjacent to the carbon steel in Fig. 6-3 correspond to the 003 reflection of GR1(Cl^-). In the pore space of Kunipia F, GR1(Cl^-) is considered to be formed.

The standard formulae of GR1(Cl^-) has been reported to be $Fe^{II}_3Fe^{III}(OH)_8Cl{\cdot}nH_2O$[9], although the composition of green rust can vary. As shown in Fig. 6-10, Fe(III) extracted from Kunipia F adjacent to the carbon steel was approximately 5×10^{-5} mol/g-Bent. Therefore, Fe(II) exceeded in the pore space of Kunipia F even when all the Fe(III) was used to form GR1(Cl^-), indicating that the other Fe(II) compounds coexisted in the pore space of Kunipia F. The Fe(II) compounds formed in Kunipia F, other than green rust, were considered to be Fe oxide, Fe hydroxide and siderite. From the result of NH_4Cl extraction, there is a possibility that Fe(II) exists as Fe^{2+} in the pore water. Siderite is known to have a 104 reflection at 32^o for CuKα radiation. However, no diffraction peak was found at 32^o in the XRD pattern adjacent to carbon steel as shown in Fig. 6-3, indicating that siderite was not formed in Kunipia F. In the selective dissolution analysis, most of Fe(II) was extracted by the oxalate extractions, while HCl extractions hardly extracted any corrosion products. The oxalate extraction was used to extract amorphous, non-crystalline or poorly ordered Fe oxides[6]. Therefore, the amorphous, non-crystalline or poorly ordered $Fe(OH)_2$ is considered to be formed in Kunipia F in addition to GR1(Cl^-). Fe(II) obtained from NH_4Cl extraction is considered to contain the Fe(II) dissolved from $Fe(OH)_2$ during the extraction. Therefore, although 5×10^{-4} mol/g-Bent of Fe, which is comparable to the CEC of Kunipia F, was obtained from the NH_4Cl extraction adjacent to the carbon steel, the concentration of Fe^{2+} in the pore water of Kunipia F is considered to be fairly lower than that obtained from the NH_4Cl extraction. This is confirmed from the fact that in the NH_4Cl extraction process the Fe concentration did not decrease remarkably, although the extraction of 1 mol/dm^3 NH_4Cl solution was repeated three times.

In the XRD pattern of powdered Kunipia F adjacent to the carbon steel, small peaks labelled L were found at approximately 27, 36 and 46^o as shown in Fig. 6-3. These peaks are considered to correspond to the small amount of lepidocrocite formed in the pore space of Kunipia F. Under the conditions in this study, the carbon steel is considered to corrode by the following reaction as described in Section 4.3.2 and 5.4.1:

$$Fe + 2H_2O = Fe(OH)_2 + H_2 . \qquad (6\text{-}1)$$

Green rust is known to be formed as intermediates in the oxidation process of $Fe(OH)_2$. The oxidation of green rust is known to yield lepidocrocite[13]. In this study, these corrosion

products coexisted in Kunipia F. Therefore, under this experimental condition, $Fe(OH)_2$ formed in Kunipia F due to the corrosion of carbon steel was oxidized to GR1(Cl^-) as intermediates, and then GR1(Cl^-) was oxidized to lepidocrocite.

6.4.3 Alteration of montmorillonite and corrosion products formed in Kunigel V1

As shown in Fig. 6-7 to 6-9, CEC of Kunigel V1 immersed in SW, SWC and LS adjacent to the carbon steel hardly decreased. The diffraction peak at approximately 12.6^o corresponding to approximately 7 Å, which corresponds to the basal spacings of most of 1:1 phyllosilicates[10], was not found. These results suggest that the alteration of montmorillonite due to the interaction with corrosion products was hardly occurred in Kunigel V1 as well. However, in contrast to the case of the XRD patterns of powdered Kunipia F in Fig. 6-3, the diffraction peak at 10.8^o was hardly found in the XRD patterns for Kunigel V1 adjacent to the carbon steel, as shown in Fig. 6-4. These results indicate that any GR1(Cl^-) was hardly formed in Kunigel V1. As shown in Fig. 6-8, the corrosion products of carbon steel barely migrated into Kunigel V1 in comparison with those in Kunigel V1 immersed in SW and LS. In the XRD patterns of Kunigel V1 immersed in SWC, the broad diffraction peak at approximately 32^o was found, while the diffraction peak was not found in the other XRD patterns, as shown in Fig. 6-4. This peak possibly corresponded to siderite, and therefore siderite might be precipitated adjacent to the carbon steel for Kunigel V1 immersed in SWC. For Kunigel V1 immersed in SW and LS, most of Fe(II) was extracted by the oxalate extractions. Therefore, the amorphous, non-crystalline or poorly ordered $Fe(OH)_2$ is considered to be formed in Kunigel V1 immersed in SW and LS.

6.5 Conclusions

In order to investigate the alteration of montmorillonite in compacted bentonite in contact with carbon steel experimentally and to investigate the mineralogical evolution of ferrous hydroxide in compacted bentonite, carbon steel was placed in contact with compacted bentonite under anaerobic conditions for ten years at 80^{o}C. From the XRD analysis, the newly formed phyllosilicates, which were produced by the alteration of montmorillonite due to the interaction with corrosion products, were not identified in compacted bentonite. The CEC of compacted bentonite adjacent to the carbon steel, from which a high concentration of Fe was extracted, hardly decreased. Therefore, although Fe(II)-rich saponite or barthierine was

expected to be thermodynamically stable under the conditions in this study[12], the alteration of montmorillonite barely occurred in compacted bentonite in contact with carbon steel for ten years. From the XRD analysis, GR(Cl^-) and lepidocrocite were identified as the corrosion products of carbon steel in Kunipia F. The selective dissolution and valence analyses suggest that $Fe(OH)_2$ coexisted in Kunipia F. Therefore, under this experimental condition, $Fe(OH)_2$ formed in Kunipia F due to the corrosion of carbon steel was oxidized to GR1(Cl^-) as intermediates, and then GR1(Cl^-) was possibly oxidized to lepidocrocite. $Fe(OH)_2$ distributed in compacted bentonite was barely crystallized within ten years at 80°C. On the other hand, any GR1(Cl^-) was hardly detected in Kunigel V1. Most of the corrosion products in Kunigel V1 immersed in SW and LS consist of $Fe(OH)_2$. In the case of Kunigel V1 immersed in SWL, siderite might be precipitated adjacent to the carbon steel.

Acknowledgements

The authors are grateful to Mr. Y. Ohuchi for assistance with the experiments.

References

1) Japan Nuclear Cycle Development Institute (JNC), *H12: Project to establish the technical basis for HLW disposal in Japan, Supporting report 3, Safety assessment of the geological system*, JNC TN1410 2000-004, (2000).
2) S. Lantenois, B. Lanson, F. Muller, et al., "Experimental Study of Smectite Interaction with Metal Fe at Low Temperature: 1. Smectite Destabilization," *Clays Clay Miner.*, 53, 597-612 (2005).
3) J. Wilson, G. Cressey, B. Cressey, et al., "The Effect of Iron on Montmorillonite Stability (II) Experimental investigation," *Geochim. Cosmochim. acta*, 70, 323-336 (2006).
4) D. Guillaume, A. Neaman, M. Cathelineau, et al., "Experimental Synthesis of Chlorite from Smectite at 300°C in the Presence of Metallic Fe," *Clay Minerals*, 38, 281-302 (2003).
5) D. Guillaume, A. Neaman, M. Cathelineau, et al., "Experimental Study of the Transformation of Smectite at 80 and 300°C in the Presence of Fe oxides," *Clay Minerals*, 39, 17-34 (2004)
6) J. W. Stucki, B. A. Goodman and U. Schwertmann, *Iron in Soils and Clay Minerals*, D. Reidel Publishing Company, Dordrecht, Holland, 83, (1988).

7) M. Ito, M. Okamoto, M. Shibata, et al., *Mineral composition analysis of bentonite*, PNC TN8430 93-003, Japan Nuclear Cycle Development Institute (JNC), (1993), (in Japanese).
8) D. M. Moore and R. C. Reynolds Jr., *X-Ray Diffraction and the Identification and Analysis of Clay Minerals, 2nd ed.*, Oxford University Press, Inc., New York, (1988).
9) P. Refait and J. M. R. Genin, "The Oxidation of Ferrous Hydroxide in Chloride-containing Aqueous Media and Pourbaix Diagrams of Green Rust One," *Corros. Sci.*, 34, 797-819 1993.
10) J. D. Bernal, D. R. Dasgupta and A. L. Mackay, "The oxides and hydroxides of iron and their structural interrelationships," *Clay Minerals Bull.*, 4, 15-30 (1959).
11) T. Misawa, K. Hashimoto and S. Shimodaira, "The Mechanism of Formation of Iron Oxide and Oxyhydroxides in Aqueous solutions at Room Temperature," *Corros. Sci.*, 14, 131-149 (1974).
12) J. Wilson, D. Savage, J. Cuadros, et al, "The Effect of Iron on Montmorillonite Stability (I) Background and Thermodynamic Considerations," *Geochim. Cosmochim. acta*, 70, 306-322 (2006).

Table 1 Composition of trace amount element in SM400B

Elements	C	Mn	Si	S	P
Content (%)	0.13	0.69	0.19	0.007	0.011

Table 2 Composition of the simulated sea water (SW) used in this study

	Concentration (mg/dm^3)
Cl^-	19,900
SO_4^{2-}	2768
HCO_3^-	144
F^-	1.4
Br^-	69
BO_3^{3-}	26
Na^+	11028
K^+	397
Ca^{2+}	418
Mg^{2+}	1328
Sr^{2+}	61

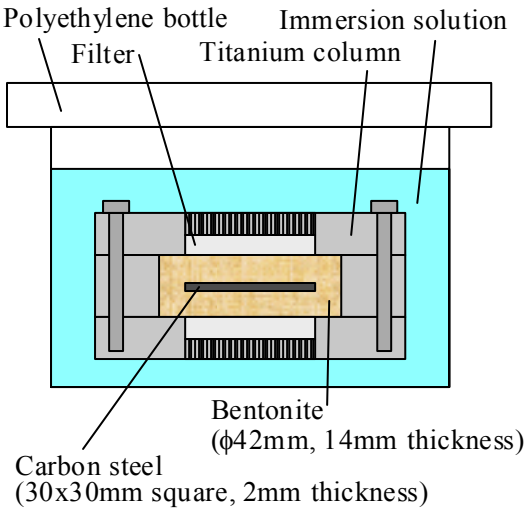

Fig. 6-1 Schematic illustration of the column

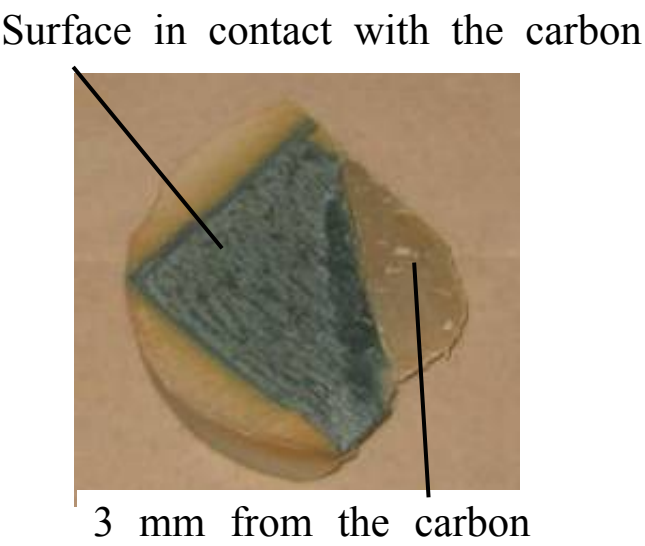

Fig. 6-2 Photograph of the surface in contact with carbon steel and the section of Kunipia F

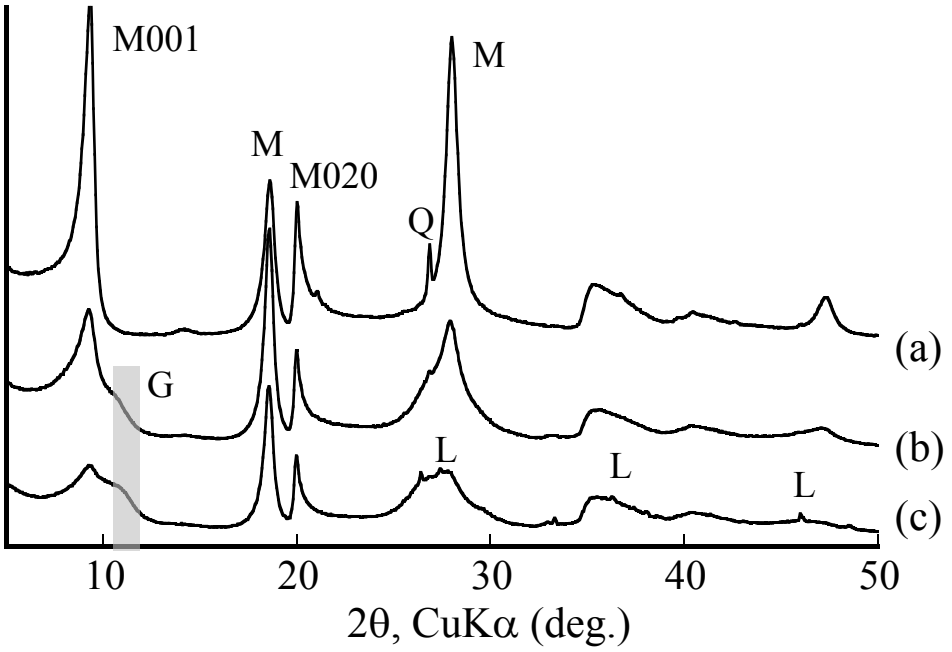

Fig. 6-3 XRD patterns of powdered Kunipia F measured at 30°C, 0% relative humidity. (a) sample at 1.1 mm from carbon steel, (b) sample at 0.5 mm from carbon steel, (c) sample adjacent to carbon steel

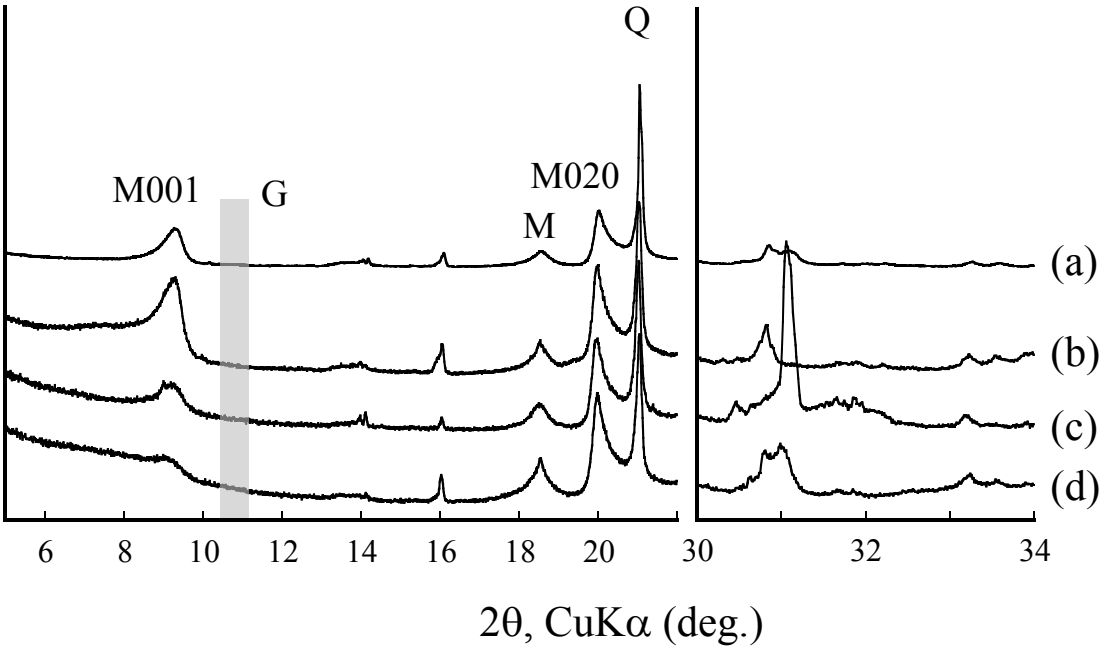

Fig. 6-4 XRD patterns of powdered Kunigel V1 adjacent to the carbon steel measured at 30°C, 0% relative humidity. (a) sample not used for experiment (b) sample immersed in SW, (c) sample immersed in SWC, (d) sample immersed in LS

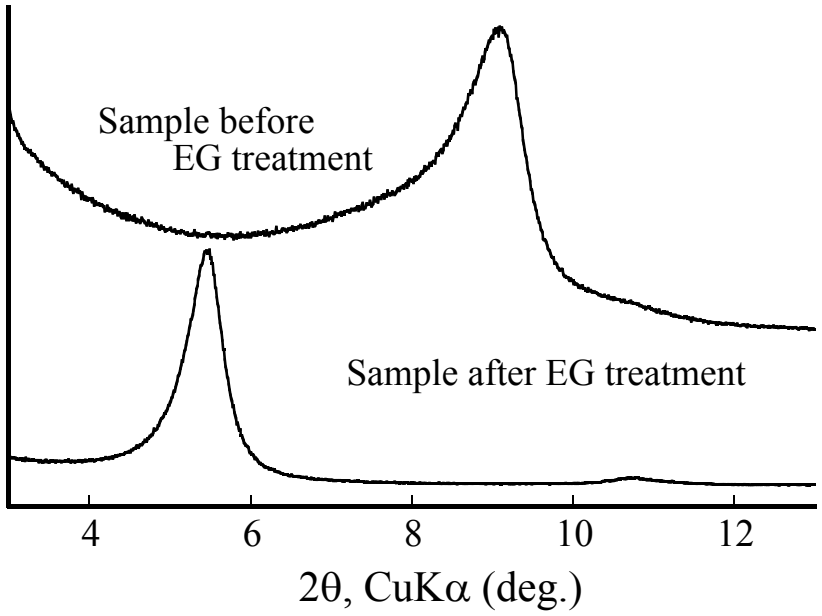

Fig. 6-5 XRD patterns of oriented samples prepared from the Kunipia F powder adjacent to the carbon steel

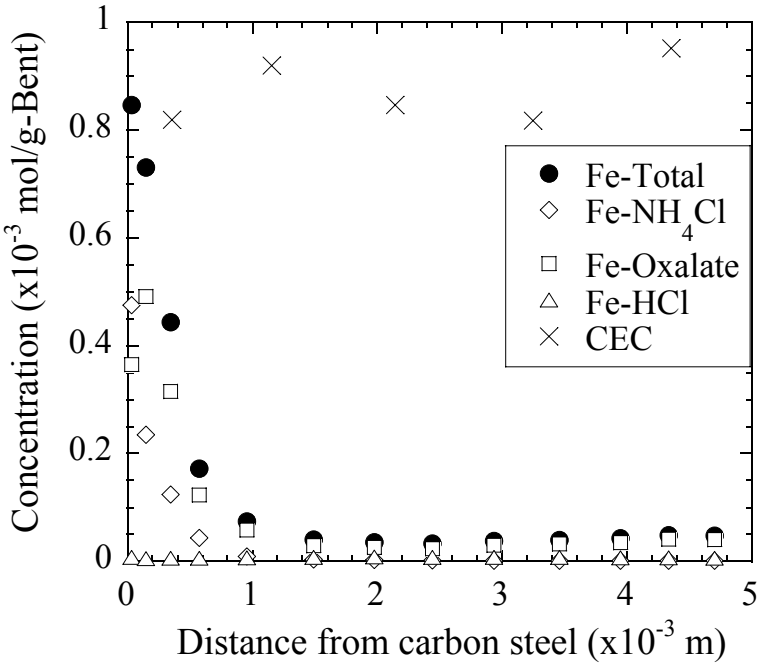

Fig. 6-6 Results of CEC and selective dissolution analyses for Kunipia F

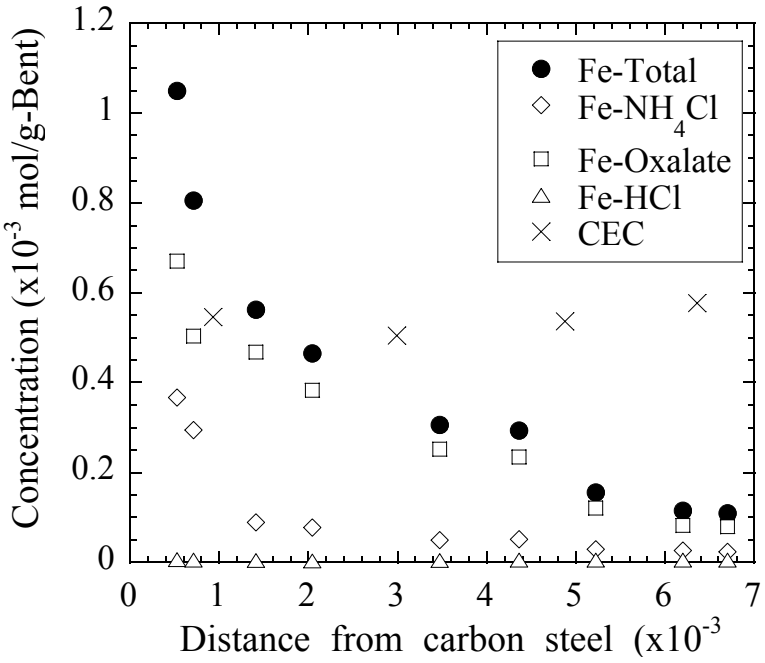

Fig. 6-7 Results of CEC and selective dissolution analyses for Kunigel V1 immersed in SW

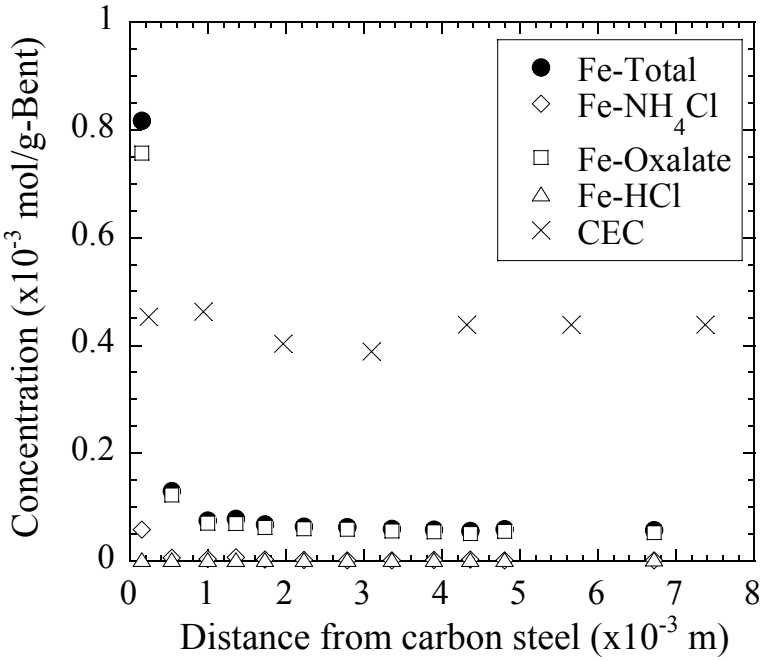

Fig. 6-8 Results of CEC and selective dissolution analyses for Kunigel V1 immersed in SWC

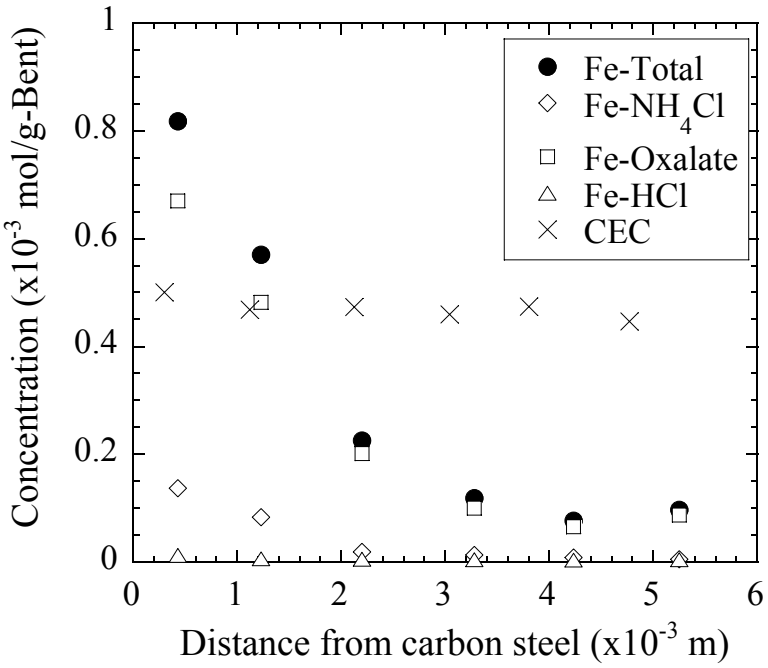

Fig. 6-9 Results of CEC and selective dissolution analyses for Kunigel V1 immersed in LS

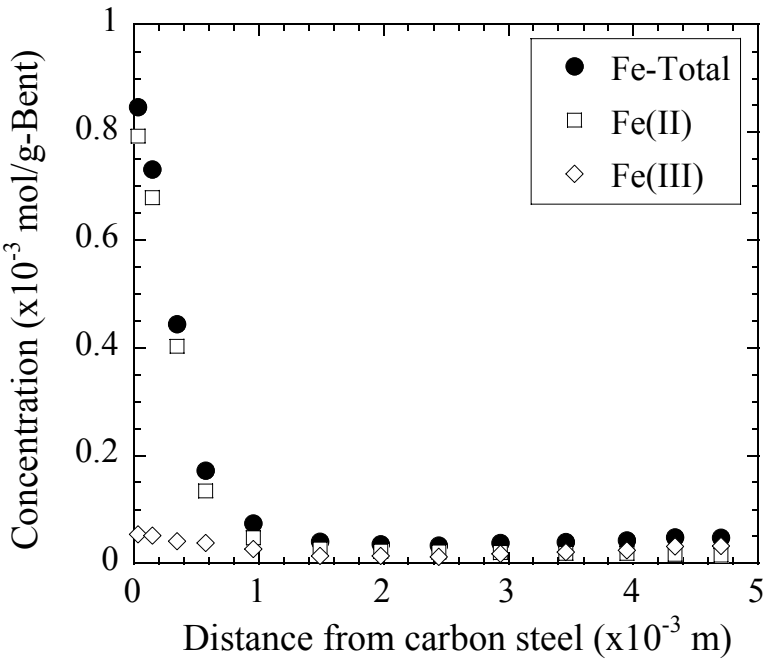

Fig. 6-10 Result of valence analysis for Kunipia F

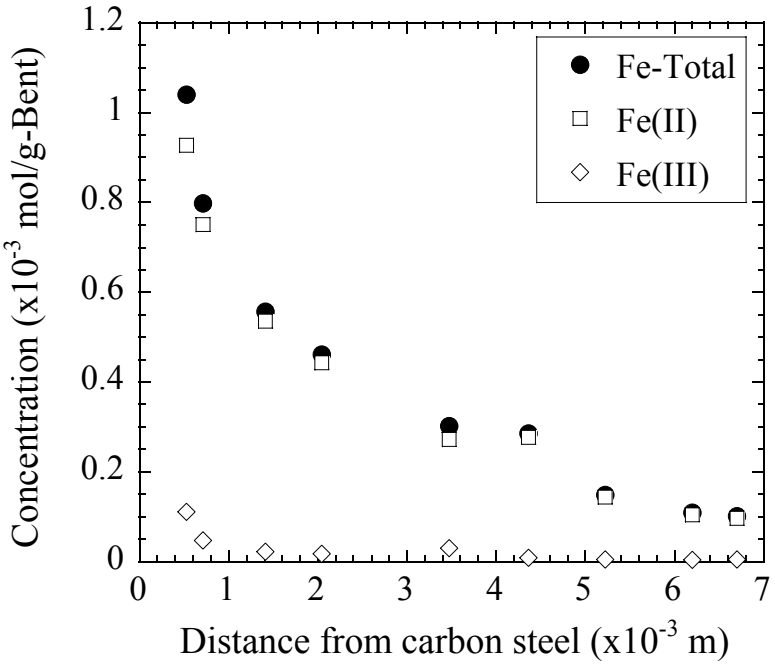

Fig. 6-11 Result of valence analysis for Kunigel V1 immersed in SW

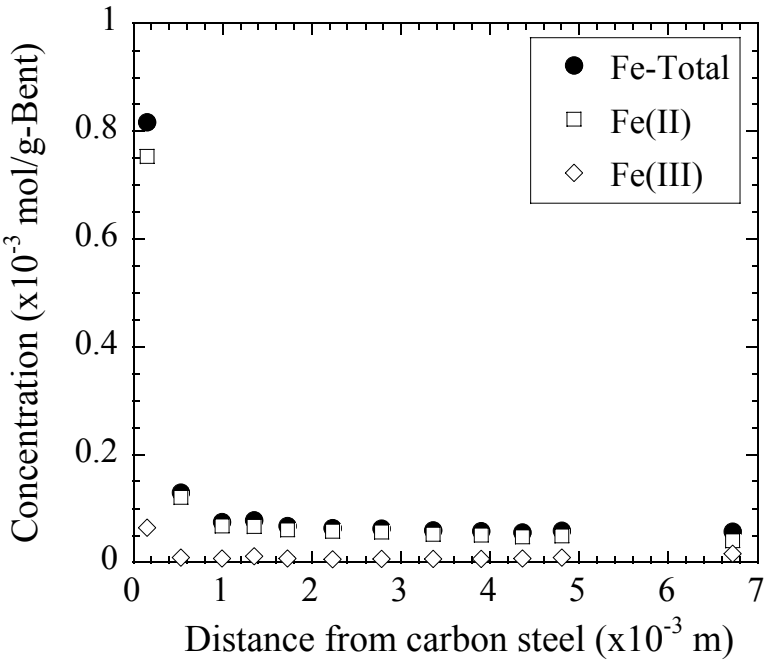

Fig. 6-12 Result of valence analysis for Kunigel V1 immersed in SWC

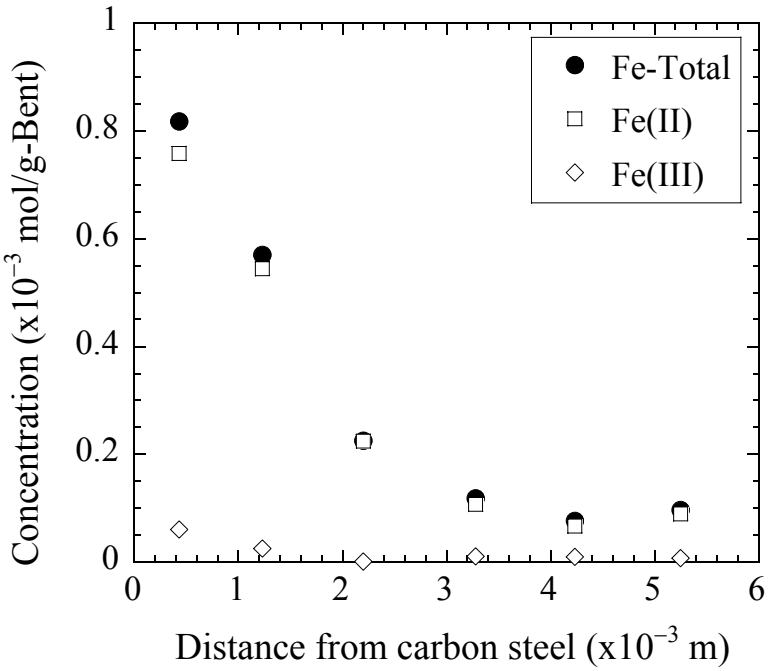

Fig. 6-13 Result of valence analysis for Kunigel V1 immersed in LS

Chapter 7
General conclusions

Diffusion of radionuclides through compacted bentonite is one of key processes of radionuclides migration to the biosphere via groundwater in safety assessment of HLW and TRU waste geological disposals. In this study, the phenomena affecting the diffusion behavior through compacted bentonite were studied.

In chapter 2, temperature dependence of effective diffusion coefficient of deuterated water in compacted sodium bentonite was determined by through-diffusion experiments conducted at elevated temperatures ranging from 298 to 333 K. Activation energies of effective diffusion coefficient were increased with increasing dry density from 0.9 to 1.35 Mg/m^3 over the range of 19-25 kJ/mol. This relationship was considered to be due to the pore structure development and the high activation energy of water near the montmorillonite surface.

In chapter 3, effective diffusion coefficients for Cl^- and I^- in compacted bentonite were determined as a function of $NaNO_3$ concentrations, ranging from 0.01 to 5 mol/dm^3. The effective diffusion coefficients for Cl^- and I^- increased with increasing $NaNO_3$ concentration. These increases in the effective diffusion coefficients were interpreted in terms of a decrease in anion exclusion. The decrease in anion exclusion indicates that the pore space in which anions are free to diffuse, namely effective porosity, increases with increasing salinity. The effective diffusion coefficients for anions in compacted bentonite were found to increase in proportion to this effective porosity in a log-log plot, although the effective diffusion coefficients in porous media generally increase in proportion to the total porosity.

In chapter 4, the corrosion of carbon steel and its effect on neptunium diffusion in compacted bentonite were studied. From thermodynamic predictions considering the condition of pore water of compacted bentonite, $Fe(OH)_2$ and Fe_3O_4 were the most possible corrosion product. Oxidation states of neptunium in the bentonite were investigated by thenoyltrifluoroacetone in xylene extraction technique. It was found that tetravalent neptunium accounted for 99% of the total neptunium in the presence of carbon steel and only 63% without. The results revealed that anaerobic corrosion of carbon steel could maintain strong reducing conditions to keep most tetravalent neptunium from being oxidized to pentavalent neptunium.

In chapter 5, carbon steel was left in contact with compacted bentonite under reducing

conditions for 3 to 4 years at room temperature. The results of selective dissolution, which can estimate crystallinity of Fe-bearing compounds, and valence analyses suggested that the corrosion products in compacted bentonite were amorphous, non-crystalline or poorly ordered $Fe(OH)_2$ and $Fe(OH)_3$. In the XRD analysis, Fe-smectite was not identified in compacted bentonite from the variation of basal spacing as a function of relative humidity. Therefore, the corrosion products in compacted bentonite had minimal effect on alteration of Na-smectite to Fe-smectite. This results is possibly caused by the sufficiently low concentration of Fe^{2+} than Na^{+} in pore water of compacted bentonite, which is controlled by the solubility of non-crystalline $Fe(OH)_2$.

In chapter 6, the alteration of montmorillonite and the form of iron corrosion products in compacted bentonite in contact with carbon steel for 10 years at 80°C were investigated. The selective dissolution and valence analyses suggest that amorphous, non-crystalline or poorly ordered $Fe(OH)_2$ existed in compacted bentonite, indicating that $Fe(OH)_2$ distributed into compacted bentonite was hardly crystallized within 10 years at 80°C. From XRD analysis, newly formed phyllosilicates resulting from the alteration of montmorillonite could not be identified in compacted bentonite. CEC of compacted bentonite was hardly decreased. Thus, the alteration of montmorillonite to other minerals was scarcely detected in compacted bentonite.

In this thesis, the experimental studies clarified the temperature dependence of effective diffusion coefficient in compacted bentonite, the effect of salinity on diffusion of anions, the corrosion process of carbon steel, the form of corrosion products and the possibility of smectite alteration due to the corrosion products. As for the corrosion of carbon steel, the phenomena which increase the diffusivity of radionuclides were not found. On the other hand, the increase in diffusivity with the increasing temperature was higher than expected. The salinity also increased the effective diffusion coefficients of anions in compacted bentonite. However, in the case that the obtained activation energy of effective diffusion coefficient, 19-25 kJ/mol, is used for the temperature correction, the increase of effective diffusion coefficient can be estimated to be approximately 1.5 times higher than that corrected by using the activation energy in free water of 15 kJ/mol at 60°C. The increase in effective diffusion coefficients with increasing salinity can be estimated from the effective porosity, since the good correlation between the effective diffusion coefficient and effective porosity was found in a log-log diagram. For safety assessment of geological disposal, it is essential to estimate

quantitatively the effect of phenomena which increase the diffusivity of radionuclides. The results obtained in this thesis are, thus, respected to estimate the effect of these phenomena on diffusivity of radionuclides in compacted bentonite.

Acknowledgements

At the end of my thesis, I am greatly indebted to Professor Dr. Hirotake Moriyama, Professor Dr. Hajime Yamana and an associate Professor Dr. Takayuki Sasaki of Kyoto University for the opportunity to summarize my studies, and also thankful to them for their comments and suggestions for the editing of this thesis.

I am greatly indebted to Dr. Satoru Suzuki, Dr. Xiaobin Xia and Professor Dr. Kazuya Idemitsu for helpful comments.

I am also thankful to the members of Japan Atomic Energy Agency (JAEA), especially to Dr. Haruo Sato and Mr. Kenichi Ueno for helpful advices.

I am grateful to Mr. Shinya Miyamoto, Mr. Seiichi Kurosawa, Mr. Yuji Ohuchi and Mr. Tadahiro Suyama for helpful advices and experimental help during my studies.

Finally, I would like to thanks all people who made this thesis possible and valuable experience for me.

Research activities by the author

Chapter 2

S. Suzuki, H. Sato, T. Ishidera, et al., "Study on anisotropy of effective diffusion coefficient and activation energy for deuterated water in compacted sodium bentonite," *J. Contam. Hydrol.*, **68**, 23-37 (2004).

Chapter 3

T. Ishidera, S. Miyamoto and H. Sato, "The Effect of Sodium Nitrate on the Diffusion of Cl^- and I^- in Compacted Bentonite," *J. Nucl. Sci. Tech.*, (2008).

Chapter 4

X. Xia, K. Idemitsu, T. Arima, et al. "Corrosion of Carbon Steel in Compacted Bentonite and its Effect on Neptunium Diffusion under Reducing Condition," *Appl. Clay Sci.*, 28, 89-100 (2005).

Chapter 5

T. Ishidera, X. Xia, K. Idemitsu and Y. Kikuchi, "Corrosion Products from Carbon Steel Formed in Compacted Bentonite under Reducing Conditions," *J. Nucl. Sci. Tech.*, (2008).

Chapter 6

T. Ishidera, K. Ueno, S. Kurosawa and T. Suyama, "Investigation of Montmorillonite Alteration and Form of Iron Corrosion Products in Compacted Bentonite in Contact with Carbon Steel for Ten Years," *Physics and Chemistry of the Earth*, (2008).